THE HONG KONG
POLYTECHNIC UNIVERSITY
香港理工大學
Pao Yue-kong Library
包玉剛圖書館

Copyright Undertaking

This thesis is protected by copyright, with all rights reserved.

By reading and using the thesis, the reader understands and agrees to the following terms:

1. The reader will abide by the rules and legal ordinances governing copyright regarding the use of the thesis.
2. The reader will use the thesis for the purpose of research or private study only and not for distribution or further reproduction or any other purpose.
3. The reader agrees to indemnify and hold the University harmless from and against any loss, damage, cost, liability or expenses arising from copyright infringement or unauthorized usage.

IMPORTANT

If you have reasons to believe that any materials in this thesis are deemed not suitable to be distributed in this form, or a copyright owner having difficulty with the material being included in our database, please contact lbsys@polyu.edu.hk providing details. The Library will look into your claim and consider taking remedial action upon receipt of the written requests.

Pao Yue-kong Library, The Hong Kong Polytechnic University, Hung Hom, Kowloon, Hong Kong

http://www.lib.polyu.edu.hk

This thesis in electronic version is provided to the Library by the author. In the case where its contents is different from the printed version, the printed version shall prevail.

The Hong Kong Polytechnic University
Department of Land Surveying and Geo-Informatics

ESTIMATION OF SURFACE VISIBILITY OVER HONG KONG USING REMOTE SENSING

Muhammad Imran Shahzad

A thesis submitted in partial fulfilment of the requirements for the Degree of Doctor of Philosophy

July 2013

CERTIFICATE OF ORIGINALITY

I hereby declare that this thesis is my own work and that, to the best of my knowledge and belief, it reproduces no material previously published or written nor material which has been accepted for the award of any other degree or diploma, except where due acknowledgement has been made.

_____ (Signed)

Muhammad Imran Shahzad (Name of student)

DEDICATIONS

I lovingly dedicate this thesis to my family for instilling the importance of hard work and higher education.

- My late grandmother, Maroof Sultana who prayed a lot for my success in every field of my life and especially during my PhD.
- My father, Muhammad Zaman who never had chance to experience the loves of his parents and get formal education but he made sure that I should not miss those. I cannot imagine the extent of his hard work from dusk until dawn as a Taxi Driver to make me reach at this stage.
- My mother, Najam-u-Nisa whose prayers have always been the keys of my mornings and locks of my evenings. I pray to Almighty to grant her health with eternal happiness. I also salute her courage for braving with her illness and at same time advising me not to come home without finishing my PhD.
- My brother and sisters, who never left my side in every difficult situation of my life.
- My very nice wife Farhat, without whom, this effort would have been worth nothing. Her love, support and constant patience have taught me so much about sacrifice, discipline and compromise. In addition, I will always be in debt to her role as a son to my family and father to my children in my absence.
- My lovely daughter Qandeel, whose smile gives me strength to accept future challenges.
- My cute son Mustaneer, who was born during this PhD.

ABSTRACT

The effects of deteriorating atmospheric visibility are more profound in rapidly growing and densely populated urban areas like Hong Kong. Existing methods to measure atmospheric visibility using ground based instruments have proven ineffective to depict regional visibility scenarios because a dense ground based network involving large cost and time is required. Previous efforts for satellite remote sensing of surface level visual range have mainly focused on stratified layers of fog, and all lack appropriate validation measurements for very clear and highly polluted days. In addition, their application in a highly polluted region like Hong Kong is untested. This study was designed to develop a remote sensing based methodology for measuring at-or-near ground level visual range (VR). The relationship between the surface extinction coefficient and columnar Aerosol Optical Depth (AOD) from four space borne sensors (MODIS, MISR, CALIPSO and OMI) was examined at two visibility recording stations; the Hong Kong Observatory (HKO) and the Hong Kong International Airport (HKIA). The highest correlation is for MISR AOD followed by MODIS AOD. MODIS AOD along with climatic data Relative Humidity (RH), Mixing Layer Height, Wind Speed (WS), Wind Direction (WD), Temperature (T), Pressure (P), V and U component of wind, advection terms VT and UT, mixing ratio (Q) and temporal change in T and P were subjected to regression analysis. A regression model using MODIS AOD, RH, VT and Q explained 84.0 % of the variance in VR with high accuracy demonstrated by a low RMSE of 0.27 km. The results of this study suggest that Q alone can explain the combined effect of P, T and RH on VR, whereas VT is sufficient to explain the effects of WS and WD on dispersion of aerosols and hence on VR. This study also proposes a new methodology to estimate VR using column-integrated aerosol physical properties from MODIS, ground-based LIDAR and AERONET sun photometer measurements of AOD. Results suggest that models utilizing satellite observations together with the near surface extinction coefficient from a visibility meter and LIDAR deployed at the Hong Kong Polytechnic University could reliably to estimate VR 35 km away at HKIA. VR estimates from the proposed models were

found to be within 20 % of ground values which is consistent with requirements of the International Civil Aviation Organization. The models did not overestimate or underestimate VR for clean and/or polluted days, as exhibited by previous studies. Results demonstrate the potential for applying passive satellite depictions of broad-scale aerosol optical properties, and suggest that passive remote sensing exhibits the potential for enhancing the performance of pre-existing ground level visibility networks.

PUBLICATIONS ARISING FROM THE THESIS

Journal Papers

Shahzad, M. I., J. E. Nichol, J. Wang, J. R. Campbell, and P. W. Chan, (2013), Estimating surface visibility at Hong Kong from ground-based LIDAR, Sun Photometer and operational MODIS products, *Journal of the Air & Waste Management Association*, 63:9, 1098-1110, DOI: 10.1080/10962247.2013.

Wong, M. S., **M. I. Shahzad**, J. E. Nichol, K. H. Lee, P.W. Chan, (2013) Validation of MODIS, MISR, OMI, and CALIPSO aerosol optical thickness using ground-based sun photometers in Hong Kong. *International Journal of Remote Sensing,* 34:3, 897-918

Shahzad, M. I., J. E. Nichol, and M. S. Wong, (2013), Evaluation of Spaceborne Sensors for Remote Sensing of Surface Visibility: a Case Study of Hong Kong, *The Journal of Energy and Environmental Science. (Accepted)*

Shahzad, M. I., and J. E. Nichol, (2014), Aerosol Optical Depth as an indicator of ground level PM2.5 mass concentration in Hong Kong, Journal of Sustainable Environment Research. *(Submitted)*

Poster Paper Presentations

Shahzad, M. I., J. E. Nichol, and M. Nazir, (2013), Evaluation of Spaceborne Sensors for Remote Sensing of Surface Visibility: a Case Study of Hong Kong, *The Journal of Energy and Environmental Science.* Advance Training Course in Ocean Remote Sensing, ESAS-Dragon 3, 21-26 Oct 2013, Hong Kong. *(Best Poster Paper Award)*

Conference Proceedings

Shahzad, M. I., J. E. Nichol, J. Wang , J. R. Campbell, S. Lolli, and P. W. Chan, (2012), Estimating surface visibility at Hong Kong from ground-based LIDAR, Sun Photometer and operational MODIS products, Aerosol and Atmospheric Optics – Visibility & Air pollution Conference, Whitefish, MT, US, Sep, 24-28, 2012.

Wong M. S., J. E. Nichol, M. Bilal, and **M. I. Shahzad,** (2011), Validation of MODIS, MISR, and OMI Aerosol Optical Thickness using ground-based sunphotometers in Hong Kong, The Asia Oceania Geosciences Society – Remote Sensing Symposium, Taipei, Taiwan, Aug 8-12 2011.

Shahzad, M. I., J. E. Nichol, and M. S. Wong, (2013), Evaluation of Spaceborne Sensors for Remote Sensing of Surface Visibility: a Case Study of Hong Kong, The Air & Waste Management Association's Annual Conference & Exhibition, Long Beach, CA, USA, June 24-27, 2014.. *(Accepted for oral presentation)*

Shahzad, M. I., and J. E. Nichol, (2014), Aerosol Optical Depth as an indicator of ground level PM2.5 mass concentration in Hong Kong, 4th International Conference on Environment Science and Engineering-ICESE 2014, 24-26 April, 2014, Erzurum, Turkey. *(Accepted for oral presentation)*

ACKNOWLEDGEMENTS

Allah is the one to whom I owe the most gratitude for enabling me to be benefited from the resources around me.

It would not have been possible to write this doctoral thesis without the help and support of the kind people around me, to only some of whom it is possible to give particular mention here.

Prof. Janet Elizabeth Nichol who under took to act as my supervisor despite her many other academic and professional commitments. I extend my gratefulness and highest reverence to her for her tolerance, restless academic and personal support. Her astuteness, knowledge and commitment to the highest standards inspired and motivated me.

I would like to acknowledge the financial, academic and technical support of The Hong Kong Polytechnic University and its staff, particularly in the award of a Postgraduate Research Studentship that provided the necessary financial support for this research. I also thank the department of LSGI, for their support and assistance since the start of my postgraduate work in 2010, especially the head of department, Prof. Xioli Ding. I would also like to thank the staff of the department of LSGI, especially Vaness, Shing, Ziki, and Justin for their support and bearing my limited Cantonese.

This research would have not completed without the good advice, support and friendship of Prof. Jun Wang. His guidance during my yearlong visit at department of Earth and Atmospheric Sciences, University of Nebraska-Lincoln, USA has been invaluable on both an academic and a personal level, for which I am extremely grateful.

I am most grateful to Dr James R Campbell for helping me in understanding the LIDAR data. It was particularly kind of him to invite me for visiting Naval Research Lab, Monterrey, USA. I highly regard his face-to-face, online and on phone discussion, when he patiently pointed out the lack of my research, and possible solutions.

Special thanks to Dr Man Sing Wong (Charles) for his valuable comments and support during my studies. His tips have been very useful to handle my PhD studies.

Amongst my fellow postgraduate students in the Department of LSGI, the effort made by Bilal, Majid, Nithi, Thom, Olympian and Alex in promoting a stimulating and welcoming academic and social environment will stand as an example to those that succeed them. I would also like to thank my colleagues and friends Richard, Bruce, Shawn, Dr Cui, Amie, Tom, Mjahid, Nichole and Sara in the Department of Earth and Atmospheric Sciences, University of Nebraska-Lincoln, USA.

Last, but by no means least, I thank my mentor Col. (Retd.) Hameed Sarwar for his support and encouragement throughout my life.

Muhammad Imran Shahzad

July 2013

Table of Contents

List of Figures

List of Tables

List of Abbreviations

VR	Visual Range
PM	Particulate Matter
RSP	Respirable Suspended Particles
PRD	Pearl River Delta
YRD	Yangtze River Delta
BC	Black Carbon
EC	Elemental Carbon
LIDAR	Light Detection and Ranging
AOD	Aerosol Optical Depth
AVHRR	Advanced Very High Resolution Radiometer
RH	Relative Humidity
WD	Wind Direction
WS	Wind Speed
T	Temperature
P	Pressure
PBL	Planetary Boundary Layer
MLH	Mixing Layer Height
HKO	Hong Kong Observatory
HKIA	Hong Kong International Airport
HKPU	Hong Kong Polytechnic University
AERONET	AErosol RObotic NETwork
ALS	Atmospheric LIDAR System
SSA	Single Scattering Albedo

Chapter 1: Introduction and Literature Review

The world's population is increasing by 1.2 % per year whereas 51 % of the world's population lives in urban areas (Population Reference Bureau, 2012). People living in cities of developing countries face worse air quality than in developed countries mainly due to the use of unclean fuel for domestic and commercial routine activities (Chow et al., 2004). Most of the time they cannot escape from the urban jungle, but sometimes they feel a strong need to escape to a place with a view of distant hills, mountains or sea. Therefore, they try to compensate by observing the blue sky or try to see a skyscraper. Their efforts for visual escape from their immediate surroundings are sometimes unsuccessful because of a grey-brown layer obscuring the view. Consequently, they start analysing the conditions of atmospheric visibility of their surroundings.

The lucidity and vibrancy in a view can affect the information extracted by the observer irrespective of his scientific knowledge. Particulates suspended in the atmosphere can degrade the clarity of the scene, and this clarity is generally evaluated in terms of atmospheric visibility. Visibility is usually expressed as Visual Range (VR) - "the greatest distance at which an observer can see a black object against horizon" (Middleton, 1952). It deals with the reception of light reflected from the objects around us. The amount of light entering our eyes, along with other factors, determines the clarity of the scene under observation.

1.1 IMPORTANCE OF UNDERSTANDING ATMOSPHERIC VISIBILITY

Visibility as a problem to be investigated gained the attention of the scientific community in early 1950s when London experienced its worst smogs due to industrial coal combustion (Brimblecombe, 1981 and 1987). Two decades later, in 1970s Los Angeles also suffered from poor visibility due to emissions from automobiles (Tiao et al, 1975). Since then, efforts have been made to improve visual air quality by identifying the factors responsible for the degradation of visibility. Such efforts have forced policy makers to implement certain "Clean Air Acts" for

many countries, such as the United States of America (CRS, 2005), United Kingdom (Clean air act, 1993) and Hong Kong (HKEPD, 2007).

1.1.1 Human perception

Appreciation of visibility depends on the aesthetic sense of the observer (Howes, 1913; Aesthetics, 2011) because a plume of the smoke can be taken as a sign of development, or on the other hand, as a sign of air pollution in the same region. The human aesthetic sense is influenced by the different elements and attributes driven by personal experience, society and education (Hyslop, 2009). Therefore, people appreciate the air quality around them according to their own perception.

1.1.2 Health

Recent rapid development and industrialization, especially in developing countries, are associated with degradation in air quality and health of the people (Dockery et al., 1993; Pope et al., 1995; EPA, 2011; Thach et al., 2010). Visual range has decreased all over the world from 1973 to 2007 except in Europe (Wang et al., 2009). It has often been used to study the effect of Particulate Matter (PM) level on Health (Thatch et al., 2010; Huang et al., 2009) because VR is often more accessible than PM. China, the world's second largest economy, experiences frequent episodes of poor air quality in its big cities (Chan and Yao, 2008; Huang et al., 2012). Huang et al., (2009) reported 2.17 % increase in mortality for each 8 km decrease in VR.

Lee and Savtchenko (2006) reported a strong association between air pollution in Hong Kong and the Pearl River Delta (PRD) region, where many manufacturing as well as service industries are established. Studies in the same region, have shown a strong correlation between respiratory illness (Peters et al., 1996; Wong et al., 1998), premature deaths due to heart disease (Wong et al., 2001, 2002a, 2002b, 2008a) and decreasing VR due to increase in PM. Also in Hong Kong, Thach et al., (2010) reported a high correlation ($R = -0.78$) between VR and the concentration of fine particulates. This explains the subsequent high correlation of $R = 0.80$ between mortality due to respiratory infections and reduced visibility (Thach et al., 2010). The authors reported a 1.13 % increase in the risk of mortality for each 6.5 km reduction in VR in Hong Kong (Thach et al., 2010) suggesting that improvements in VR can improve life expectancy.

1.1.3 Value of visibility

A cost benefit analysis for improving VR can help to set air quality objectives for a region. Such analysis can also help to estimate the social price tag for the forth-coming strategy for improving regional air quality and may reveal some alternatives to promote efficient use of public funds. Valuation of visibility is important because the relationship between the costs of reducing the emission of PM does not linearly relate to the cost of improvement in visibility (Hyslop, 2009). Delucchi et al., (2002) and Loehman et al., (1994) deduced that improving visibility can cost 10 % to 40 % of the total cost for improving health and air quality.

It is perhaps surprising that there has not been any study to evaluate visibility in Hong Kong because according to Hong Kong Tourism Board (HKTB), site seeing is the second most popular activity after shopping by tourists (HKTB, 2003). Reduction in visibility can affect tourism and hence the economy of Hong Kong in many ways, such as by shortening or diverting the tourist's stay, by lowering property prices and reducing local investment in areas affected by reduced visibility. Therefore, visibility can be considered not only a meteorological phenomenon, but also a commercial product or an economic indicator.

1.1.4 Navigation and transportation

Reduced visibility is a well-known problem in the field of navigation and transportation as it often makes drivers behave inappropriately, which has frequently resulted in fatal accidents (Kang et al., 2008; Caro et al., 2009). Accidents may result in road closures and hence diversions of the traffic route, entailing higher cost in the form of fuel and time to passengers.

In the skies, reduced visibility causes disruption and delays in air traffic as well, which sometimes leads to the closure of airports resulting in heavy losses to the aviation industry (Pejovic et al., 2009). Kulesa, (2002) reported that reduced visibility caused 24 % of general aviation accidents in the air and 37 % on the ground during taxiing. Unanticipated visibility problems in the design of the airport runways can cause heavy losses and sometimes become a key factor in relocation of the whole airport. For example, runway 13's approach at the old Hong Kong airport was impossible in low visibility (http://en.wikipedia.org/wiki/Kai_Tak_Airport#Runway _13_approach). Similar situations have also occurred in naval navigation (Morel and

Chauvin, 2006) and eight vessels collided in August 2004 in Hong Kong due to reduced visibility (Hogg, 2004).

According to road traffic accident statistics of 2010, Hong Kong has 2,076 km length of road with 594,723 licensed vehicles. On average these vehicles faced 7.2 accidents per km in 2010 (Road traffic accidents statistics, 2010). In 2010, Hong Kong's air space was used by 306,534 aeroplanes and more than 420,000 vessels passed through Hong Kong's waters (Road traffic accidents statistics, 2010). A reliable and convenient method to estimate VR can increase the safety of commuters in the presence of this huge road, sea and air traffic.

1.1.5 Indicator of air quality

Degradation in atmospheric visibility is "the pollution that people can see" or the visual air quality (Yuan et al., 2002; Hyslop, 2008) and many studies have reported the inverse relationship between the concentration of aerosols and changes in VR (e.g. Wan et al., 2011, Chan et al., 2008; Wang et al., 2003). Therefore, these changes in VR can be used to indicate air quality (Watson, 2002).

Table 1.1. *Indexing system to estimate the PM level using VR.

VR (Miles)	Levels of Health Concern	Hourly Average PM Levels
Greater than 11	Good	0-38
6 to10	Moderate	39-88
3 to 5	Unhealthy for Sensitive Groups	89-138
1.5 to 2.75	Unhealthy	139-350
1 to 1.25	Very Unhealthy	351-526
Less than 1	Hazardous	Greater than 526

* modified from (www.co.shasta.ca.us/.../ Visually_Estimating_PM_Levels. sflb. Ashx)

Vajanapoom et al., (2001) estimated PM_{10} (Particulate matter with radius less than 10 μm) in Bangkok using VR data with $R^2 = 0.51$. Such studies enabled some cities, such as Shahsta in Canada *(*www.co.shasta.ca.us), to use VR to develop an index for estimating PM levels (Table 1.1).

1.2 PHYSICS OF ATMOSPHERIC VISIBILITY

It is important to understand the Physics involved in the process of visibility because the process of human perception of visibility involves a complex interaction

of light, atmosphere, the human eye and the brain (Henry et al., 2000; Mahadev and Henry, 1999). When the atmosphere is clear and there is no, or less light than that coming from the object, then the human eye can see up to 200 km in the horizontal direction and can even detect light coming from the stars (Watson, 2002). Human vision uses the contrast between the object under observation and its surroundings to detect the edges of the object. Therefore, the human eye works more efficiently if there is high contrast (Malm et al., 1982). Along with the sensitivity of the human eye to the contrast, the threshold for the spatial visual frequency (repetition of structures per unit distance) is also important because sometimes we have to move further away from the object (like a tree line on a hill) to increase the visual distinction by increasing the visual frequency (of the trees) (Watson, 2002). Therefore, the unique thresholds of contrast and spatial visual frequency for each observer give rise to the differences in their visual observations. Moreover, such differences in visual observation can increase in the presence of aerosols as the incoming light disperses away from the observer (Ross et al., 1997).

Interaction between light and the atmosphere has been discussed since 569 B.C (Zanjonc, 1993). Later, Koschmieder, (1924) presented the most practical explanation with the help of his famous "Koschmieder's Equation" (Eq 1.1), which is still being used to explain the combined effect of contrast and extinction on visibility.

$$VR = \frac{\ln C}{B_{ext}} \tag{1.1}$$

Here, C is the contrast threshold of the human eye (0.02 – 0.05) that depends on the health of the eye, and B_{ext} (km^{-1}) is the coefficient of extinction for light coming from the object to the eye. The application of the equation is possible if (Horvath, 1971)

- The illumination in the atmosphere is uniform otherwise, an error up to 5 % can occur.
- The composition of the air in which light is travelling is uniform making the coefficient of extinction constant over large distances to make it closer to the real atmosphere, if the average of the extinction coefficient over a distance is used then the occurrence of the error is zero.

- The object under observation is ideally black (i.e. its reflectivity is zero) giving an error up to 50 % if a non-black object is illuminated in the sunlight.
- By using Eq. 1.1 in the above-mentioned ideal conditions, one can estimate visibility with a maximum error of 10%.

All the wavelets reflected or emitted from the object are unable to reach the observer and may be scattered and or absorbed in different directions. The amount of light lost on its way to the observer is called extinction (absorption + scattering). Other than relative humidity, scattering also depends on the size of the particle (van de Hulst, 1957; Finlayson-Pitts and Pitts, 2000), whereas absorption depends on the chemical composition of the particles e.g. NO_2, and Black and Elemental Carbon (BC and EC) absorb light (Wang and Martin, 2007). Usually, the coefficient of absorption is ignored because light absorption has an overall share of 5 to 10 % in rural areas and 20 to 30 % in polluted urban areas due to EC, in the total extinction of light (White, 1990; Jacobson, 2002). Scattering becomes stronger when the concentration of particles with size corresponding to visible wavelengths increases, and more and more light energy is transmitted in the forward direction. Therefore, the presence of aerosols and gases in the air reduces the contrast by adding noise in the form of scattered light into the signal (light reflected from the target). Hence, the light received at the observer's eyes contains a small portion of the actual light reflected from the target. Total extinction (B_{ext}) is the sum of absorption and scattering due to particles and gases in the air (Eq 1.2).

$$B_{ext} = B_{sca(p)} + B_{sca(g)} + B_{abs(p)} + B_{abs(g)} \quad (1.2)$$

Here $B_{sca(p)}$ and $B_{sca(g)}$ are coefficient of scattering due to particles and gases respectively. $B_{abs(p)}$ and $B_{abs(g)}$ are coefficient of absorption due to particles and gases respectively.

1.3 MEASUREMENT OF VISUAL RANGE

There are different scales and units for measuring VR because the perception of visibility and its appreciation is somewhat subjective to the psychology of the observer. Each measuring unit and scale for measuring atmospheric visibility is assessed for its proximity for human perception but all methods have some

limitations. Because of these limitations, the obtained readings do not match human observations. The limitations in the measuring methods are difficult to mitigate due to the involvement of the complex synergistic process between human vision and the brain system (Henry, 2006). Methods for measuring atmospheric visibility are compared below.

1.3.1 Human eye observation

The most commonly used and easiest method to estimate VR is spotting and identifying a most distant object across the horizon. The object to be spotted is preferred to be black in order to get maximum contrast with the background but in common practice manmade objects, like trees, mountains, buildings or natural objects at known distances are used as a target, whereas illuminated targets are used at night time. The distance of the farthest spotted target will be VR.

The human observer method may not have high accuracy under certain atmospheric conditions that alter the contrast of the target with the horizon, e.g. bright or dark cloud behind the target, target under the cloud, the sun in front of or behind the observer or the target roofed by snow or dust. In addition, consistency among the readings is difficult due to the difference in the contrast threshold of the individual observer. Most importantly, human observation for estimating VR is a subjective approach and mechanical as well as electronic methods have replaced it since 1990 (Hyslop, 2009).

In Hong Kong, human observation is used at the HKO and at the HKIA on an hourly basis by two trained observers. At the HKIA, this method is used when atmospheric visibility is less than 8 km, whereas, normally VR is measured from six forward scatterer visibility meters (FDP) installed along each runway and a scanning Light Detection and Ranging (LIDAR) installed between two runways.

1.3.2 Ground based optical measurements

Transmissometer

A Transmissometer measures attenuation during the forward scattering of the light (from LED, infrared or laser) transmitted from a transmitter and received by a transceiver over a certain distance (Eq 1.3; Horvath, 1981).

$$B_{ext} = \frac{\ln(\frac{I_o}{I_r})}{r} \quad (1.3)$$

Here "I_o" is the actual irradiance at transmitter and "I_r" is the recorded irradiance at the receiver. Malm et al., (1981) found a linear relationship between the human observation and B_{ext}. There are two types of transmissometers; short range, in which the receiver and transmitter are fixed at a short distance on a metallic arm and long range, in which the receiver and transmitter are placed at some distance (meters).

Such instruments can replace human observation in order to get VR at minute intervals. However, they are limited by using a light source of lower power in order to avoid affecting the optical properties of nearby air by a heating effect, and also a Transmissometer cannot measure VR at longer distances (more than 50 km) than human observation (Watson, 2002).

Nephelometer

A Nephelometer measures the scattering coefficient (B_{scat}) by filling it in with a sample of air and heating it before exposing the air sample to light of known wavelength. The scattered light is measured at an angle 90^0 with respect to the incident light. B_{abs} can be computed by subtracting the b_{scat} from b_{ext}. A Nephelometer can also be used to study optical properties of aerosols of any size using filters of different sizes (Anderson, 1998, Han et al., 2009).

This device has some structural design limitations, which make it impossible to measure scattering beyond 170^0. In addition, it is calibrated at a unique index of refraction of a gas, which gives the biased scattering properties (Horvath and Kaller, 1994).

Teleradiometer

A Teleradiometer measures the changes in the inherent contrast of a target with the horizon and perceived contrast at the radiometer over a certain distance by focusing a telescope coupled with photodiode on the target (Malm, 1981; Watson, 2002). Therefore, its measurements can be representative of human observations. The advanced form of this instrument is the telephotometer (Horvath, 1981). Such photometric devices for the measurement of the VR require frequent maintenance and calibration to reduce signal attenuation.

Digital camera

Instruments mentioned above have a common disadvantage of high cost of their installation and operation (Babari et al., 2011). Therefore, a well-developed low cost method to estimate atmospheric visibility using ordinary cameras is often used (Baumer et al., 2008; Duda and Hart, 1972). Visibility is derived by computing the contrast of the target with its background using advanced techniques of digital image processing. The HKO has installed sixteen digital cameras all over Hong Kong but these are for weather monitoring only (Fig 1.1).

The availability of portable devices such as mobile phone and handy camera makes estimation of VR economical and more mobile as compared to the above instruments but they still cannot give full representation across a region. Additionally, it is usually necessary to develop an algorithm according to local atmospheric conditions for increasing the accuracy of estimated VR (Baumer et al., 2008).

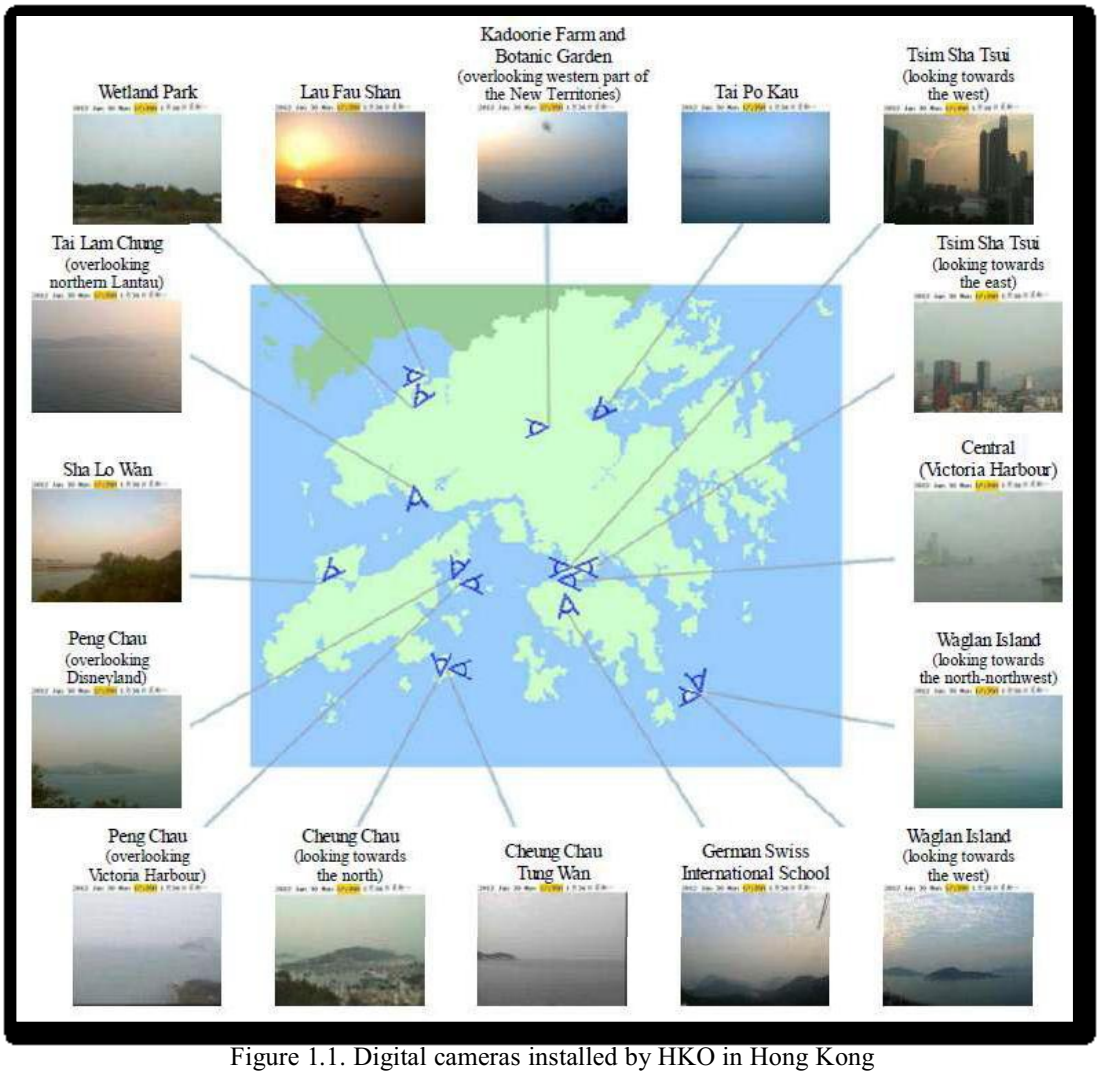

Figure 1.1. Digital cameras installed by HKO in Hong Kong (http://www.weather.gov.hk/wxinfo/ts/index_e_webcam.htm)

1.3.3 Physic-chemical measurements

Visibility is measured in the USA's national parks using chemical speciation method in a campaign called IMPROVE (Malm et al, 1994), where extinction coefficient of the respective species are calculated by selecting a regression fit (Eq 1.4).

$$B_{ext} \cong 2.2 \times f_s(RH) \times [Small\ (NH_4)_2\ SO_4] + 4.8 \times f_L(RH) \times [Large\ (NH_4)_2\ SO_4] + 2.4 \times f_s(RH) \times [Small\ NH_4\ \ NO_3] + 5.1 \times f_L(RH) \times [Large\ NH_4\ \ NO_3] + 2.8 \times [Small\ POM] + 6.1 \times [Large\ POM] + 10 \times [EC] + 1 \times Fine\ Soil] + 1.4 \times f_{ss}(RH) \times [Sea\ Salt] + 0.6 \times [Coarse\ Mass] + Rayleigh\ Scatering + EE_{NO_2} \times NO_2 \quad (1.4)$$

This method can be used as an empirical formula (Malm et al., 2003). In spite of its successful use in the USA, this formula underperforms by 30 % in the PRD region (Jung et al., 2009). Recently Bian (2011) has modified this formula (Eq 1.5) for the PRD and Hong Kong region but it still underestimates visibility with an uncertainty of ± 10 %. This formula needs validation over large time series of ground data before becoming operational. The method is also expensive and time-consuming as ground level aerosol mass concentrations over a region are required.

$$B_{ext} \cong a \times [[\ (NH_4)_2\ SO_4] + [NH_4NO_3] + [NH_4HSO_4]] \times f(RH) + b[OC \times 1.6] + 7.70 \times [EC] + CM + Soil \quad (1.5)$$

1.3.4 Estimation of VR from space

From the above discussion, it is clear that all methods for measuring visibility are representative of only a specific cylinder of the nearby air and they assume the air across a whole region to be identical to that near the measuring instrument. However, in reality, it is common to find different concentrations of aerosol in adjoining areas. Therefore, a method for estimation of visibility over a large region is required that can report VR representing both locale and direction without integrating a local result (representative of a small area of few hundred m^2).

Modern advancements in the field of satellite meteorology have enabled us to estimate large numbers of climatic parameters at high temporal and spatial resolutions (Hadjimistsis et al., 2010). Atmospheric visibility is also an important

climatic parameter and a number of studies have been reported in the literature for estimation of VR from satellite remote sensing (Williams and Cogan, 1991; Bendix, 1995; Vincent, 2003; Haung et al., 2006; Yang et al., 2008; Riffler et al., 2009; Nichol et al., 2010; Hadjimistsis et al., 2010). However, these satellite-based techniques are not yet able to fill the data gaps due to insufficient and rather impossible deployment of ground instruments over a big region (Williams and Cogan, 1991).

Efforts have been reported to supplement surface networks with satellite remote sensing to estimate surface level atmospheric VR (Kaufman and Fraser, 1983; Hadjimitsis et al., 2010), using one, or a combination of approaches. Some relevant examples are; (1) The use of solar albedo for deriving geometric and optical thickness of fog from the Advanced Very High Resolution Radiometer (AVHRR; Mishchenko et al., 2003) and SOnic Detection And Ranging (SODAR), including a radiative transfer model for calculating the extinction coefficient (Bendix, 1995). (2) The use of luminance and contrast in spatial and frequency domains derived from radiative transfer models from satellite images (Diner, 1985; Williams and Cogan, 1991). (3) Atmospheric transmittance derived from satellite Aerosol Optical Depth (AOD) measurements (Hadjimitsis et al., 2010; Nichol et al., 2010) and (4) The use of statistical regressions with different combinations of band radiances to estimate VR (Haung et al., 2006).

Bendix (1995) estimated visibility in the fog from NOAA-AVHRR band 1, 4 and 5 and calculated the spectral and geometrical depths. He computed fog spectral depth using surface and top of fog albedo with a radiation transfer model, and geometrical fog depth by superimposing a digital elevation model (DEM) over a binary image of fog layer with uniform thickness. Although he reported results with accuracy of $R^2 = 0.82$, $R = 0.9$ and standard deviation = 100 m his findings are valid only if the fog layer is of uniform thickness. Therefore, his approach lacks consideration of the vertical extinction profile of the non-homogeneous layer of the fog. In addition, this approach is not reliable in the case of aerosols that have almost similar reflectance to that of urban surfaces. Therefore it can be challenging to use this method when there is no well-defined stratified layer of fog.

Williams and Cogan, (1991) used the luminance and contrast in RS images over a time series to measure the effects of atmospheric attenuation in the

degradation of the VR. They assumed that the transmittance of the beam to the sensor is dependent on an attenuation length (L(z)) and zenith angle (θ). The authors assumed zenith and azimuth angles to be same for a given region in all images. Minimum computed contrast range from each image in the time series, was designated as the inherent contrast of the atmosphere, which was used to compute L(z) and hence VR for each image. In their work, there was no validation with the ground data and hence its operational use is untested. Moreover, using the same azimuth and zenith angle for each image was not realistic. In addition, the method is highly sensitive to the cloud contaminated images as clouds can mask true transmittance of the beam. Therefore, such an algorithm may not be a good choice for Hong Kong that experiences frequent cloud cover. Moreover, this algorithm was computationally expensive.

Hadjimistsis et al. (2010) used a graph between AOD and VR proposed by (Turner and Spenser, 1972) to report VR from the retrieved AOD through an algorithm based on the Darkest-pixel approach using Landsat images at Heathrow Airport, England. They assumed zero reflectance from the selected dark pixel and the radiance recorded for that pixel was assumed to be from the aerosols in that pixel. In addition, they oversimplified their algorithm by ignoring the effects of multiple scattering, Relative Humidity (RH), water vapour and ozone in the atmosphere. Although, they reported an estimated VR with an accuracy of $R^2 = 0.97$ based on only seven images but so many assumptions in algorithm development question its reliability for highly polluted and humid regions like Hong Kong.

The only study using satellite retrieved AOD to estimate VR over the Hong Kong was by Nichol et al., (2010), which used the MODIS AOD computed from the minimum reflectance technique (MRT) at 500m resolution (Wong et al., 2010) to estimate the 3D VR (Eq 1.6).

$$VR = (3.912 \times Z)/AOD \tag{1.6}$$

Here Z is the scaling height where the extinction due to the vertical distribution of AOD becomes zero. This height was used to estimate the vertical profile of the VR corresponding to the n^{th} floor of any building in the region. More over this was the first study considering the importance of visibility in terms of direction, location, and height. Their results still lack the validation from real time ground VR, as large differences are expected, as reported by other studies discussed above.

Haung et al., (2006) used principal component regression (PCR) for computing VR from the radiance of five channels of NOAA-AVHRR over 458 images during 2001- 2002 and found a high correlation for low visibility (< 5 km) with Ch1, Ch2 andCh1/Ch2 (Visible and NIR), possibly due to absorption and scattering from water vapour. The correlation for high visibility (> 15 km) and the NIR channel was highest, whereas for moderate visibility it had the same correlation values for all channels. The results were reported with accuracy of 94.98 % (R = 0.82) for the foggy conditions and the computed visibility with PCR method underestimated the high visibility and overestimated the low visibility.

The studies mentioned above focus only on stratified layers of fog, and all lack appropriate validation measurements for very clear or highly polluted (i.e., high AOD) days or cases. Therefore, their use for a highly polluted and humid region like Hong Kong is untested.

1.4 VISIBILITY IN HONG KONG

Rapid urban industrial development in China mainland has given rise to megalopolises like the Yangtze River Delta (YRD) and the PRD region, and created visibility problems for their own areas as well as neighbouring regions such as Hong Kong. Hong Kong's skyline and mountain horizons are frequently obscured due to reduced visibility (HKO, 2012). This is primarily the result of high aerosol particulate loading, with mean annual AOD values exceeding 0.60 at 550 nm (Wu et al., 2005). Air quality in urban Hong Kong is considered worse than in surrounding rural areas (Louie et al., 2005), and, for context, is worse than in most urbanized coastal areas of eastern USA (Yuan et al., 2002).

Several studies have shown that Hong Kong's declining visibility is closely related to local and regional air pollution (Chan and Yao, 2008), as light extinction correlates strongly with concentrations of respirable suspended particles (RSP - particles with a diameter of less than 10 μm) within the planetary boundary layer (PBL) (Chin, 1997; Lee and Gervat, 1995; Sequeira and Lai, 1998). It is a continuing debate in Hong Kong, whether low visibility is due to regional transport of pollutants under the prevailing meteorological conditions (Lee and Hills, 2003; Lee and Sequeira, 2002; Zhuang et al., 1999) or due to local sources (Ho et al., 2006; Lu and Wang, 2004; Wang et al., 2003). Some researchers suggested both regional and local

sources (Lind and Kok, 1999; Chan et al., 1998, Xiao et al., 2006). Local anthropogenic activities, as well as aerosol particle transport, most commonly in the form of sulphate (SO_4) from neighbouring China, are primary contributors (Cheung et al., 2005; Qun et al., 2009; Zhuang et al., 1999). Lai and Sequeira (2001) showed that NO_2 and RSP are responsible for 79 % of light extinction in Hong Kong. In comparison, Wan et al., (2011) reported a high correlation between visibility and PM_{10} between 2001 and 2008, when the latter decreases by 0.004 mg/m^3 and with NO_2 when NO_2 decreases from 0.05 to 0.02 mg/m^3 in the nearby PRD region. Deteriorating visibility has prompted concern for health as well as for transportation, aviation and other routine civil operations (Thach et al., 2010). Therefore Wan et al., (2011) defined the degradation of visibility in Hong Kong as a multifaceted problem.

Figure 1.2. Long range (left) and short range (centre) Transmissometers at HKIA. Locations of four visibility-monitoring stations (right) in Hong Kong.

Surface VR is measured operationally at five locations in and around Hong Kong's main land areas by qualified weather observers, forward scattering radiometers and transmissometers. These include an urban site at the Hong Kong Observatory (HKO at 22.301° N, 114.174° E) across Victoria Harbor, as well as in the outer suburbs at the Hong Kong International Airport (HKIA at 22.309° N, 113.922° E; Fig 1.2). Although, these monitoring sites have contributed a number of new and important data sets for better characterization of visibility, they are not sufficient to cover all of Hong Kong. In addition, such estimates are valid only for a specific sample of space or direction (Anderson et al., 2003).

1.5 OBJECTIVES OF THIS STUDY

It is evident from the discussion in previous sections that none of the methods to estimate VR has addressed the estimation of visibility at regional scale effectively because it requires a dense ground based network that is costly and time consuming. Although satellite remote sensing has played a vital role in the field of meteorology, it cannot yet be fully utilized because VR is horizontally measured and satellite measures attributes of the atmosphere vertically. However, these different viewing perspectives can also present an opportunity to estimate VR more effectively over a region.

Therefore, the main objective of this study is to develop a remote sensing based methodology for measuring atmospheric visibility at or near ground level. Such a method can improve understanding of the effects of atmospheric visibility in the field of transportation, navigation, health, tourism, and air quality. The following secondary objectives arise from the stated main objective;

- To examine the relationship between columnar AOD and ground visibility; one being measured horizontally and the other being measured vertically.
- To evaluate the potential of space borne optical sensors for remote sensing of VR at surface level.
- To identify the parameters required to estimate VR using ground and satellite remote sensing.

1.6 ORGANIZATION OF THESIS

This thesis is organised in five chapters as follows

- Chapter 1 describes the background, reviewed literature, research gaps, motivation and objectives.
- Chapter 2 depicts study area and data used.
- Chapter 3 evaluates the satellite sensors for estimation of surface visibility using their AOD products. This chapter further identifies the parameters required to improve the estimation of visual range.

- Chapter 4 presents the methods to estimate surface visibility using AOD from MODIS, AERONET and LIDAR. This chapter also describes the validation of each method.
- Chapter 5 highlights the overall outcome and recommendation of this research.

Chapter 2: Research Tools

2.1 STUDY AREA

The Hong Kong domain studied here represents an aggregate surface area of 1104 km^2, located in a sub-tropical region surrounded by the South China Sea to the east, south and west, and bordering Shenzhen, China mainland to the north (Fig. 2.1). The maximum altitude above mean sea level (MSL) is 957 m and approximately 40 % of the land area is preserved as country parklands. Hong Kong experiences local as well as regional trans-boundary air pollution. In the warm summer months, southwesterly winds bring fresh marine air, resulting in a relatively clean, hot and humid atmosphere (Cheng et al., 2006). From October to April, cold air masses from South China mainland transport regional pollutants (Cheng et al., 2006) making air quality poor. Local visibility is highest in the hot humid summer, with southerly winds from the South China Sea, and lowest in the winter and spring, with dry northerly winds from continental China mainland (Chang and Koo, 1986; Mui et al., 2009).

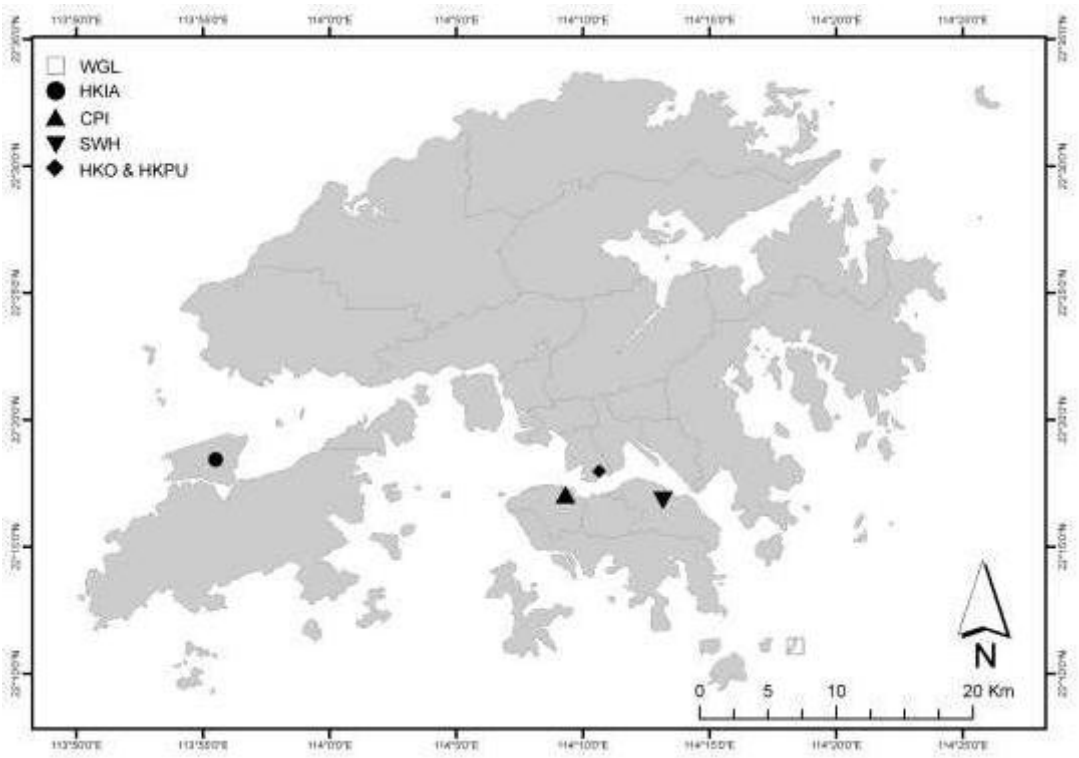

Figure 2.1 Locations of the visibility monitoring stations in Hong Kong, (HKO and HKPU are 0.5 km apart.)

2.2 DATA USED

A brief description of the data used is given below (Tab. 2.1);

Table 2.1 Summary of the data use in the study.

Data Type	Level/Resolution	Wavelength (nm)	Period
MODIS AOD	10 (km)	550	2000 - 2009 Apr, 2011 – Sep, 2012
MISR AOD	17.6 (km)	558	2005 – 2009
OMI AOD	27.8 (km)	483	2006 – 2009
LIDAR (B_{ext}, MLH, AOD)		355	Apr, 2011 – Sep, 2012
AERONET AOD	Level 2.0	550	Apr, 2011 - Oct, 2011
	Level 1.5	550	Nov, 2011 – Sep, 2012
Visual Range	Human observation	550	2002 - 2009
	Visibility meter	875	Apr, 2011 – Sep, 2012
Climatic	Surface level		2005 - 2008

2.2.1 AERONET

Direct level 2.0 AOD from Aerosol Robotic NETwork (AERONET) station of HKPU (operating from 2005 onwards) is used in this study. The HKPU AERONET station (22.303^0 N, 114.179^0 E) is on the rooftop (5^{th} floor) of a building. The AERONET sun photometer database includes AOD over a range of wavelengths (0.35 to 1.05 μm), with an accuracy of ± 0.015 (Rainwater and Gregory, 2005). Generally, instruments are calibrated annually. Typically, measurements are collected and reported at 15 min resolution. Value added Level 2 products aside from AOD include aerosol single scattering albedo, size distribution, fine and coarse mode fraction, phase function and asymmetric function (Dubovik and King, 2000). AERONET data are widely used for the validation of satellite AOD retrievals and model simulations (Yu et al., 2003).

We note recent work suggesting that Level 2 AERONET screening algorithms may be limited by optically-thin cirrus clouds, most common in tropical and sub-tropical locales, thus leading to a positive definite AOD bias of 0.03 to 0.06 when

such clouds go unscreened (Chew et al., 2011). In Singapore, for instance, this can approach 35 % of the Level 2 sample. In this study however, we apply the Level 2 archive directly and presume the cloud screening procedures are robust. Atmospheric Lidar System (ALS; Lolli et al., 2011) data (discussed in the next section) is also used in this study. Despite the presence of ALS measurements, during daytime, when the passive radiometric observations used here are available, the ALS proves insensitive to cloud presence at heights and temperatures most commonly associated with optically thin tropical cirrus. Thus, no consideration of potential cloud bias in the AERONET sample is possible.

2.2.2 Atmospheric LIDAR System (ALS)

The ALS at HKPU collects data at 15 m and 1 min spatial and temporal resolutions, respectively. The ALS is a single channel elastic backscatter LIDAR, operated at 355 nm, with an outgoing energy pulse near 16 μJ at 20 Hz. The ALS data used in this study do not account for Rayleigh scattering and gas and particle absorption. Signals are processed for a relative backscattering coefficient (β; $m^{-1}sr^{-1}$), which can be interpreted for significant aerosol particle layers, such as the surface-detached mixed aerosol layer (referred to as Mixing layer low; ML-Low) and diffuse elevated layers decoupled from the primary surface layer (ML-High) and advecting within the free troposphere. Further processing can yield an estimated extinction coefficient (Lidar extinction coefficient at HKPU; σ_{LU} - m^{-1}), where AOD (Lidar AOD at HKPU; τ_{LU}) is either constrained and extinction solved iteratively through an inversion solution to the Lidar equation (Fernald, 1984; Klett, 1985), or by setting the relationship between extinction and backscatter coefficients (Lidar ratio) constant within an assumed turbid layer and again constraining total transmission to solve extinction bin-by-bin from the top of the layer to the surface.

In this work, the latter technique for solving the extinction is applied using built-in software provided by the ALS manufacturer that includes a predefined set of extinction-to-backscatter ratios that limited the choices of extinction-to-backscatter ratios. The extinction-to-backscatter ratio can fluctuate depending on the region of interest, particularly in Southeast Asia (Campbell et al., 2013). At Hong Kong, it is found to fluctuate seasonally between 18 sr to 44 sr at 532 nm (He, 2006). In this study, a value ratio of 36 sr was chosen from the available list in LIDAR's built-in software because it was the most appropriate choice among the available predefined

set. This value ratio of 36 sr (e.g., Ackerman et al., 1998) reflects urban pollution as the primary aerosol type regionally.

Note that overlap of the ALS system is achieved at a range approximating 170 m. Thus, in order to estimate near surface VR effectively, we use data as close to the surface as possible and extrapolate downward (described below). Therefore, the hourly average extinction coefficient (Lidar extinction coefficient at HKPU; σ_{LU}) at 355 nm is retrieved from the LIDAR measurements at heights between 75 m and 150 m.

2.2.3 Image data from satellite

The objective of this study is to estimate the atmospheric visibility using the AOD retrieved from the satellite. Therefore, in order to select the most appropriate sensor and its AOD product a comparison is also carried out between potential AOD retrieving sensors. This study used all available satellite data: (i) MODIS 10 km AOD product at 550nm from 2000 to 2009, (ii) MISR 17.6 km AOD product at 558 nm from 2005 to 2009, (iii) OMI 27.8 km AOD product at 483 nm from 2004 to 2009 and (iv) CALIPSO 5 km AOD product at 532 nm from 2006 to 2009. Following is the brief description of each sensor and their AOD products used in this study;

MODIS

The MODerate resolution Imaging Spectroradiometer (MODIS) is a sensor aboard the Terra and Aqua satellites. Terra was launched in 1999 and passes from north to south in the morning (ca. 10:30 a.m. local time) and Aqua was launched in 2001, passing from south to north in the afternoon (ca. 1:30 p.m. local time). With 36 wavebands at 250 m, 500 m and 1 km resolution, MODIS can be used for atmospheric, oceanic and land studies at both global and local scales. MODIS also provides specific products such as atmospheric aerosols, ocean colour, land cover maps and fire products. The MODIS aerosol operational product (MOD04) devised with the 10 km resolution has been upgraded from collection 4 (Kaufman et al., 1997; Kaufman and Tanré, 1998) to collection 5 (Levy et al., 2005) with more consideration of aerosol types and dark pixel selection during retrieval. The rationale of multi-wavelength algorithm used in MODIS is to take advantage of different aerosol scattering properties at different wavelengths. Thus, by virtue of their

spectral differences, the amount of aerosol reflectances can be inferred from a combination of longer and shorter wavelengths. Then fit the derived aerosol reflectances in Look-Up Tables created from different aerosol types to derive AOD.

MISR

Multi-angle Imaging SpectroRadiometer (MISR) was launched in 1999 in a polar orbiting sun-synchronous satellite (Terra) at an altitude of 705 km with temporal resolution of 16 days, nine cameras with four spectral bands (446, 558, 672 and 867nm) are used for observing forward, nadir and rear 9 different viewing angles (Diner et al., 1998). The spatial resolution of MISR is 250 m, 275 m and 1.1 km respectively. The radiances at 1.1 km resolution are processed in the standard level 2 MISR aerosol product at 17.6 km^2 pixel size. The heterogeneous land algorithm has been developed by Martonchik et al. (1997) for application with multiple view angle sensors when no Dense Dark Vegetation (DDV) is present and when sufficient spatial contrast is present in a scene. It differs from the dark water and DDV retrieval methods in that it does not use the observed radiances directly, but instead uses the presence of spatial contrasts to derive an Empirical Orthogonal Function (EOF) representation of the angular variation of the scene reflectance. This is then used to estimate the scene path radiance (the radiance field reflected from the atmosphere without interacting with the surface), which is used in turn to determine the best fitting aerosol models (Martonchik et al., 1997; Diner et al., 1998).

OMI

The Ozone Monitoring Instrument (OMI) was launched in 2004 on a 705 km sun synchronous polar orbit with an ascending node equator crossing time of 13:45 (LST). The OMI instrument (Levelt et al., 2006) with advance viewing capabilities is an inheritor of the instruments such as the Total Ozone Mapping Spectrometer (TOMS; Bhartia and Wellemeyer, 2002; Heath and Park, 1978), the Solar Backscatter Ultraviolet Instrument (SBUV; Heath and Park, 1978), the Global Ozone Monitoring Instrument (GOME; Burrows et al., 1999) and the Scanning Imaging Absorption Spectrometer for Atmospheric Cartography (SCIAMACHY; Burrows et al., 1995; Bovensmann et al., 1999). The OMI instrument is a push broom nadir viewing ultraviolet to visible (ultraviolet: 270-365 nm and visible part: 365-500 nm) imaging spectrometer with a wide instantaneous across track field of view (115^o). These wavelengths range are used to retrieve the OMI data products that are

available at four processing levels (level 0, level 1B, level 2, and level 3). The OMI operational algorithms to retrieve these data products heavily depend on experience gained from TOMS, GOME, SBUV and SCIAMAMCHY. There are two aerosol operational products developed for OMI sensor: OMAERUV aerosol product (near-UV algorithm) and OMAERO aerosol product (multi-wavelength algorithm). The near-UV algorithm derives AOD from 342.5 and 388nm. Its rationale is first deriving aerosol index from these two wavelengths, then using aerosol index to determine the corresponding aerosol type. Lastly, it uses the corresponding aerosol types to generate look up table and making use of look up table to derive AOD and Single Scattering Albedo (SSA). The multi-wavelength algorithm derives AOD using eight UV and visible wavelengths from 340 to 500 nm. Its rationale is by fitting the spectrum to fifty aerosol models, and find the model with the least systemic error (Root Mean Square Error - RMSE), then further derive AOD value from the appropriate aerosol model (Torres et al., 2005). In this study, the OMAERO aerosol grid product by multi-wavelength algorithm (at 27.8 km spatial resolution) was used since it provides AOD values at visible wavelengths that are compatible with human observation of VR.

CALIPSO

CALIPSO (Cloud-Aerosol Lidar and Infrared Pathfinder Satellite Observation) spacecraft was launched in 2006 to observe the vertical structure and properties of clouds and aerosols (Winker et al., 2003, 2007, 2010). CALIPSO is the first polarization LIDAR in a 705 km sun-synchronous polar orbit providing global coverage between 82^{o} N and 82^{o} S with a local afternoon equator crossing time at 13:30 (ascending node). CALIPSO payload consists of the CALIOP (Cloud-Aerosol Lidar with Orthogonal Polarization), an active and polarization sensitive lidar instrument with passive visible and infrared sensors (Winker et al., 2003). The main objective of CALIPSO is to provide the high-resolution vertical profiles, and spatial and optical properties of aerosols and clouds to improve the global climate, weather forecast and air quality models (Winker et al., 2007). The accuracy of CALIOP data products depend on the calibration of the 532 nm backscatter profiles and these products are divided into level 1 and level 2 (King et al., 2004). The level 1 data products consist of geo-located and calibrated profiles. The level 2 data products have three types of data: layer products (provide properties of clouds and aerosols

layers), profile products (provide backscatter and extinction profiles), and vertical feature mask (provide location and types of aerosol and clouds). In this study, the column AOD from level 2 products with spatial resolution at 5 km was used.

2.2.4 Climatic data

Climatic data from HKO for the years 2004 to 2008 were used in this study. Meteorology plays an important role in dispersion and accumulation of aerosols. For instance, northerly winds reaching Hong Kong in winter are mostly polluted. Regional pollutants combined with local are trapped under an inversion layer developed within height of few hundred meters. On the other hand, southwesterly winds in summer bring marine air mass to region. Mostly pollutants are vertically dispersed due to increased surface temperature in summer. This results in to increased VR due to decreased mass concentration of particulates near the surface. Therefore, Mixing Layer Height (MLH), wind speed (WS), wind direction (WD), temperature (T), pressure (P), V and U component of wind, advection terms VT and UT, mixing ratio (Q) and temporal change in T and P (ΔT and ΔP) were used to further explore the physics of their relationship with visibility.

Visibility studies are often performed under dry conditions as relative humidity (RH) impacts the aerosol optical properties (Charlson et al., 1992). Increase in RH can cause many fine particles with diameters less than 1 μm to grow up to 1 μm and hence increase the scattering (Bohren and Huffman, 2004; Seinfeld and Pandis, 2006). The extent of the effect of RH on the optical properties of the aerosols depends on the size and chemical composition whereas other influential factors are difficult to identify for the region (e.g. Hong Kong) where there is a frequent exchange of large air masses (Zieger et al., 2011). The effect of RH some time dominates the role of aerosols in the visibility degradation, for example, visibility in Beijing is reported to degrade under the effect of RH when PM level and visibility both are found to decrease simultaneously (Chan and Yao, 2008). Therefore, hourly values of the RH were also used in this study to analyse the effect of RH on visibility.

Sequeira and Lai, (1998) mentioned PBL height and seasonality in the Hong Kong as the key climatic parameter to affect the aerosol loading. Significant relationship (R^2 = 0.82 - 0.85) between aerosol and visibility are reported when PBL height is lower (Zieger et al., 2011, Liu et al., 2009) and the atmosphere is stable. In

Hong Kong PBL height is measured twice daily (0800 and 2000 HKT) at King's Park using Balloon Radiosonde. It is also useful to have the PBL data from the LIDAR of the HKPU because some data of the Radiosonde and LIDAR have shown good agreement below the height of 12 km in Hong Kong (Keckhut et al., 1993). Therefore, PBL and ML height data from the NCEP FNL Operational Model Global Tropospheric Analyses dataset and lidar were also used.

2.2.5 Visual range

In this study, we used VR from Human observation as well as from visibility meter. Hourly visibility data from human observer were collected from the two stations of HKO and HKIA whereas VR from visibility meter are collected from two stations of HKIA and HKPU stations. HKO is located in Tsim Tsa Tsui (TST) within few hundred meters of the HKPU's AERONET, LIDAR and visibility monitoring station in a highly commercialized urban area and HKIA is in the eastern side of PRD near Tung Chung (TC). Human observation of the visibility was used in the time series, correlation and regression analyses.

Chapter 3: Evaluation of Spaceborne Sensors for Remote Sensing of Surface Visibility

3.1 INTRODUCTION

In order to explore the potential of different satellite sensors to estimate VR from their AOD products, a comparison was carried out by extracting the AOD value from different sensors from the pixels corresponding to the VR monitoring stations. This part of the study will compare the AOD products from four satellite sensors (MODIS, MISR, OMI and CALIPSO) with human observations of VR measured at two stations in Hong Kong. The two stations HKO and HKIA collect VR data for the urban area and a coastal area respectively. The results from this evaluation can suggest the best parameters for reliable satellite-based VR estimation.

3.2 IMAGE AND CLIMATIC DATA USED

The study used satellite products for many years from four different sensors, namely: (i) MODIS 10 km AOD product at 550 nm from years 2000 to 2009, (ii) MISR 17.6 km AOD product at 558 nm from years 2005 to 2009, (iii) OMI 27.8 km AOD product at 483 nm from years 2004 to 2009, and (iv) CALIPSO 5 km AOD product at 532 nm from years 2006 to 2009. The AOD products in the green or near green regions of the visible spectrum were compared with hourly human observations of VR from two stations in Hong Kong i.e. HKO and HKIA.

Climatic data were considered because meteorological conditions affect the concentration and optical properties of pollutants and hence can influence VR (Du et al., 2013; Zieger et al., 2011). For instance, relative humidity (RH) causes many fine particles of $< 1\mu m$ to grow in size up to $1\mu m$ and, hence increase the scattering (Bohren and Huffman, 2004; Seinfeld and Pandis, 2006). The effect of RH may exceed the role of aerosols in visibility degradation (Chan and Yao, 2008). Therefore, hourly values of RH were also used in this study to analyse the effect of RH on visibility. Preliminary analysis in this study (not discussed here) depicted a decrease in the correlation between AOD and VR by increasing RH until RH = 90 %. Correlation did not increase for RH above 90 %. This finding is also in line with by

other studies investigating the relationship of VR with climatic data (Chang et al., 2009; Tsai, 2005). Therefore, data corresponding to RH greater than 90 % and with rainfall were excluded from the analysis.

Wind speed (WS) can alter the aerosol loading and the aerosol residence time in a region. Wind direction (WD) can also increase aerosol loading in a region if wind is coming from an emission source. Lee and Savtchenko (2006) reported that seasonal variation in regional air quality of Hong Kong is due to seasonal variation of cyclonic and anticyclonic activities bringing alternatively fresh and polluted air to the region. Leung and Lam, (2008), did a quantitative analysis on this and proposed three wind sectors based on wind direction (Fig 3.1): (1) West to North - air enters from PRD (2) Northeast to Southeast - air enters from southeastern coastal areas of China mainland (3) South - air enters from South China Sea. They found the highest number of hours of reduced visibility for Hong Kong Observatory (HKO) to be in the NE to SE sector (59 - 80 %) followed by W to N (14 - 34 %) and S (2 - 12 %) for the years 2003 - 2007.

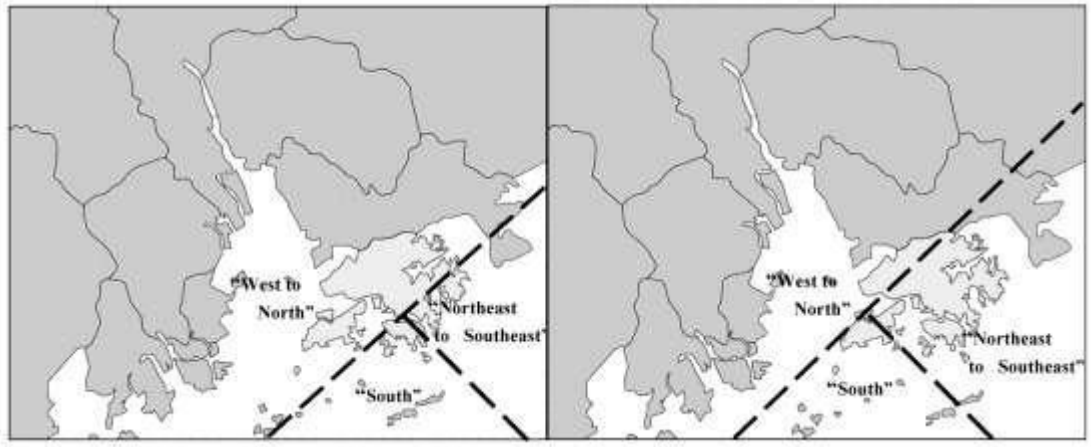

Figure 3.1. Division of study area into wind sectors of West to North, Northeast to Southeast and South for HKO (left) and HKIA (right) (Leaung and Lam, 2008).

Both Lee and Savtchenko, (2006) and Leung and Lam, (2008) in Hong Kong focused on the role of WS and WD in the degradation of VR but they failed to draw any final conclusion on the use of WS and WD for predicting VR because a detailed study is required for identifying important wind sectors at a finer scale. Similarly, to quantify the effect of WS, Wu et al., (2005) combined the role of PBL and wind as Wind Flux using the U and V component of wind from a wind Profiler. This enabled them to study the combined effect of MLH and WS at different heights in order to understand the vertical dispersion of the aerosols. Therefore, it appears that the effect

of WD and WS on visibility may be quantified using a wind profiler along with MLH data. Therefore, V and U components of the wind are also used in this study to analyse the subsidence and dispersion of aerosol.

High temperature can disperse aerosols through thermal turbulence, thus increasing VR (Lin et al., 2011; Du et al., 2013). Mui et al. (2009) developed a regression model to estimate VR from climatic parameters and found temperature to be the only significant parameter, reporting a correlation coefficient of 0.76. In other studies, the importance of the temperature was discussed by dividing data into seasons (Zhang et al., 2010). Moreover, in some studies, the advection terms UT, VT, temporal change in T and P along with mixing ratio (Q), which itself is a function of P, T and RH, have also proven to be good indicators for convection and advection of aerosols. Leung et al., (2009) reported that visibility in Hong Kong is affected as a whole by changes in the source of air masses under the effect of convergence of horizontal and vertical airflows, temperature inversions, and wind speed.

Sequeira and Lai (1998) noted that the Mixing Layer Height (MLH) and seasonality in the Hong Kong were the key climatic parameters affecting aerosol loading. They reported a more significant relationship (R^2 = 0.82 - 0.85) between aerosol and visibility when MLH is low (Zieger et al., 2011, Liu et al., 2009) and the atmosphere is stable, as scattering of light increases with low MLH because aerosols are trapped close to the surface. Recently, Yang et al., (2013) reported a decrease in daytime maximum MLH with decrease in temperature over Hong Kong from May 2003 to Dec 2009. They explained that a decrease in maximum MLH increased the near surface extinction of light because a decrease in maximum MLH reduces the volume of air containing aerosols near to the surface.

Therefore, MLH may be used as a scaling height because most of the scattering occurs within the MLH of 1 to 5 km (Chin et al., 2007). MLH in Hong Kong is measured twice daily (0800 HKT and 2000 HKT) using Radiosonde at King's Park. Since, there is a two to three hour difference in the time of sounding and satellite overpass, during which MLH can change significantly, MLH data from Radiosonde were not included in this study. However, MLH data corresponding to satellite pass time was obtained from NCEP FNL Operational Model Global Tropospheric Analyses dataset (NCEP, 2000).

Overlapping of cold and warm front due to pressure difference has been observed to disturb the vertical dispersion of aerosols (Zhang et al, 2009). This frontal inversion creates a stable temperature inversion layer between the two fronts that acts as a mixing layer to trap aerosols below it (Zhang et al., 2009). This kind of situation may occur in Hong Kong in the winter when a high concentration of the aerosols is trapped under the mixing layer due to prevailing high pressure. Aerosols can also be trapped in the presence of two MLHs due to frontal inversion. This traps the majority of aerosols near the ground in a well-mixed layer and the remaining aerosols reside above the inversion layer forming a secondary mixing layer. Hence, the effects of P are translated into the changes of MLH and concentration of the aerosols below it.

Due to the above reasons, climatic data of temperature – T, pressure – P, relative humidity – RH, wind speed – WS, wind direction – WD, MLH, U and V component of wind, water vapour mixing ratio (Q), and temporal change in T and P (ΔT, ΔP) from HKO from 2004 to 2008 are used in this study to construct linear multiple regression against AOD from a potential remote sensor for estimating visibility.

3.3 METHODOLOGY

This study was conducted in two parts. First, the relationship between AOD and surface level extinction coefficient (B_{ext}) was analysed to evaluate the potential of satellite sensors for remote sensing of VR. The relationship was analysed in terms of correlation coefficient (R), Root mean square error (RMSE) and Mean absolute deviation (MAD). Secondly, multiple linear regression was implemented with each satellite AOD along with the climatic data from HKO to simulate B_{ext}.

3.3.1 Evaluation of satellite sensors

VR values from HKIA and HKO were converted to Surface level extinction coefficient (B_{ext}) using Koschmieder's equation. The OMI, MODIS, MISR, and CALIPSO AOD products were compared with B_{ext} observations within a period of ± 30 minutes of the overpass time (Ichoku et al., 2002). VR can vary significantly over time and VR may be greater or less than the standard spatial resolution of an AOD product. This variation can affect the underlying relationship of that AOD product and VR. Therefore, the AOD from each sensor was extracted at HKO and HKIA

using kernels (K) of 1 by 1, 3 by 3, 5 by 5 pixels, and so on until the kernel size was greater than or equal to 50 by 50 km^2. The maximum kernel size of 50 by 50 km^2 was used because time series analysis showed that VR in Hong Kong did not exceed 50 km throughout the study period. In addition, a kernel window greater than 50 by 50 km^2 would be unable to separate the AOD extracted at the HKO and HKIA ground visibility measurement sites. The variable kernel size helps to select an optimal spatial window for a given satellite AOD product, and to understand its relationship with surface level VR. The relationship between AOD and B_{ext} was analysed statistically using R, RMSE and MAD.

3.3.2 Regression modelling

The AOD product having a significant relationship with B_{ext} was included in multiple linear regression along with climatic data for the years 2005 to 2008. Time matched data for 2005 to 2007 were used for building an empirical model for simulating B_{ext} using the satellite retrieved AOD product, and data for the year 2008 were used for validating the simulated B_{ext} from the empirical model.

Originally, VR and B_{ext} were positively skewed, which could violate the assumption of ordinary least square (OLS) regression that requires regression variables to be normally distributed. Therefore several transformations were applied, including square root (sqrt), natural logarithm (ln), square (sqr) and inverse (inv) transformations, to produce normal distributions. Such transformations were also applied to the independent variables MODIS AOD, T, P, RH, WS, WD, MLH, UT, VT, ΔT, ΔP and Q. This resulted in a total of ten dependent and fifty five independent variables.

Anderson-Darling statistics (AD) and correlation coefficients for each of the independent and dependent variables were computed. The independent and dependent variables with maximum correlation coefficient at p-value less than 0.1 and minimum AD value were grouped together as potential candidates for multiple linear regression because correlation value alone cannot completely imply the cause and effect relationship. A variable with minimum AD value was included in regression because its distribution would be more normal than others would. The condition of p-value less than 0.1 was imposed to select a sufficient number of independent variables to be analysed with regression modelling.

Each group of variables was subjected to multiple linear regression and further selection of variables from each group was done on the basis of their p-value, T statistic, F statistic, variance inflation factor (VIF), coefficient of determination (R^2) and error in prediction (PRESS). Independent variables with significantly larger p-value and VIF as well as variables with smaller T and F statistics were omitted one by one and regression was repeated until all the variables correspond to p-value less than 0.001. The basic assumptions of regression (variance of the error population should be constant, and residuals are independent and normally distributed) were validated by analysing the standard residual plot and Durbin-Watson statistics (DWS) where the residual should be randomly distributed without any pattern in their spread, and DWS should be near to 2.0.

Each statistical set satisfying the above mentioned criteria was further subjected to two more modelling approaches namely, 'stepwise' and 'best subset' regression. This helped to examine the principal factors affecting B_{ext} using climatic data. Stepwise regression is based on "add" and "drop" approaches where the "add" approach, allows only those independent variables to enter into regression one by one that can improve model fitting, based on their p-value of correlation. A variable is retained in the regression equation until the p-value of its correlation is less than a threshold value. Inclusion of another variable can reduce the significance of the previously added variable and hence it will be removed from the regression equation. A "drop" approach is opposite to the "add" approach (Lin et al., 2011). A combination of both approaches was used in this study at threshold p-value equal to 0.001 unless otherwise stated.

Stepwise regression adopts a single path through the independent variables whereas best subset regression explores all pathways to select the best combination of independent variables (Hudak et al., 2005). Therefore, a regression model with 'n' number of variables developed using best subset approach is expected to perform better than one with the same number of variables developed using a stepwise approach. Therefore, the set of variables selected using stepwise regression was also analysed with best subset regression. A model was selected if it's Cp-value was approximately equal to the number of independent variables in it (Eq. 3.1; Mallows, 1973).

$$Cp = \frac{SSE}{MSE} - N + 2n \quad (3.1)$$

where SSE is the sum of square errors of the model with n parameters including independent variables and intercept. MSE is the mean square error of the model. N is the number of samples. The selected model was then validated using the validation data from the year 2008.

3.4 RESULTS AND DISCUSSION

3.4.1 Columnar AOD and surface level extinction coefficient

OMI AOD and B_{ext}

The correlations between OMI AOD and B_{ext} at HKIA and HKO are both low with R = 0.303 and 0.244 at HKIA (Fig 3.2) and R = 0.418 and 0.386 at HKO (Figure 3.3) for kernel windows of 1 by 1 and 3 by 3 respectively. The overall low correlations may be due to OMI's general overestimation of AOD due to sub pixel cirrus cloud contamination, as reported by Curier et al., (2008) and Livingston et al., (2009) because a pixel size of 27.8 km can easily be mixed with cloud cover and thus underestimate the single scattering albedo (Torres et al., 1998). Therefore, it is suspected that uncertainty in retrieval of OMI AOD over Hong Kong may be associated with sub pixel cloud contamination due to frequent cloud cover. Other than, wavelength (483 nm) of the OMI AOD is expected to experience relatively more extinction than the human observation at wavelength of 550 nm. This may also be the cause of high bias for OMI extinction.

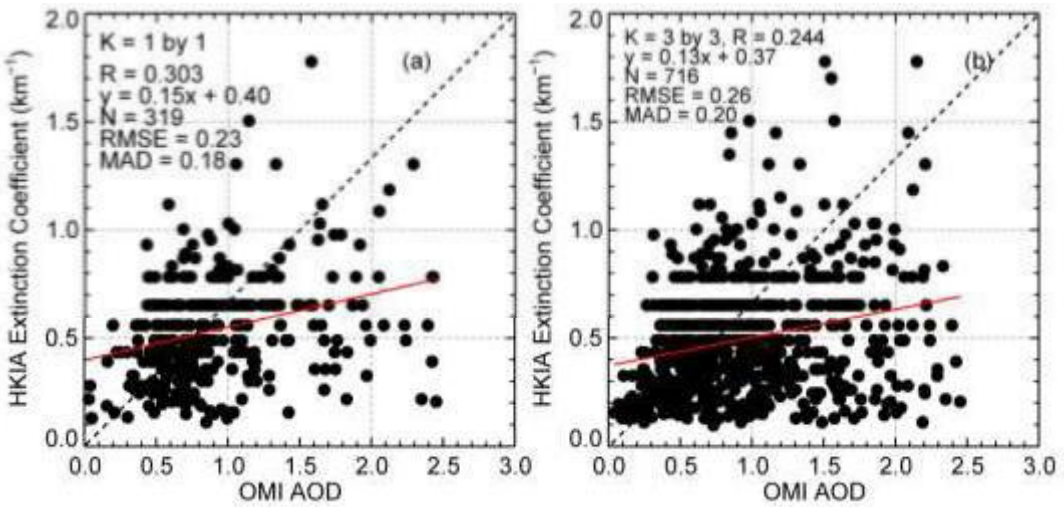

Figure 3.2. Correlation of Extinction Coefficient at HKIA with OMI AOD (27.8 km product at 483 nm) for kernel window of (a) 1 by 1 and (b) 3 x3. Dashed line represents a 1:1 line whereas solid line is the resultant regression line.

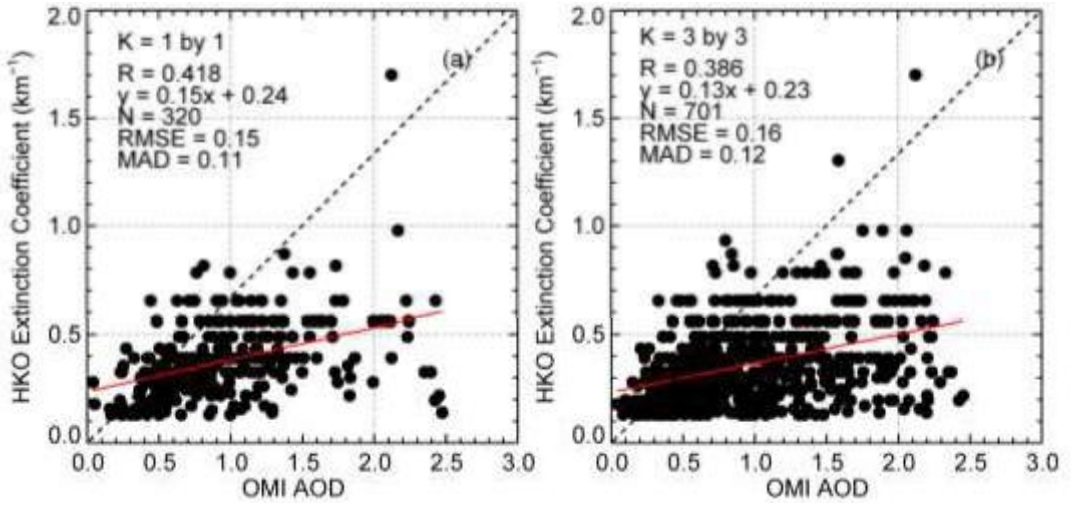

Figure 3.3. Correlation of Extinction Coefficient at HKO with OMI AOD (27.8 km product at 483 nm) for kernel window of (a) 1 by 1 and (b) 3 x3. Dashed line represents a 1:1 line whereas solid line is the resultant regression line.

CALIPSO AOD and B_{ext}

The main objective of the CALIPSO sensor is to measure the aerosol vertical profile from space-borne LIDAR. The sum of extinction coefficient at different heights is deemed equal to AOD. Low correlations are observed between CALIPSO AOD and B_{ext} at both HKO (R = -0.888, 0.467 and 0.167 for kernel windows of 7 by 7 to 11 by 11 respectively; Fig 3.4 a-c) and at HKIA (R = 0.320, 0.391, 0.248, 0.297, 0.239 and 0.115 for kernel windows of 1 by 1 to 11 by 11 respectively; Fig 3.5 a-f).

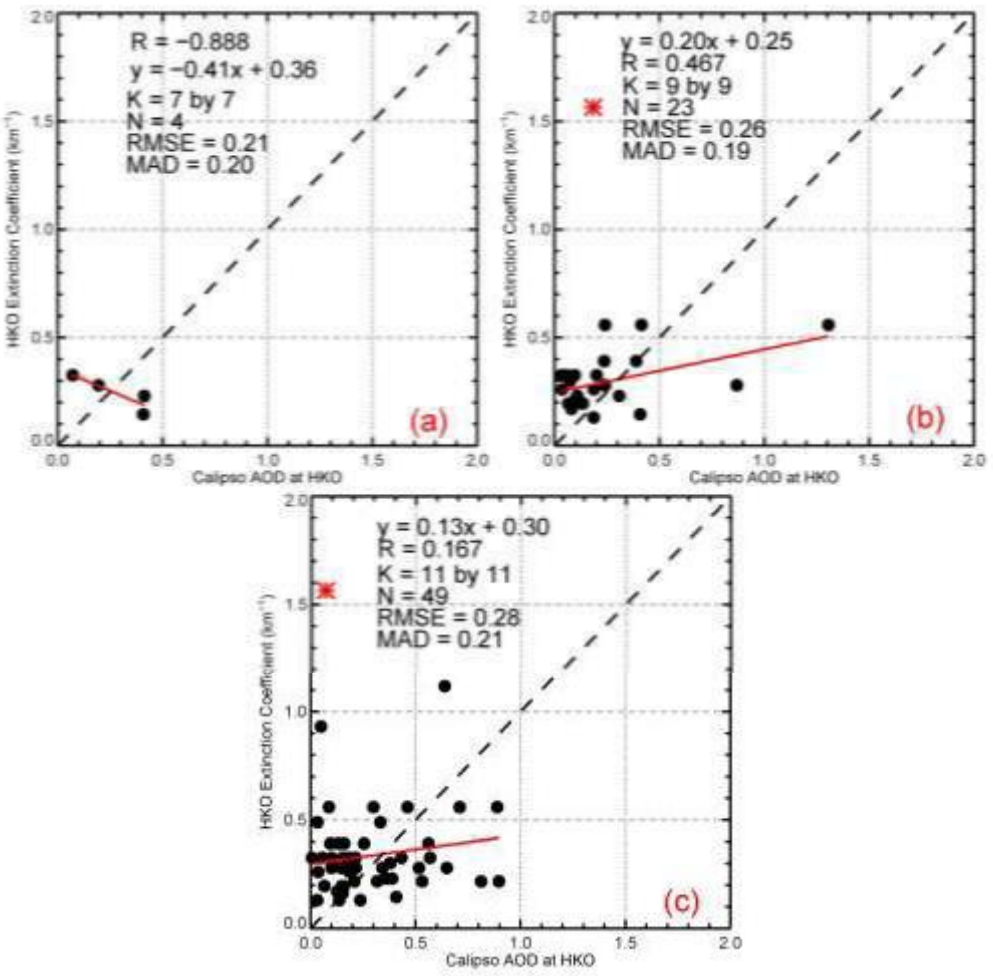

Figure 3.4. Correlation of Extinction Coefficient at HKO with CALIPSO AOD (5 km product at 532 nm) for kernel window of (a) 7 by 7 (b) 9 x9 and (c) 11 by 11. There was no valid AOD retrieval for kernel windows of 1 by 1 to 5 by 5. Dashed line represents a 1:1 line whereas solid line is the resultant regression line. * - potential outlier in the data.

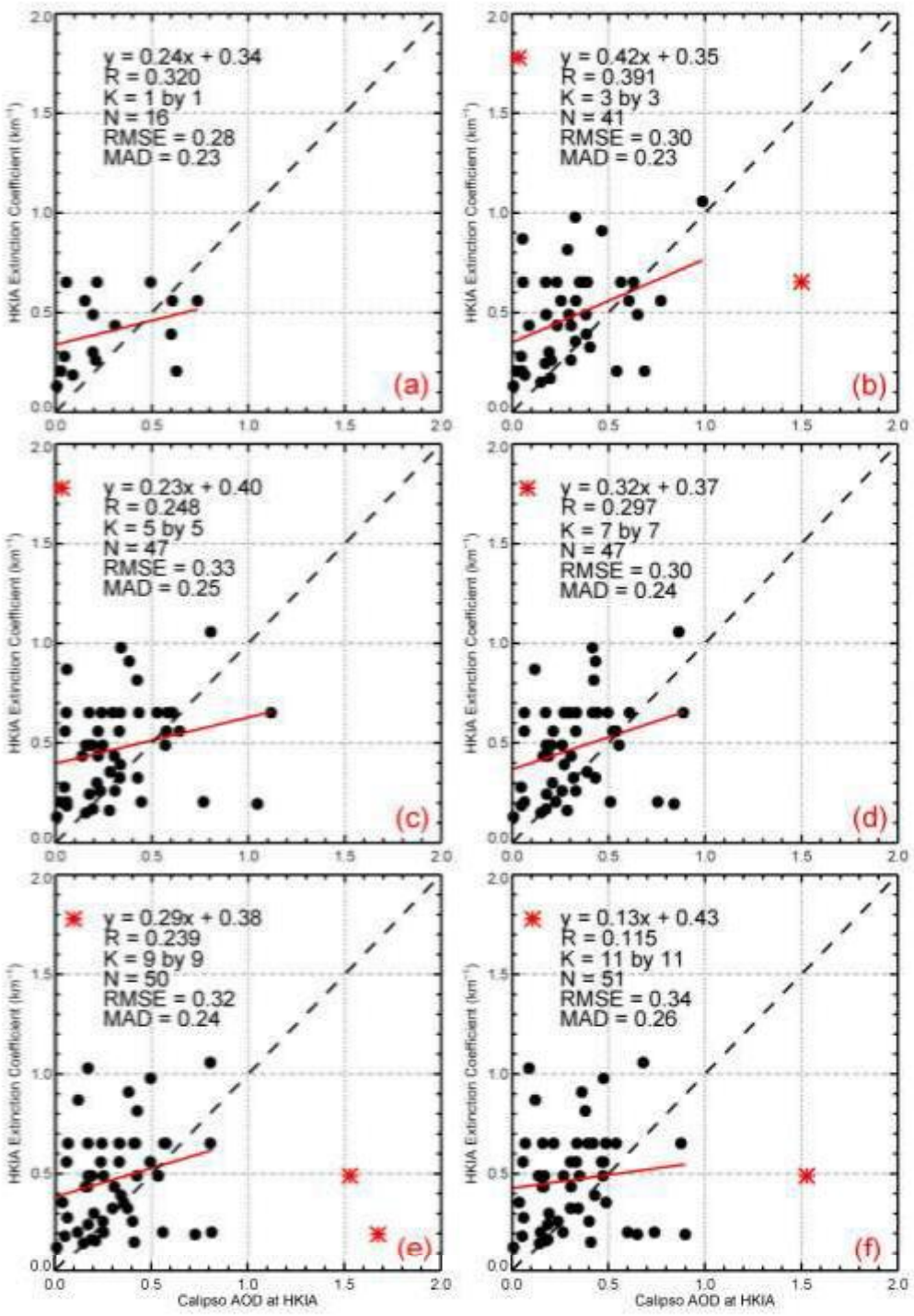

Figure 3.5. Correlation of Extinction Coefficient at HKIA with CALIPSO AOD (5 km product at 532 nm) for kernel window of (a) 1 by 1 (b) 3 by 3 (d) 5 by 5. (e) 7 by 7 (f) 9 x9 and (g) 11 by 11. Dashed line represents a 1:1 line whereas solid line is the resultant regression line. * - potential outlier in data.

Other researchers observed that low correlations from CALIPSO may be due to its limitations in collecting data from near ground level during the day because of lower signal to noise ratio in the presence of high solar background (Hoff and Christopher, 2009). This means that the backscatter signal near ground can become

contaminated by the solar zenith radiance (solar background signals). These backscatter signals combine to give a backscatter profile using a daytime calibration constant that is also contaminated due to the above-mentioned reason. Therefore, a night time calibration constant is used by the CALIPSO team to derive the daytime profiles to overcome this problem. Even with this amendment, CALIPSO is reported to underestimate AOD by a factor of two compared with AERONET AOD (Kacenelenbogen et al., 2011).

MISR AOD and B_{ext}

The correlations between MISR AOD product and B_{ext} at HKIA are R = 0.601 and 0.509 (Fig 3.6 a-b), whereas the observed correlations for HKO are R = 0.260 and 0.631 for kernel windows of 1 by 1 and 3 by 3, respectively (Fig 3.7 a-b). This correlation is reported after excluding the potential outliers (data shown with *) due to exceptionally high AOD representing extreme cases for the MISR observations. Outliers are detected only for MISR observation at HKIA only might be due to presence of mix pixel. Lower MADs and RMSEs are obtained from HKO site than for HKIA.

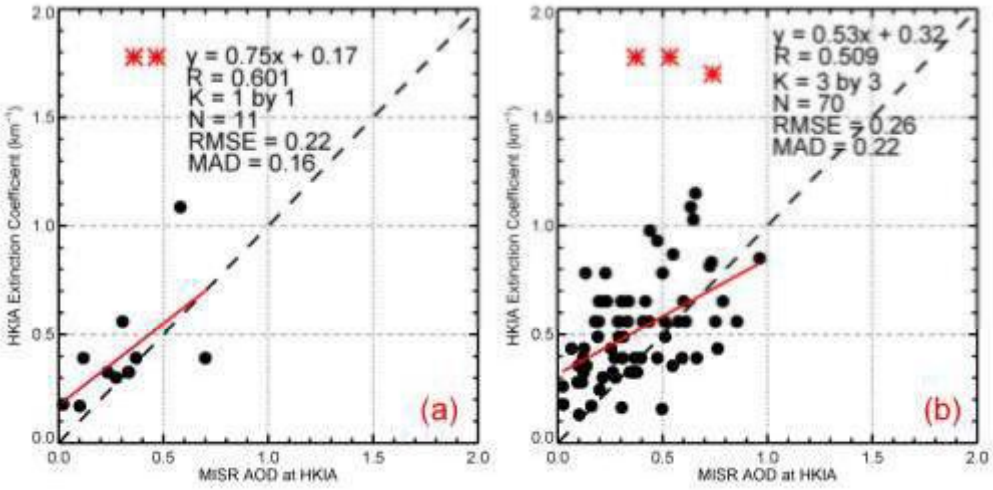

Figure 3.6. Correlation of Extinction Coefficient at HKIA with MISR AOD (17km product at 558 nm) for kernel window of (a) 1 by 1 and (b) 3 x3. Dashed line represents a 1:1 line whereas solid line is the resultant regression line. * - potential outlier in the data.

The higher correlations observed over urban (HKO) and coastal (HKIA) areas are in line with the findings reported by Liu *et al.* (2010) and Jiang *et al.* (2007) in China. MISR AOD showed a stronger correlation with B_{ext} than OMI and CALIPSO, which may be because a large number of aerosol models, incorporating aerosol mixtures from different aerosol parameters including shape, size and mass are

considered in the MISR AOD retrieval algorithm (Martonchik *et al*., 1998; Kahn *et al*., 2001), thus the AOD product is more accurate.

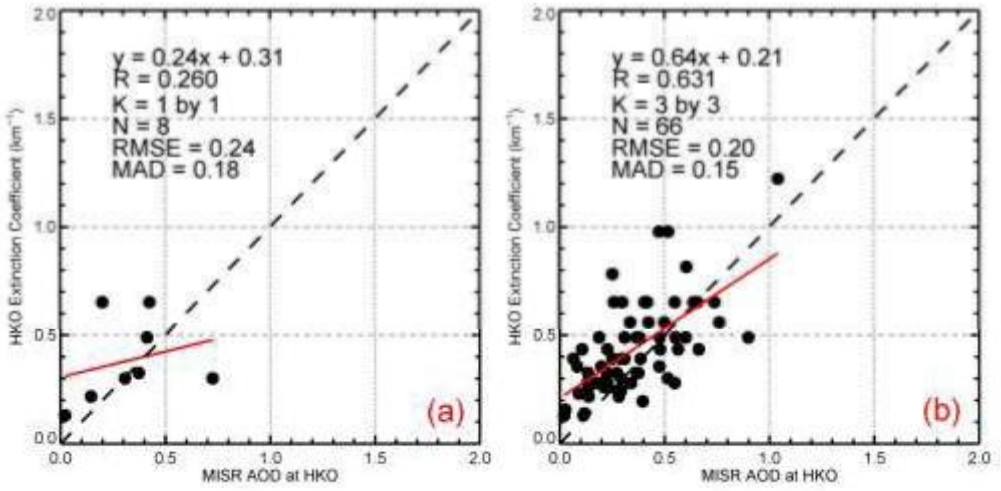

Figure 3.7. Correlation of Extinction Coefficient at HKO with MISR AOD (17km product at 558 nm) for kernel window of (a) 1 by 1 and (b) 3 x3. Dashed line represents a 1:1 line whereas solid line is the resultant regression line.

MODIS AOD and B_{ext}

The MODIS AOD is better correlated with B_{ext} at HKO than at HKIA (Fig 3.8). The correlations between MODIS AOD and B_{ext} at HKO are R = 0.379, 0.510 and 0.529 (Fig 3.8 d-f), whereas the observed correlations at HKIA are R = 0.112, 0.350 and 0.256 (Fig 3.8 a-c) for kernel windows (K) of 1 by 1, 3 by 3 and 5 by 5 respectively. Similar to MISR, some outliers are also detected at HKIA for MODIS observation and hence are excluded from calculation of correlation due to probable presence of mix pixel.

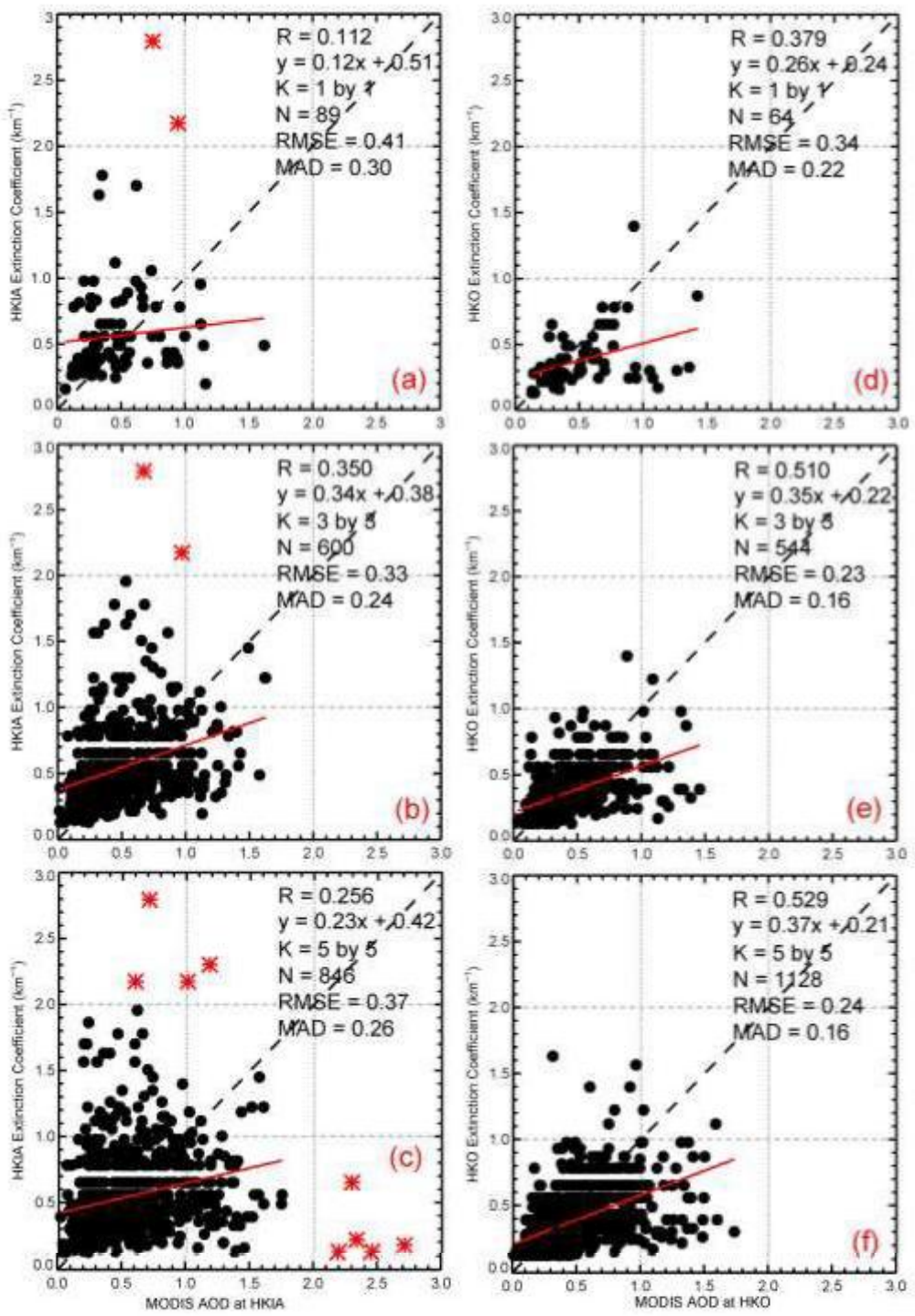

Figure 3.8. Correlation of Extinction Coefficient with MODIS AOD (10 km product at 550 nm) for HKIA (left) and HKO (right) for kernel window of 1 by 1 (top row), 3 by 3 (middle row) and 5 by 5 (bottom row). Dashed line represents a 1:1 line whereas solid line is the resultant regression line. * - potential outlier in the data.

3.4.2 Evaluation of sensors

Among the different sensors evaluated, there are great differences in the R, RMSE and MAD for both coastal (HKIA) and non-coastal (HKO) areas (Fig 3.9). The difference in R, RMSE and MAD may be due to the satellite sensor measuring columnar value of AOD whereas visibility refers to the value of light extinction along a horizontal path usually at ground level. Fig 3.9 is a comparison between the values of R, RMSE and MAD with changing spatial resolution for MODIS, MISR, OMI and CALIPSO. The highest correlation at HKIA is for MISR AOD for kernel window of 1 by 1 (R = 0.60) followed by MISR AOD for kernel windows of 3 by 3 (R = 0.51) and Calipso for kernel window of 3 by 3 (R = 0.39) (Fig 3.9 top). However, the highest correlation at HKO is for MISR AOD for kernel window of 3 by 3 (R = 0.63) followed by MODIS AOD with kernel windows of 5 by 5 (R = 0.53) and 3 by 3 (R = 0.51) respectively (Fig 3.9 top). Hence, MISR AOD has the highest correlation with the surface level extinction of coefficient followed by MODIS. Similarly, MISR has lower RMSE and MAD at both HKO and HKIA than other sensors.

Although the correlation, RMSE and MAD at both HKO and HKIA for B_{ext} and MISR AOD are slightly higher than MODIS, the high temporal and spatial resolution of MODIS along with its comparable RMSE and MAD to MISR, makes it a better potential sensor for operational estimation of surface visibility at Hong Kong. Therefore, further analyses are done using MODIS AOD products for kernel windows of 5 by 5.

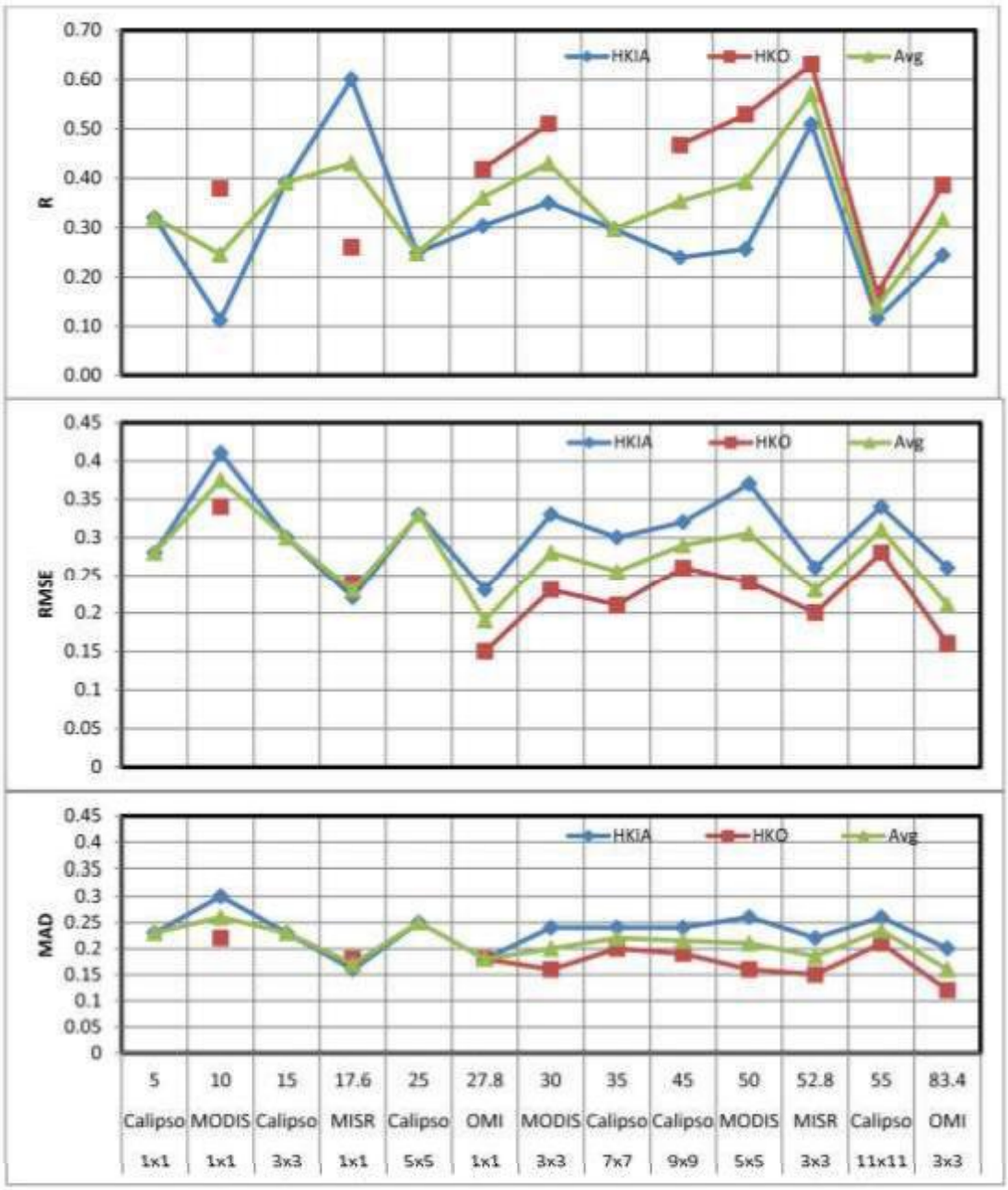

Figure 3.9. Variations in R (top), RMSE (middle) and MAD (bottom) at different spatial resolutions of MISR, MODIS, OMI and CALIPSO for HKIA, HKO and their Average. Spatial resolution (km), sensors name and size of kernel window is labelled in first, second and third x-axis respectively. The scales of R, RMSE and MAD are on the y-axis. Negative correlation values for CALIPSO AOD are not shown.

3.4.3 Derivation of surface visibility range from AOD

Simple linear regression

MODIS AOD data for kernel window of 5 by 5 and VR at HKO were divided into a training set (from years 2002 to 2006 and 2008) and validation set (from years 2007 and 2009), to estimate and validate MODIS B_{ext}. Similar to Fig 3.8, the training data set also showed significant correlation between MODIS AOD and B_{ext} at HKO (Eq 3.2; Fig 3.10a).

$$B_{ext} = 0.36\ (\text{MODIS AOD}) + 0.22 \qquad (3.2)$$

Consequently, Eq 3.2 was designated Model-0 (M1) and was tested against the validation data set (Fig 3.10b). The result shows a significant agreement between simulated and observed extinction coefficients suggested by a slope close to 1 and decreased RMSE and MAD. However, most of the data points in validation fell outside the 95 % confidence interval, depicting a weak estimation power for M1. Therefore, it was thought that the estimation of B_{ext} might improve further by adding climatic data in a multiple linear regression model.

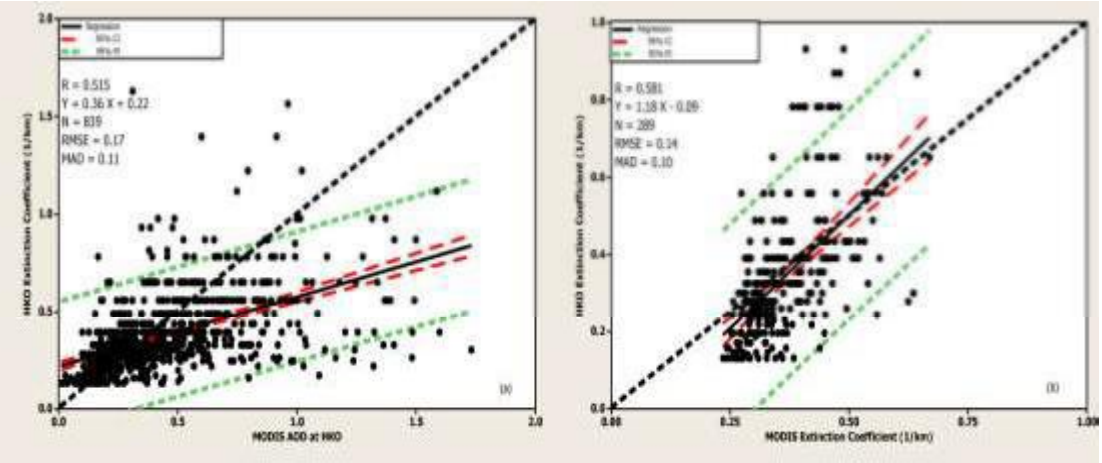

Figure 3.10. Correlation of Extinction Coefficient with MODIS AOD (10 km product at 550 nm) using Model-0 for HKO (a) linear regression of training data for years 2002 to 2006 and 2008 (b) estimated MODIS extinction coefficient using MODIS AOD from years 2007 and 2009. Black dashed line represents a 1:1 line whereas black solid line is the resultant regression line.

Time series analysis

By and large, a direct relationship of visibility with P, T, VT, Q, RH and AOD was observed with VR (Fig. 3.11). The values of P, T, VT, Q, RH and AOD were smoothed and standardised between -1 to +1 to analyse their relationship. The relationships between P, T, RH, VT, AOD and Q were able to explain the variations in visibility in terms of subsidence and uplift of the aerosols. The relationship is

rather seasonal with highest visibility in the summer and lowest in the winter. Overall, VR is noted to increase with decreasing P, RH and AOD. Low pressure generally makes the atmosphere turbulent, shortening the aerosol's residence time, whereas low RH decreases the aerosol's scattering efficiencies by inhibiting the increase in aerosol size. However, VR is noted to increase with increasing T, VT and Q. Low temperature indicates the prevalence of the winter continental northeast monsoon bringing regional anthropogenic aerosols to Hong Kong and reducing the VR, whereas high temperature is associated with summer and early autumn bringing clean and fresh maritime winds from the southwest (Mui et al., 2009). It is also noted that the number of hours with reduced visibility (visibility less than 8 km) in winter and summer are associated with the "-VT" and "+VT". A total 78% of the reduced visibility hours during the study period are associated with "-VT" due to advection of aerosols from the north and northeast. It is also noted that VR increases with increasing Q due to increased rate of mixing. A high value of Q indicates a turbulent atmosphere increasing the vertical and horizontal aerosol dispersion, whereas decrease in Q is associated with a trough due to increase in air density causing subsidence of aerosols. Situations with low value of Q are commonly associated with cold season and/or cold air mass, whereas high value of Q suggests warmer weather conditions. Hence, Q can explain the effect of T, P and RH on VR.

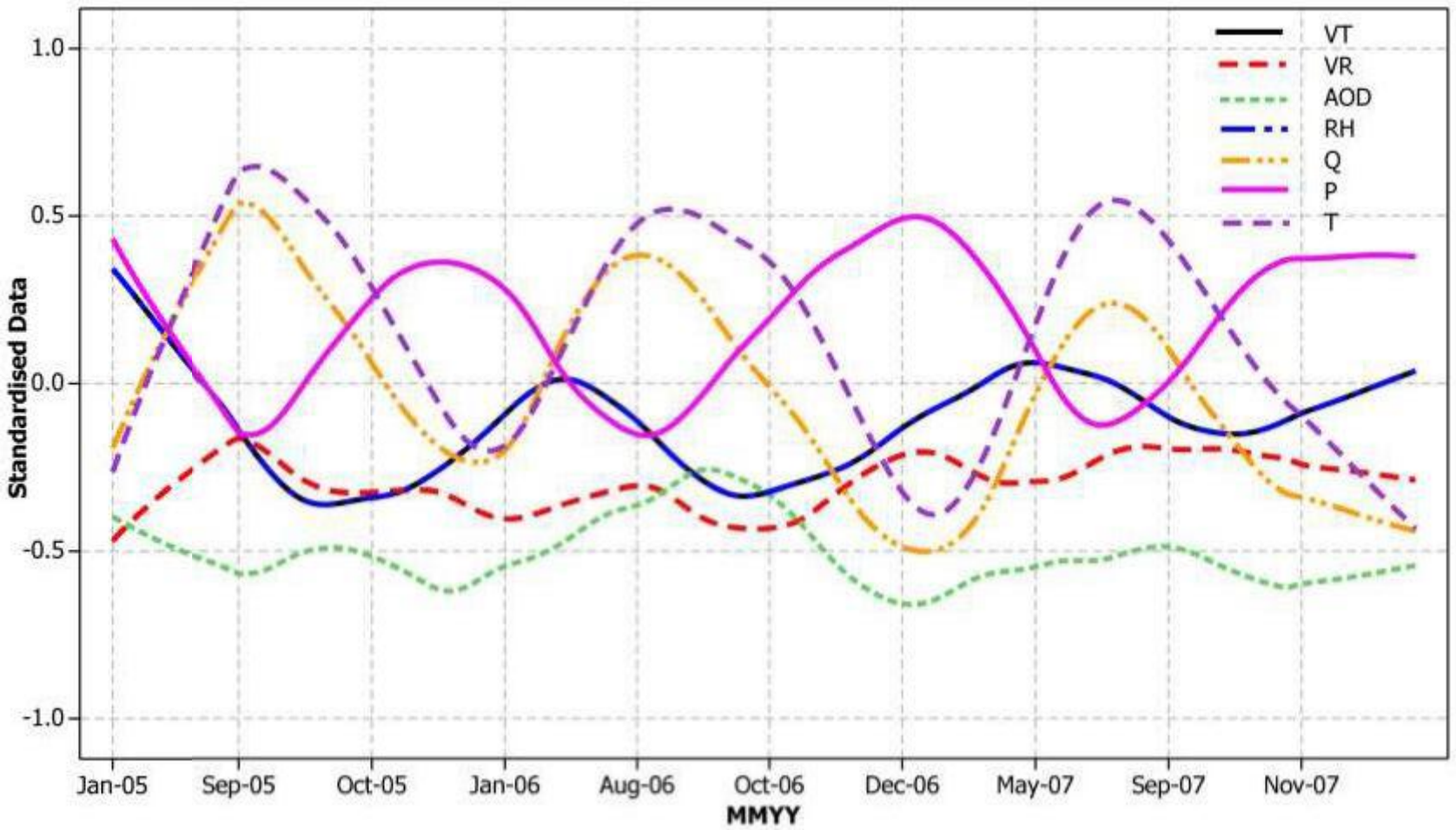

Figure 3.11. Time series of smoothed and standardised VR, AOD, RH, VT, Q, P and T
Note: VT and RH are overlapping throughout the study period

Multiple linear regression

Climatic data from HKO for years 2005-2008 were divided into a training data set (years 2005-2007) and a validation data set (2008) to explore the effects of climatic parameters on VR or B_{ext}. Correlation analysis was used to explore the relationship between B_{ext}, VR and climatic parameters. It is often instructive to apply some transformations to data before regression analysis if data do not follow normal distribution (as discussed in the Methodology). Therefore, transformations (inverse, square, square root and natural log) were applied to VR, B_{ext} and climatic data to obtain a normal distribution. This resulted in a set of ten independent and fifty five dependant variables. The correlation matrix and AD statistics for these variables was analysed to select potential parameters for constructing a regression model using climatic data and MODIS AOD at HKO. Part of the correlation matrix containing potential parameters is shown in Table 3.1, and the respective p-values are italicized in next line to each variable.

The correlations improved due to some of the transformations. For example, the correlation between B_{ext} and AOD improved from 0.78 to 0.79 when B_{ext} and AOD were transformed into $\ln(B_{ext})$ and ln(AOD). Similarly the correlation between VR and AOD improved from -0.74 to -0.80 when VR and AOD were transformed into $(VR)^{1/2}$ and ln(AOD). The parameters with highest correlation and lowest p-value from each column were selected for constructing a multiple linear regression model, followed by stepwise and best subset regression models as described in the methodology. However, the regression model involving the bold variables in Tab. (3.1) performed far better than the rest and therefore, only regression models involving the bold variables will be discussed.

As a first attempt, all the selected variables (bold variables in Tab. 3.1) were subjected to regression analysis, as the Full model gave a poor fit. Some of the independent variables with significant correlation (Table 3.1) turned out to be insignificant in the full model (Table 3.2). The P value for UT, VT, U, V, $(T)^2$ and $(P)^2$ was not significant in the Full model with largest VIF of 68.52. It is to be noted that a VIF close to zero or one shows no, or minimum colinearity among the regression variables. Multicolinearity for the Full model was significant and hence a regression variable, $(T)^2$ having highest p-value and VIF was dropped from the model and the regression was repeated for the remaining variables. The new model is

designated as Model A. This time $(P)^2$ was omitted as previously explained, and the process was repeated until Model E was achieved. The regression statistics of each model are shown in Table 3.2.

Table 3.1. Correlation matrix for independent and dependent variables in their transformed and untransformed forms.

	VR	$(VR)^{-1}$	$(VR)^2$	$\mathbf{(VR)^{1/2}}$	ln(VR)	B_{ext}	$\ln(B_{ext})$	$(B_{ext})^{1/2}$	$(B_{ext})^{-1}$	$(B_{ext})^2$
AOD	-0.74	0.78	-0.66	-0.76	-0.78	0.78	0.78	0.78	-0.74	0.74
	0.00	*0.00*	*0.00*	*0.00*	*0.00*	*0.00*	*0.00*	*0.00*	*0.00*	*0.00*
T	0.12	-0.08	0.13	0.11	0.10	-0.08	-0.10	-0.09	0.12	-0.07
	0.09	*0.23*	*0.06*	*0.12*	*0.15*	*0.23*	*0.15*	*0.19*	*0.09*	*0.31*
P	-0.11	0.05	-0.13	-0.09	-0.08	0.05	0.08	0.07	-0.11	0.03
	0.13	*0.46*	*0.07*	*0.18*	*0.26*	*0.46*	*0.26*	*0.35*	*0.13*	*0.66*
RH	-0.08	0.16	-0.04	-0.10	-0.13	0.16	0.13	0.15	-0.08	0.19
	0.25	*0.02*	*0.57*	*0.14*	*0.07*	*0.02*	*0.07*	*0.04*	*0.25*	*0.01*
MLH	0.01	-0.07	-0.02	0.03	0.04	-0.07	-0.04	-0.05	0.01	-0.08
	0.88	*0.35*	*0.81*	*0.72*	*0.57*	*0.35*	*0.57*	*0.44*	*0.88*	*0.26*
UT	-0.15	0.18	-0.13	**-0.16**	-0.17	0.18	0.17	0.18	-0.15	0.18
	0.03	*0.01*	*0.06*	***0.02***	*0.01*	*0.01*	*0.02*	*0.01*	*0.03*	*0.01*
VT	0.21	-0.18	0.21	**0.21**	0.20	-0.18	-0.20	-0.19	0.22	-0.14
	0.00	*0.01*	*0.00*	***0.00***	*0.00*	*0.01*	*0.00*	*0.01*	*0.00*	*0.04*
Q	0.11	-0.02	0.15	0.09	0.07	-0.03	-0.07	-0.05	0.11	0.01
	0.11	*0.73*	*0.03*	*0.20*	*0.33*	*0.73*	*0.33*	*0.52*	*0.11*	*0.91*
U	-0.17	0.20	-0.14	**-0.18**	-0.19	0.20	0.19	0.19	-0.17	0.20
	0.02	*0.00*	*0.05*	***0.01***	*0.01*	*0.00*	*0.01*	*0.01*	*0.02*	*0.00*
V	0.18	-0.15	0.18	**0.18**	0.17	-0.15	-0.17	-0.16	0.18	-0.13
	0.01	*0.03*	*0.01*	***0.01***	*0.01*	*0.03*	*0.01*	*0.02*	*0.01*	*0.07*
WD	0.02	0.03	0.05	0.01	0.00	0.03	0.00	0.02	0.02	0.05
	0.73	*0.66*	*0.49*	*0.88*	*0.96*	*0.66*	*0.96*	*0.80*	*0.73*	*0.44*
WS	0.00	-0.06	-0.01	0.02	0.03	-0.06	-0.03	-0.05	0.00	-0.10
	0.95	*0.36*	*0.87*	*0.82*	*0.67*	*0.36*	*0.67*	*0.51*	*0.96*	*0.15*
ln(AOD)	-0.79	0.74	-0.76	**-0.80**	-0.79	0.74	0.79	0.77	-0.79	0.67
	0.00	*0.00*	*0.00*	***0.00***	*0.00*	*0.00*	*0.00*	*0.00*	*0.00*	*0.00*
ln(RH)	-0.09	0.16	-0.05	**-0.11**	-0.13	0.16	0.13	0.15	-0.09	0.19
	0.21	*0.02*	*0.50*	***0.12***	*0.06*	*0.02*	*0.06*	*0.03*	*0.21*	*0.01*
$\mathbf{(T)^2}$	0.14	-0.09	0.15	**0.13**	0.11	-0.09	-0.11	-0.10	0.14	-0.08
	0.05	*0.18*	*0.03*	***0.07***	*0.10*	*0.18*	*0.10*	*0.14*	*0.05*	*0.27*
$\mathbf{(P)^2}$	-0.11	0.05	-0.13	**-0.09**	-0.08	0.05	0.08	0.07	-0.11	0.03
	0.13	*0.46*	*0.07*	***0.18***	*0.26*	*0.46*	*0.26*	*0.35*	*0.13*	*0.67*
$\mathbf{(Q)^2}$	0.16	-0.06	0.20	**0.14**	0.11	-0.06	-0.11	-0.09	0.16	-0.02
	0.02	*0.39*	*0.00*	***0.05***	*0.11*	*0.39*	*0.11*	*0.22*	*0.02*	*0.79*

Note: P-value of correlation is italicized in next line to each variable and variables selected for construction of regression model are shown in bold letters.

Table 3.2. Multiple linear regression models for predicting $(VR)^2$. The final model selected for estimating $(VR)^2$ is highlighted.

Model	Const	UT	VT	U	V	ln(AOD)	ln(RH)	$(T)^2$	$(P)^2$	$(Q)^2$	S	R^2	R^2_{adj}	PRESS	R^2_{pred}	SS	F	DWS	Largest VIF	CP
Full	ns	ns	ns	ns	ns	****	****	ns	ns	***	0.34	72.38	70.97	24.33	69.50	57.74	51.37	1.69	68.52	x
A	ns	ns	ns	*	ns	****	****	x	ns	****	0.33	72.34	71.07	24.09	69.79	57.71	57.24	1.69	65.43	x
B	****	*	ns	*	ns	****	****	x	x	****	0.33	72.31	71.20	23.84	70.11	57.69	64.65	1.68	66.73	x
C	****	**	***	**		****	****	x	x	****	0.33	71.79	70.94	23.91	70.03	57.26	84.82	1.66	35.28	x
D	****	x	***	ns		****	****	x	x	****	0.33	71.21	70.49	24.20	69.64	56.81	99.40	1.66	1.62	x
E	****	**x**	****	**x**		****	****	**x**	**x**	****	**0.33**	**71.10**	**70.53**	**24.07**	**69.83**	**56.71**	**124.20**	**1.67**	**1.62**	**x**
Stepwise	****	x	****	x		****	****	x	x	****	0.33	71.10	70.53	24.01	69.83	x	x	x	x	5
Best Subset	****	x	****	x		****	****	x	x	****	0.33	71.10	70.53	x	x	x	x	x	x	5

Note: Significance levels are as follows: **** - $p < 0.001$; *** - $p < 0.01$; ** - $p < 0.05$; * - $p < 0.1$; ns – not significant.

X – N/A and variable excluded from regression; Const – Intercept of regression model. "Full" refers to the multiple linear regression models involving all parameter

All variables of Model E were significant with P-value of zero and VIF between 1.0 and 1.62. Moreover the prediction error (PRESS) for Model E was also the smallest, and F statistics the highest among all models. Therefore, Model E was further subjected to stepwise and best subset regression analyses to further examine the principal factors affecting VR as explained in methodology. The regression statistics remained the same as Model E suggesting Model E as optimal regression model for estimating VR. Therefore, Model E was designated henceforth as Model 2 (M2; Eq 3.3; Fig 3.11).

$$\sqrt{V} = 6.43 + 0.00079\,VT - 1.96\,\ln(AOD) - 2.30\,\ln(RH) + 0.017\,Q^2 \qquad (3.3)$$

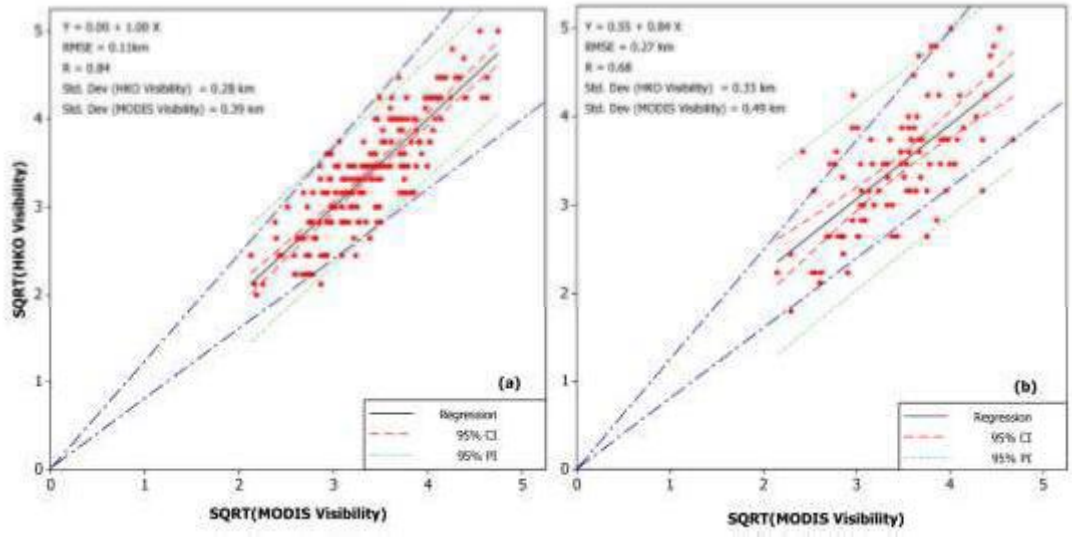

Figure 3.12. Correlation between Square root of MODIS visibility at HKO (SQRT(MODIS Visibility)) and Square root of ground visibility at HKO (SQRT(HKO Visibility)) using Model 2 (a) linear multiple regression of training data for years 2005 to 2007 (b) simulated MODIS visibility using validation of data (MODIS AOD and Climatic data) from years 2008. Blue Dotted Dashed lines show the upper and lower limit of ± 20 % of the ground visibility at HKO whereas black solid line is the resultant regression line.

With the addition of climatic parameters having significant relationship with VR Model 2 (Eq. 3.3) actually performed better than Model 1, having significantly high values of R = 84 %, R^2 = 71.1%, predicted-R^2 = 69.8% and RMSE = 0.11 km (Fig. 3.12a). Model 2 was also able to simulate the real time VR at HKO with high accuracy demonstrated by a low RMSE of 0.27 km (Fig. 3.12b). The selected model can explain the physical forces behind the influence of regression parameters on visibility in terms of subsequent changes in air density, turbulence and advection. Respective signs (+ and -) for the coefficients of regression model M2 suggest that a unit increase in any one or combination of "T", "RH", "VT", "Q^2" also increases the visibility whereas a unit increase in ln(AOD) or P decreases the visibility. This is

also in agreement with the physical forces explained in section "Time series analysis". Although ln(RH) has the highest coefficient, M2 is highly sensitive to changes in ln(AOD) with F-value of 401.00 followed by Q^2, ln(RH) and VT with F-values of 41.10, 28.24 and 10.567 respectively. This may be due to the fact that Q depends on P, T and RH and therefore acts as a confound variable whose interaction with VR can also explain the combined effect of P, T and RH on VR. The performance of M2 also suggests that VT is sufficient to explain the effects of WS and WD on dispersion of aerosols and hence on VR. The presence of VT, RH and Q in a model can also increase the multicolinearity but DWS values close to one (Tab. 3.2), suggest no multicolinearity in M2. This explains why M2 was able to accurately estimate VR at HKO as shown by the summary statistics of real-time and simulated VR at HKO for the year 2008 (Tab. 3.3).

Table 3.3. Summary statistics for the real-time (HKO VR) and simulated (MODIS VR) VR at HKO for the year 2008.

	HKO VR (km)	MODIS VR (km)
Total observations	95	95
Mean	12.25	12.10
Standard Error	0.51	0.40
Mean	4.92	3.94
Median	12.00	12.18
Maximum	25.00	21.93
Minimum	3.20	4.64
Standard Deviation	0.33	0.49
First Quartile	9.00	9.08
Third Quartile	15.00	14.87

Eighty one percent of the simulated VR using M2 was found to be also well within ±20% of the HKO VR (Fig. 3.13) which is consistent with Annex 3 of the International Civil Aviation Organization (ICAO) that suggests that an uncertainty of ±20 % in estimated VR is acceptable when actual VR is above 1.5 km. The results of this study are far better than previous studies on the same topic for Hong Kong and the Chinese mainland (Tab. 3.4).

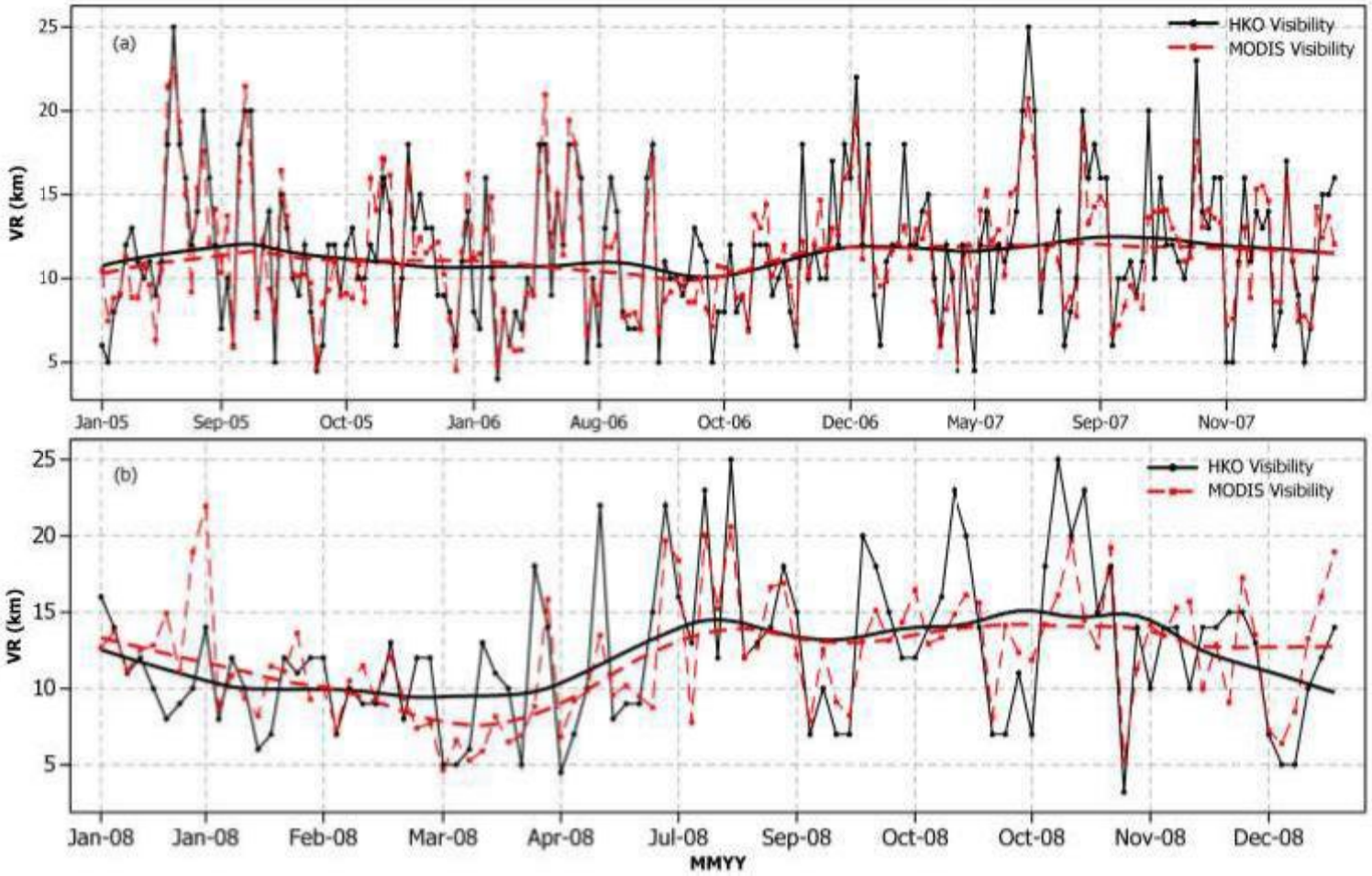

Figure 3.13. Time series of the real-time and simulated VR at HKO using Model 2 for (a) Training data set of 2005-2007 and (b) Validation data set of 2008. Black solid line and Dotted red line show the smoothed trend line for HKO and MODIS visibility respectively.

All these previous studies have used expensive and time consuming data of mass concentrations of pollutants, along with available meteorological data. In addition these studies used averaged daily data which cannot serve real-time operational purposes, whereas this study used satellite derived AOD along with hourly meteorological data.

Table 3.4 Results of the previous studies on the same topic for Hong Kong and China mainland.

	Dependant Variable	Independent Variables	R^2
Lai et al., (2001)	B_{ext}	NO_2, RSP, RH	0.76
Ke et al., (2013)	VR	RH, WS, P, T, Prec.	0.39
Mui et al., (2009)	VR	T, API	0.77
Mang et al., (2011)	VR	PM_{10}, NO_2, RH	0.80
Wan et al., (2011)	VR	SO_2, NO_2, PM_{10}	0.51

Note: RSP – Respirable Suspended Particles; Prec. – Precipitation; API – Air Pollution Index

3.5 CONCLUSION

The potential of MODIS, MISR, OMI and CALIPSO AOD products was evaluated for remote sensing of visibility at two stations for monitoring visibility in Hong Kong. The highest correlation at HKIA is for MISR AOD for kernel window of 1 by 1 (R = 0.60) followed by MISR AOD for kernel windows of 3 by 3 (R = 0.51) and Calipso for kernel window of 3 by 3 (R = 0.39) and the highest correlation at HKO is for MISR AOD for kernel window of 3 by 3 (R = 0.63) followed by MODIS AOD with kernel windows of 5 by 5 (R = 0.53) and 3 by 3 (R = 0.51) respectively. Although the correlation, RMSE and MAD for MISR AOD and B_{ext} is the highest at HKO and HKIA than MODIS AOD with a kernel window of 5 by 5 but due to higher temporal and spatial resolution of MODIS than MISR and comparable RMSE and MAD MODIA AOD was used in regression modelling to simulate VR. A simple linear regression model (M1) with only MODIS AOD was able to explain 58.1 % of variance in B_{ext} whereas a multiple linear Regression model (M2) combining MODIS AOD with climatic data explained 84.0 % of the variance in VR with a high accuracy, i.e. RMSE of 0.27 km. The results of this study suggest that Q alone can explain the combined effect of P, T and RH on VR. The Results also suggest that VT alone is sufficient to explain the effects of WS and WD on dispersion of aerosols and hence on VR.

Chapter 4: Estimation of Surface Visibility using Operational Products of LIDAR, AERONET and MODIS

4.1 INTRODUCTION

From the discussion in section 1.4, it is evident that recent efforts to estimate surface visibility have not been successful. This is because passive aerosol remote sensors do not resolve aerosol distributions vertically with reliably high resolution (in the order of 1-100 m). Although spaceborne LIDAR instruments, of which the NASA Cloud Aerosol Lidar with Orthogonal Polarization instrument (CALIOP; Winker et al., 2010) is currently the only operational sensor, do offer this measurement, CALIOP's limited sensor swath width and orbital track make these data difficult to apply practically in a routine/daily operational setting relative to other passive sensors. Instead, we consider the opportunity to combine the benefits of regional passive satellite aerosol observations with surface-based LIDAR profiling to better constrain local VR estimates.

Therefore, in this study, the vertical profile of aerosol particle scattering and distribution is estimated from a single-channel elastic-scattering LIDAR at Hong Kong Polytechnic University (HKPU at 22.30° N, 114.197° E). Six algorithms are then described and tested, where regional VR is estimated using coincident ground-based LIDAR, sun photometer and AOD datasets of the Moderate Resolution Infrared Spectroradiometer (MODIS; Ackerman et al., 1998). Using the 355 nm extinction coefficient profile derived from the LIDAR measurements at one location, MODIS AOD data are scaled down to the surface to generate a regional composite depiction of surface VR. We assume the vertical distribution of aerosol particle mass concentration over the Hong Kong study domain is constant relative to its horizontal distribution. We evaluate this assumption by comparing our results with independent VR measurements at locations where LIDAR data do not exist. By applying this technique, it is possible to optimize information from a relatively limited number of

available ground visibilities to estimate VR across the entire area from passive remote sensing datasets, which provide the necessary spatial coverage.

4.2 DATA USED

This study considers hourly-averaged datasets collected with a 355 nm elastic scattering LIDAR instrument, a multi-channel sun photometer, deployed as part of NASA's federated Aerosol Robotic Network (AERONET; Holben et al., 1998), and a Vaisala visibility meter, all installed on the urban campus of HKPU. The data are evaluated from April 2011, beginning with the availability of routine LIDAR observations at HKPU, through October 2011, corresponding to the availability of quality assured Level 2 AERONET products that are cloud screened as well as pre and post-field calibrated. However, in order to sample a larger number of MODIS data for validating our method, we extend the study period beyond October 2011 to September 2012 using only Level 1.5 AERONET data, which are cloud screened but without a final post-operation calibration applied. Overall, though, only six data points of these level 1.5 data were available for use for our validation study.

4.2.1 MODIS

The AOD from MOD04 and MYD04 are extracted for the HKPU (τ_{MU}) and HKIA (τ_{MA}) sites using spatial windows of 5x5 pixels, which are then compared to hourly average values of data from AERONET, the LIDAR and visibility meter. These temporal and spatial windows were designed in accordance with Anderson et al. (2003), who report a significant correlation ($r > 0.90$) between AOD measurements from ground, air and space using a temporal window of less than 3 hours and a spatial window of less than 60 km.

4.2.2 AERONET Data

We used the hourly averaged Level 2.0 and Level 1.5 AOD from the AERONET station at HKPU. We note recent work suggesting that Level 2 AERONET screening algorithms may be limited by optically-thin cirrus clouds, most common in tropical and sub-tropical locales, thus leading to a positive-definite AOD bias of 0.03-0.06 when such clouds go unscreened (Chew et al., 2011). In Singapore, for instance, this can approach 35% of the Level 2 sample. In this study however, we apply the Level 2 archive directly and presume the cloud-screening procedures are

robust. In this study time matched values from ALS and Level 2.0 data from AERONET were also used to avoid potential cloud bias in the ALS sample.

4.2.3 LIDAR Data

The Atmospheric LIDAR System (ALS; Lolli et al., 2011) at HKPU collects data at 15 m and 1 min spatial and temporal resolutions, respectively. The ALS is a single-channel elastic backscatter LIDAR, operated at 355 nm, with an outgoing energy pulse near 16 μJ at 20 Hz. The ALS data used in this study do not account for Rayleigh scattering and gas and particle absorption. Signals are processed for a relative backscattering coefficient (β; $m^{-1}sr^{-1}$), which can be interpreted for significant aerosol particle layers, such as the surface-detached mixed aerosol layer (referred to as Mixing layer-low; ML-Low) and diffuse elevated layers decoupled from the primary surface layer and advecting within the free troposphere (ML-High). Further processing can yield an estimated extinction coefficient (σ_{LS} - m^{-1}), where AOD (τ_{LU}) is either constrained and extinction solved iteratively through an inversion solution to the LIDAR equation (Fernald, 1984; Klett, 1985), or by setting the relationship between extinction and backscatter coefficients constant within an assumed turbid layer and again constraining total transmission to solve extinction bin-by-bin from the top of the layer to the surface.

In this work, the latter technique for solving the extinction is applied using built-in software provided by the ALS manufacturer which includes a predefined set of extinction-to-backscatter ratios. The extinction-to-backscatter ratio can fluctuate depending on the region of interest, particularly in Southeast Asia (Campbell et al., 2013). At Hong Kong, it is found to fluctuate seasonally between 18 sr to 44 sr at 532 nm (He, 2006). This led us to choose an extinction-to-backscatter ratio of 36 sr (e.g., Ackerman et al., 1998), reflecting urban pollution as the primary aerosol type regionally. Note that overlap of the ALS system is achieved at a range approximating 170 m. Thus, in order to estimate near surface VR effectively, we use data as close to the surface as possible and extrapolate downward (described below). Therefore the hourly average extinction coefficient (σ_{LU}) at 355 nm is retrieved from the LIDAR measurements at heights between 75 m and 150 m.

4.2.4 Surface Visibility Data

A Vaisala visibility meter is collocated with the sun photometer and LIDAR at HKPU. This meter uses a forward-scattering method to estimate Visual Range at 875 nm. Intensity of infrared light scattered at 33^{o} is measured and converted to VR. VR readings from this station (V_{HKPU}) are used below to construct model estimates. VR readings from a similar visibility meter deployed at HKIA (V_{HKIA}) are used for validation. Human observations of visibility are also important for such a study but could not be used, as none was available for HKPU.

4.3 STATISTICAL ANALYSES

4.3.1 Descriptive statistics

Histograms depicting hourly averages of the parameters (V_{HKPU}, V_{HKIA}, ML-High, ML-Low, σ_{LU}, τ_{AU} and τ_{LU}) used by the various models for estimating VR are shown in Fig. 4.1. Lognormal distributions are observed in all except for ML-High, V_{HKPU} and V_{HKIA}, which exhibit bimodal distributions. Summary statistics for these hourly averages, including sample size, mean, median, standard deviation and maximum/minimum values are given in Table 4.1.

Table 4.1. Summary statistics for hourly averages of visibility, LIDAR AOD, AERONET AOD, Extinction coefficient and ML heights presenting sample size (N), mean, median, standard deviation (SD) and maximum/minimum (Max/Min).

Parameter	N	Mean	Median	SD*	Max	Min
V_{HKPU} at 875 nm (km)	489	21.77	20.82	10.41	46.17	3.965
V_{HKIA} at 875 nm (km)	492	24.28	25.79	11.39	44.03	4.28
τ_{LU} at 550 nm	183	0.28	0.23	0.24	1.41	0.01
τ_{AU} at 550 nm	492	0.39	0.28	0.30	1.80	0.04
σ_{LU} at 335 nm (km^{-1})	181	0.22	0.19	0.16	0.72	0.008
Z_H (km)	216	1.56	1.55	0.72	2.82	0.36
Z_L (km)	216	0.97	0.76	0.64	2.51	0.23

*Standard Deviation, Z_H = ML-High and Z_L = ML-Low

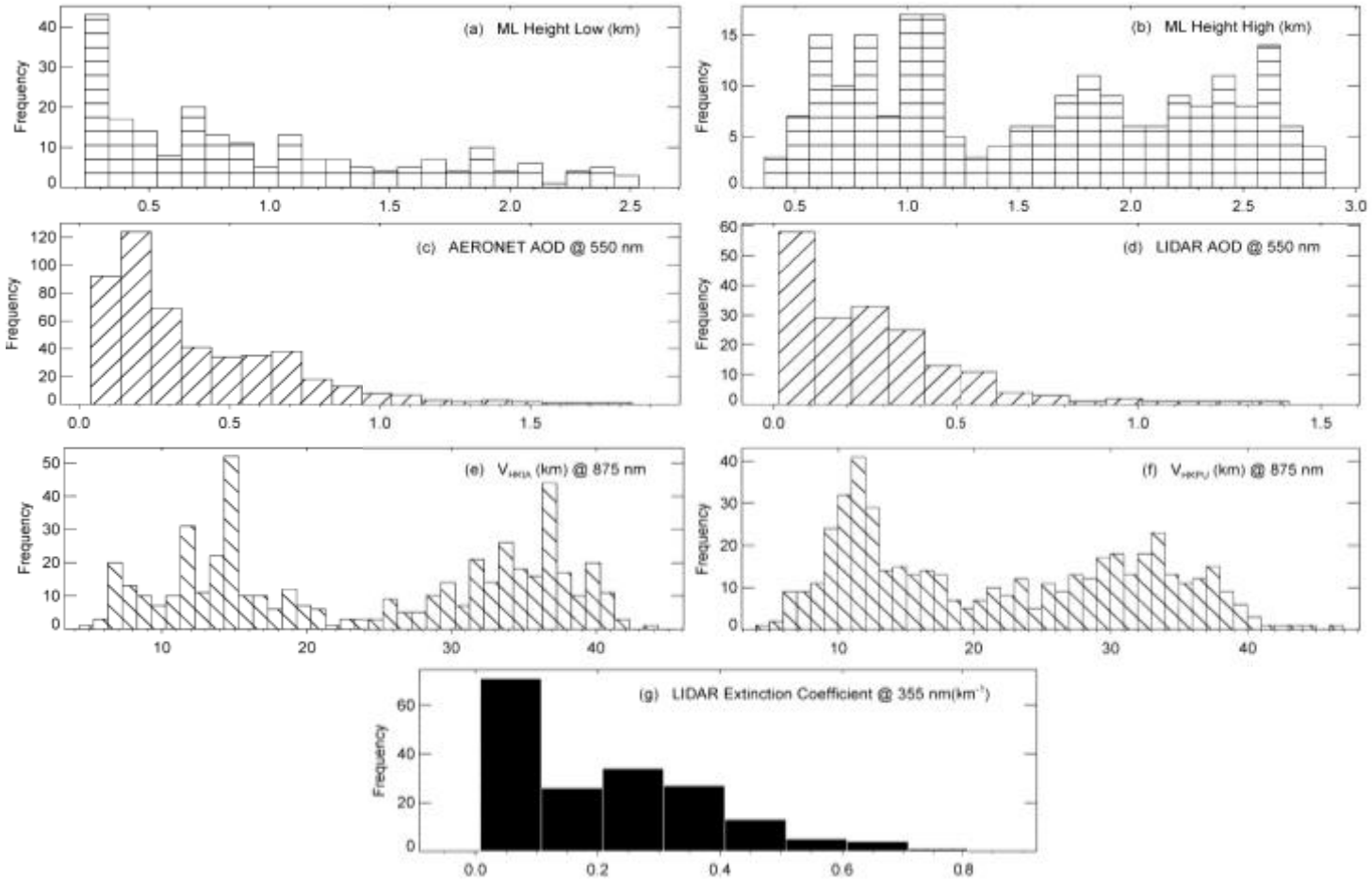

Figure 4.1. Frequency distribution hourly averages of (a) ML-Low, (b) ML-High, (c) AOD from AERONET, (d) AOD from ALS (e) Visibility at HKIA (f) Visibility at HKPU and (g) Extinction coefficient from ALS for height between 75 m – 150 m.

The highest values for ML-High and ML-Low during the study period were 2.82 km and 2.51 km, respectively. The lowest values were 0.36 km and 0.23 km, respectively. On average, the majority of aerosol particles were present within a finite layer near the surface. This is suggested by the observation that ML-High (ML-Low) remained below 1 km 31.01 % (60.01 %) of the time. The average value of σ_{LU} was 0.22 km^{-1}, with maximum (minimum) values of 0.72 km^{-1} (0.16 km^{-1}) that correspond to VR of 5.43 km (24.45 km) according to Koschmieder's equation. Although τ_{LU} and τ_{AU} exhibit log-normal distributions, the lidar-derived AOD, which is based on an assumption of constant extinction-to-backscatter ratio, was low compared with AERONET retrievals. Average values of τ_{LU} and τ_{AU} were 0.28 and 0.39, respectively. These smaller values of τ_{LU} can be reconciled by using Eq. 4.4 to represent V_{HKPU}.

We note that VR between 20 and 30 km was more frequent than VR below 20 km or above 30 km for both HKIA and HKPU. The peak frequency at HKPU was ~11-12, and that at HKIA was ~15 and standard deviation and mean values for V_{HKPU} and V_{HKIA} are significantly different (p-value = 0.00) with values of V_{HKPU} and V_{HKIA} of 21.77 ±10.41 km and 24.28 ±11.39 km, respectively. This supports our assumption of spatial variability of aerosol mass concentrations in Hong Kong.

4.3.2 Correlation analyses

Scatter plots of V_{HKPU} versus σ_{LU}, τ_{LU}, ML-Low, τ_{AU} and V_{HKIA} are shown in Fig. 4.2, and each shows significant correlation (p-values < 0.05), thus indicating the relevance of applying these parameters to estimate VR. Studies involving the light extinction properties of aerosol particles have shown similarly good correlations (R^2 = 0.82 - 0.85) between ML height and AOD when ML height is relatively low (Liu et al., 2009; Zieger et al., 2011) and the atmosphere is relatively stable. As noted by Xue et al (2010), light scattering increases as the height of the ML decreases because a lower ML reduces the volume of the air containing aerosol particles. Thus increasing the aerosol loading per unit volume and hence the scattering of light. This likely explains the positive correlation (R = 0.70) observed for V_{HKPU} with ML-Low. Therefore, ML height can be approximated as a scaling height. A possible inverse relationship for V_{HKPU} and σ_{LU}, τ_{LU} and τ_{AU} occurs since an increase in the aerosol concentration increases the scattering and absorption. This results in increased extinction of light and hence decreases visibility, which has been shown in various

studies over Hong Kong (e.g. Wang et al., 2003; Chan and Yao, 2008; Nichol et al., 2010; Wan et al., 2011). The difference in the number of data points for ML heights, σ_{LU} and τ_{LU} derived from ALS, is due to the use of a constant extinction-to-backscatter ratio. This setting caused some retrievals to fail, which is a likely reflection of its true variance over time. Hence, τ_{LU} and σ_{LU} were not retrieved for every day.

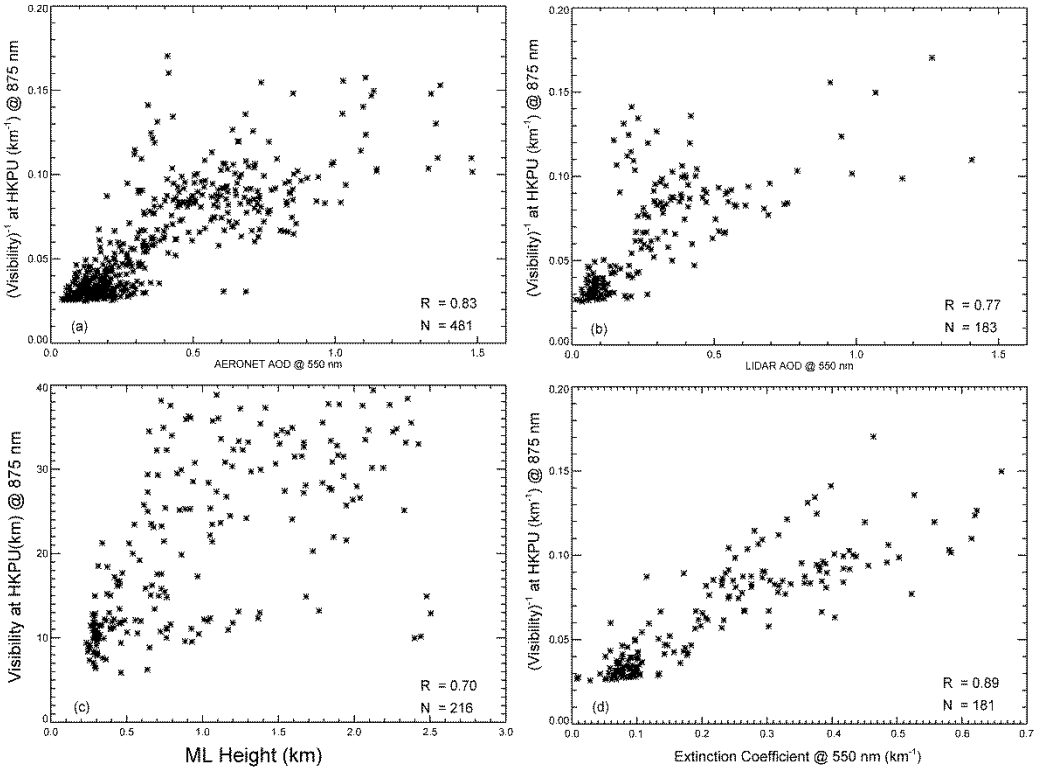

Figure 4.2. Relationship between visibility at HKPU derived from visibility meter at 875 nm wavelength and (a) AOD from AERONET (b) AOD from ALS (c) ML-Low and (d) Extinction coefficient from ALS for height between 75 m – 150 m at HKPU. Here R is correlation coefficient and N is the number of data points.

4.4 METHODOLOGY

4.4.1 ALS Extinction Coefficient Profiles

Although ALS data are collected at 15 m and 1 minute resolution, integrated profiles can improve the signal to noise ratio (SNR) (e.g., Campbell et al., 2008). Therefore, hourly averages of the extinction coefficient profile at 75 m resolution were computed. The arithmetic mean ($\sigma(t,r)$) and standard deviation ($\Delta\sigma(t,r)$) for each 1 minute and 15 m profile were first computed after resolving the profile to 75 m resolution (i.e., 5 bin averages at 15 m resolution). Next, the hourly average of 75 m and 1 minute extinction coefficient profiles was derived by computing, once again

the arithmetic mean of each 75 m and 1 min profile available in an hour (Eq. 4.1). The relative uncertainty in the hourly averaged profile was then computed using Eq. 4.2.

$$\sigma_{LU}(t,r) = \frac{\sum_{t=0}^{t=59} \sigma_t(r)}{N} \tag{4.1}$$

$$\Delta\sigma_{LU}(t,r) = \frac{\sqrt{\sum_{t=0}^{t=59} [\Delta\sigma_t(r)]^2}}{N} \tag{4.2}$$

Here, N is the total number of profiles in an hour and σ_{LU} and $\Delta\sigma_{LU}$ are the hourly averaged profiles of extinction coefficient and their corresponding relative uncertainty at 75 m resolution. Ratio of Eqs. 4.1 and 4.2 give the SNR for the corresponding profile, as

$$SNR(r) = \frac{\sigma_{LU}(r)}{\Delta\sigma_{LU}(r)} \tag{4.3}$$

To extract a representative ALS surface extinction coefficient (Scaled Surface Extinction Coefficient, σ_S at 355 nm) from signals measured within the overlap region of the LIDAR, some correction or scaling is necessary due to possible uncertainty corresponding to the overlap region and use of a static ratio of extinction and backscatter (as described above) of 36 Sr. To overcome this problem the ratio of τ_{AU} and τ_{LU} are used in order to constrain the LIDAR equation and scale extinction coefficient (σ_S) relative to AERONET as

$$\sigma_S = \frac{\tau_{AU}}{\tau_{LU}} * \sigma_{LU} \ (at\ r = 75\ m) \tag{4.4}$$

where σ_{LU} (extinction coefficient from LIDAR) is reported at 355 nm. Note here that τ_{AU} and τ_{LU} are scaled up to 550 nm using corresponding values of Angstrom Exponent ($\alpha_{440\,nm-675\,nm}$ and $\alpha_{340\,nm-500\,nm}$) from the AERONET Level 2 datasets, since τ_{AU} and τ_{LU} are measured at 500 nm and 355 nm from AERONET and ALS, respectively.

4.4.2 Nonlinear Regression Analysis

It is assumed that σ_S and V_{HKPU} will exhibit an inverse empirical relationship, in a form similar to Koschmieder's law (Koschmieder, 1924) that can be applied to the entire Hong Kong domain under our assumption of constant and persistent aerosol vertical distributions. Therefore, a formula is proposed to estimate V_{HKPU} using σ_S as

$$V_{HKPU} = \frac{a}{\sigma_S + b} \tag{4.5}$$

where a (unitless) and b (km^{-1}) are constants that can be estimated using a non-linear regression fit between σ_S and V_{HKPU}. Values of parameters "a" and "b" are estimated using the AERONET AOD, LIDAR AOD and LIDAR extinction coefficient for the time period of March, 2011 to December, 2011 at HKPU only. These estimated values of "a" and "b" will be used to estimate and validate at HKIA. The values of parameters "*a*" and "*b*" will be different from the 3.912 and 0.0 km^{-1} prescribed by Koschmieder's equation, which correspond to an assumed visual contrast of (0.02) and extinction of light due to gases as well as particles, whereas σ_S in Eq. 4.5 accounts for extinction of light due to particles in air only. Also V_{HKPU} accounts for scattering due to particles only. Hence values of parameters "a" and "b" also account for absorption due to gases such as NO_2 as well as brown and black carbon, which are important contributors to visibility reduction in an urban atmosphere.

4.4.3 Modelled Extinction Coefficient

As noted in the previous section (Fig 4.1e and 4.1f), there is significant spatial variability in VR between HKIA and HKPU, such that a measurement of VR in one location cannot be representative of another location. Therefore, in this study six models are developed (Table 4.2) to use MODIS data to spatially extrapolate either σ_{LU} measurements (Models 1 to 3) or VR measurements at HKPU (Models 5 and 6) to the HKIA. Development of these models is based on the assumption that at any given time vertical distribution of AOD is constant in Hong Kong compared to their horizontal distribution at any given time. All proposed models use MODIS AOD at HKIA to estimate surface visibility at HKIA. MODIS AOD retrieved at HKIA is scaled to near surface using LIDAR ML height (Model 4), LIDAR AOD (Model 1), AERONET AOD (Model 2 and 6) and MODIS AOD (Model 3 and 5) at HKPU.

Table 4.2. Proposed models for estimating MODIS extinction coefficient (σ_{MA}) and MODIS VR (V_{HKIA}^{mod}) at HKIA.

Model 1	$\sigma_{\mathrm{MA}} = \frac{\tau_{MA}}{\tau_{LU}} * \sigma_{LU}$
Model 2	$\sigma_{\mathrm{MA}} = \frac{\tau_{MA}}{\tau_{AU}} * \sigma_{LU}$
Model 3	$\sigma_{\mathrm{MA}} = \frac{\tau_{MA}}{\tau_{MU}} * \sigma_{LU}$
Model 4(a,b)	$\sigma_{\mathrm{MA}} = \frac{\tau_{MA}}{Z_{(L,H)}}$
Model 5	$V_{HKIA}^{mod} = \frac{\tau_{MA}}{\tau_{MU}} * V_{HKPU}$
Model 6	$V_{HKIA}^{mod} = \frac{\tau_{MA}}{\tau_{AU}} * V_{HKPU}$
Model 7	$V_{HKIA} = V_{HKPU}$

σ_{MA} = MODIS extinction coefficient at HKIA
τ_{MA} = MODIS AOD at HKIA
τ_{MU} = MODIS AOD at HKPU
τ_{AU} = AERONET AOD at HKPU
τ_{LU} = LIDAR AOD at HKPU
$Z_{(L,H)}$ = Low and High ML heights at HKPU
V_{HKIA} = VR from visibility meter at HKIA
V_{HKPU} = VR from visibility meter at HKPU

Model 1

$$MODIS\ Ext.Coeff.at\ HKIA = \frac{MODIS\ AOD\ at\ HKIA}{ALS\ AOD\ at\ HKPU} * ALS\ Ext.Coeff.at\ HKPU$$

Model-1 estimates MODIS derived surface level extinction coefficient at HKIA at 355 nm using MODIS AOD at HKIA, ALS AOD at HKPU and near surface ALS extinction coefficient at HKPU. This model first scales the MODIS AOD at HKIA with ALS AOD at HKPU. Multiplication of the resultant scale factor with near surface extinction coefficient from the ALS at HKPU gives the near surface MODIS extinction coefficient at HKIA.

Model 2

$$MODIS\ Ext.Coeff.at\ HKIA\ = \frac{MODIS\ AOD\ at\ HKIA}{AERONET\ AOD\ at\ HKPU} * \ ALS\ Ext.Coeff.at\ HKPU$$

Model 2 estimates MODIS derived surface level extinction coefficient at HKIA at 355 nm using MODIS AOD at HKIA, AERONET AOD at HKPU and near surface ALS extinction coefficient at HKPU. This model first scales the MODIS AOD at HKIA with AERONET AOD at HKPU. Multiplication of the resultant scale factor with near surface extinction coefficient from the ALS at HKPU gives the near surface MODIS extinction coefficient at HKIA. Model 2 is expected to perform better than Model 1 because the performance of Model 1 depends on the LIDAR AOD computed by using a fixed backscatter-to-extinction ratio that may not estimate AOD as reliable as AOD from LIDAR.

Model 3

$$MODIS\ Ext.Coeff.at\ HKIA\ = \frac{MODIS\ AOD\ at\ HKIA}{MODIS\ AOD\ at\ HKPU} * \ ALS\ Ext.Coeff.at\ HKPU$$

Model 3 estimates MODIS derived surface level extinction coefficient at HKIA at 355 nm using MODIS AOD at HKIA, AERONET AOD at HKPU and near surface ALS extinction coefficient at HKPU. This model first scales the MODIS AOD at HKIA with MODIS AOD at HKPU. Multiplication of the resultant scale factor with near surface extinction coefficient from the ALS at HKPU gives the near surface MODIS extinction coefficient at HKIA.

Model 4(a,b)

$$MODIS\ Ext.Coeff.at\ HKIA\ = \frac{MODIS\ AOD\ at\ HKIA}{ALS\ Mixing\ Layer\ Height\ at\ HKPU}$$

Model 4 estimates MODIS derived surface level extinction coefficient at HKIA at 355 nm using MODIS AOD at HKIA and mixing layer heights (Low and High) from ALS at HKPU. This is reasonable since on average the majority of AOD measured at Hong Kong is the result of particle scattering below ML-Low (He et al., 2008; Campbell et al., 2012). As mentioned above, Eq. 4.5 uses σ_S at 355 nm to derive V_{HKPU} at 875 nm. Therefore σ_{MA} should also be at 355 nm. Hence, σ_{MA} from Model 4 was also scaled to 355 nm using the Angstrom Exponent values from AERONET.

MODIS extinction coefficient at HKIA (σ_{MA}) from Models 1 to 4 simulates VR at HKIA from MODIS (V_{HKIA}^{mod}) at 875 nm wavelength when substituted in Eq. 4.6 similar to Eq.4.5, where values of "a" and "b" are the same as in Eq. 4.5.

$$V_{HKIA}^{mod} = \frac{a}{\sigma_{\mathrm{MA}}+\mathrm{b}} \tag{4.6}$$

It is also important to note that Eq. 4.4 and Eq. 4.5 play imperative roles in estimating visibility at HKIA (Eq. 4.6) using models 1-4. Therefore, to ensure the independent and robust validation of the simulated visibility values at HKIA, Eq. 4.4 and Eq. 4.5 do not involve any data from HKIA.

Model 5

$$MODIS\ Visibility\ at\ HKIA\ = \frac{MODIS\ AOD\ at\ HKIA}{MODIS\ AOD\ at\ HKPU} * \ Visibility\ at\ HKPU$$

To study the effect of possible uncertainties involved in retrieval of ALS products due to use of a constant extinction to backscatter ratio, Model 5 was developed independent of the LIDAR data. This model uses MODIS AOD at HKPU to scale MODIS AOD at HKIA. The resultant scaling factor when multiplied to surface level visibility at HKPU from the visibility meter at 875 nm, reports the modelled MODIS visibility at HKIA without involving Eq. 4.4 - 4.6.

Model 6

$$MODIS\ Visibility\ at\ HKIA\ = \frac{MODIS\ AOD\ at\ HKIA}{AERONET\ AOD\ at\ HKPU} * \ Visibility\ at\ HKPU$$

Model 6, like Model 5 is also independent of the LIDAR data. However, model 6 uses AERONET AOD at HKPU to scale the MODIS AOD at HKIA. Hence, like Model 5, Model 6 also reports the modelled MODIS visibility for HKIA at 875 nm without involving Eq. 4.4 to 4.6.

Model 7 (Reference Model)

$$Surface\ visibility\ at\ HKIA = \ Surface\ visibility\ at\ HKPU$$

Models 1 to 6 use MODIS data to account for the spatial variability in VR in Hong Kong with the assumption that this reduces uncertainty in the extrapolation of VR measured at one location to another. However, MODIS AOD contains some errors (More et al., 2013) and it is unknown if inclusion of these data adds useful information to the estimates of VR. Therefore, to evaluate the usefulness of the

MODIS data in estimating VR, a "Reference Model" (Model 7) was also developed where VR at HKIA and HKPU are compared.

4.5 RESULTS AND DISCUSSION

4.5.1 Model fitting

A nonlinear regression model (Eq. 4.5) was fit to the data for the relationship between VHKPU and σ_S (Fig. 4.3).

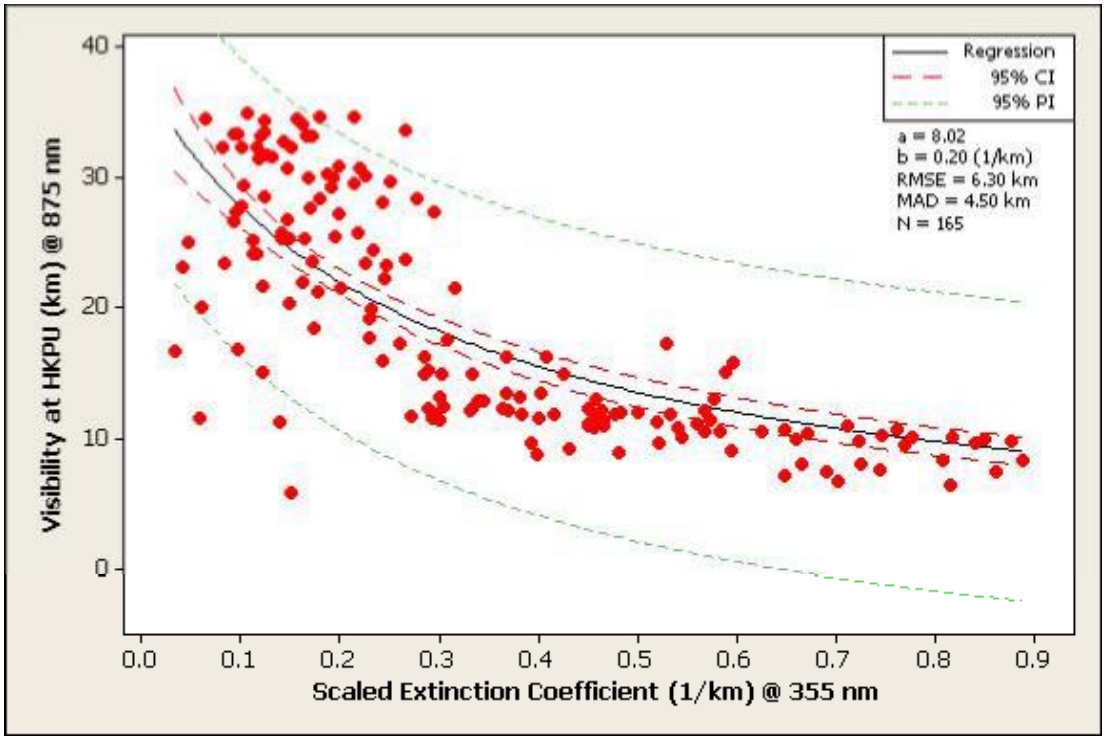

Figure 4.3. Non-linear regression fit for scaled extinction coefficient and visibility at HKPU. Estimated values of regression coefficients *a* and *b,* and N are reported along with root mean square error (RMSE), Mean absolute deviation (MAD) and coefficient of determination (R^2) for 165 measured values of visibility at HKPU and scaled surface extinction coefficient.

The value of the first parameter, a, is approximately two times greater than that prescribed by Koschmieder's equation (8.02 compared to 3.912). Koschmieder's values assume a visual contrast threshold of the eye at 0.02, where the absorption and scattering of the optical medium correspond to the 500 nm wavelength. However, two of the terms in Eq. 4.5 are derived at different wavelengths: the σ_S in Eq. 4.5 is derived at the ultraviolet 355 nm wavelength and visibility at HKPU (V_{HKPU}) is derived from a forward scattering instrument, considering only scattering in the infra-red region at 875 nm. Additionally, the calculated values for 'a' comply with the fact that for a given particle with single scattering albedo of 1 (SSA = 1), the scattering cross-section can increase significantly (Hansen and Travis, 1974) (i.e.

approx. 2 times in the case of SO_4^- a major pollutant reported for Hong Kong; Cheung et al., 2005; Qun et al., 2009; Zhuang et al., 1999) when the wavelength is changed from 550 nm to 335 nm.

A larger value of 'b' (of 0.2 km^{-1}) is also observed in the model, which may have one or two possible causes, including the extinction of light due to absorption by gases and particles, or due to the regression analyses which are based on least squares regression. This does not account for errors in the dependent variable i.e. V_{HKPU}, which will result in an overestimated intercept value i.e. '*b*'. The fitting of the model with V_{HKIA} was able to explain only 50 % of the variability in V_{HKPU}, possibly due to use of the LIDAR extinction coefficient from the overlap region where reliability may be an issue (Kovalev and Eichinger, 2004). Overall, 95 % confidence interval (red dotted line in Fig. 4.3) of fitted regression line is fairly narrow predicting a significant estimation power of the model. This is the reason that only 4 % of data points fall out of the prediction interval (green dotted line in Fig. 4.3). The estimated error in prediction of the proposed model is 23.59 %.

4.5.2 Validation

Each model requires a valid retrieval of MODIS AOD over HKIA. For the entire study period there were only 46 MODIS images with valid AOD retrieval, and only 14 of these (8 from 2011 and 6 from 2012) could be matched to concurrent LIDAR data as required by Models 1 to 4 in Table 4.1.

Performance of models 1 to 4 depends on the values of estimated parameters 'a' and 'b' based on LIDAR, AERONET and VR data at HKPU whereas performance of Models 5 and 6 depends on the VR data at HKPU for the period March 2011 to December 2011. These models are validated for VR from the visibility meter at HKIA (V_{HKIA}) using MODIS AOD for the period March 2011 to March 2012. This allows an independent validation of algorithms at HKIA. We could not include data beyond March 2012 for validation due to unavailability of LIDAR data at HKPU.

Modelled VR for those 14 days along with visibility meter readings at HKIA are shown in Fig. 4.4. The error bars for V_{HKIA} correspond to the 20 % expected uncertainty of the visibility meter (from its manual), which is consistent with Annex

3 of the International Civil Aviation Organization (ICAO) that suggests that an uncertainty of ±20 % in estimated VR is acceptable when actual VR is above 1.5 km.

Most of the proposed models (Table 4.1) are able to reproduce variations in V_{HKIA}. Here, Models 2 and 3 combined with Eq. 4.6 give the best estimate of surface VR, followed by Models 5 and 6 that estimate VR independent of Eq. 4.6. It can also be noted that estimation of VR at HKIA is independent of any bias for clear or polluted days, whereas previous studies (Diner, 1985; Haung et al., 2006; Otterman, 1985; Williams and Cogan, 1991) have overestimated (underestimated) those conditions. In fact, the modelled visibilities from Models 2, 3, 5 and 6 all fall within one standard deviation (6.17 km) of V_{HKIA} for validation days.

Model 1 underestimates VR most of the time, primarily because AOD estimates from the ALS are found to be biased low relative to AERONET. This is the reason that when τ_{AU} replaces τ_{LU} in Model 2 the modelled VR is fairly close to V_{HKIA} for most days. A similar argument is also valid for Model 3, whose performance is similar to Model 2.

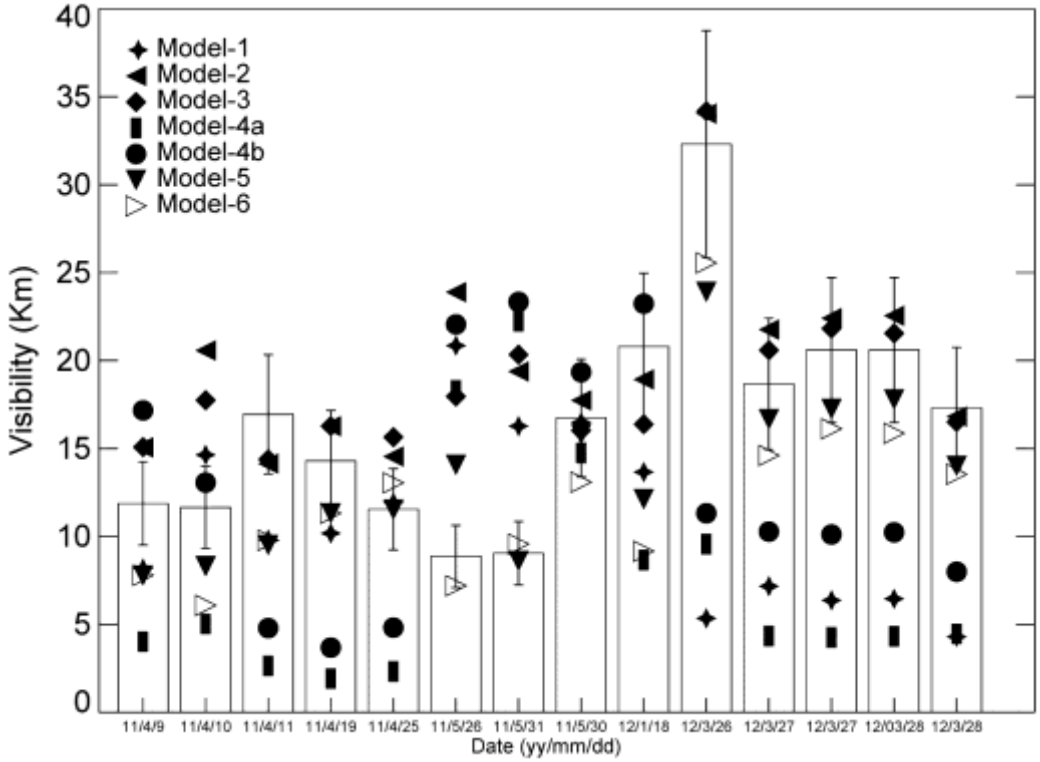

Figure 4.4. MODIS derived modelled visibility at HKIA from the proposed models listed in Table 1and actual visibility (Histogram bars) from visibility meter at HKIA. In addition to MODIS AOD, Model 1-4 uses AOD, ML heights as well as extinction coefficients from ground based instruments at HKPU whereas Model 5-6 uses visibility readings from visibility meter at HKPU. Error bars are ±20% of the visibility at HKIA from the manual of visibility meter.

Models 4a and 4b underestimate V_{HKIA} most of time. There are two primary reasons for this. The first is that the atmosphere was not well mixed for days with underestimated modelled VR. The second is that Models 4a and 4b depend on ML heights estimated from the ALS at HKPU. ML heights were derived from the LIDAR extinction profile based on a constant extinction-to-backscatter ratio, and we have seen that τ_{LU} is lower than τ_{AU}. Hence, the retrieved vertical distribution of AOD from ALS is expected to be lower, which influences the computation of ML. Results for Models 4a and 4b may suggest that underestimated ML heights caused overestimation in the corresponding σ_{MA} and hence decrease the modeled VR.

It is noted that Models 1-4 are unable to estimate VR on 26 May 2011 and 31 May 2011 when V_{HKIA} is much lower than on other days. In addition, Models 1 and 4 underestimate V_{HKIA} for most days, which are thought to be due to uncertainties associated with ALS data. Therefore, Models 5 and 6, which are independent of ALS data, were introduced, as they isolate the effect of possible uncertainties in σ_{LU} because both depend on AOD from MODIS and AERONET along with surface VR at HKPU. Both gave better estimates of V_{HKIA} than Models 2 and 3. In addition, Model 6 was also able to estimate V_{HKIA} for both 26 May 2011 and 31 May 2011, whereas Model 5 was only able to estimate V_{HKIA} for 31 May 2011, in addition to other days. No other model was able to estimate V_{HKIA} for 26 May 2011 and 31 May 2011. Overall, the highest correlation between modelled and ground visibilities is for these two models (Fig. 4.5), which overall, are best able to reproduce variations of V_{HKIA}.

Further assessments of the respective models are shown by scatter plots of modelled VR versus ground VR estimated at HKIA (Fig. 4.5). Model 1 (Fig. 4.5a) shows a strange inverse relation between estimated and ground visibility at HKIA. Further analysis showed that there is an inverse relation between AOD from LIDAR and MODIS at HKIA for 8 days that also caused an inverse relationship between estimated and ground visibility at HKIA for Model 1. Discrepancy in the LIDAR AOD may be attributed to the use of fixed backscatter-to-extinction ratio, which can be avoided by calculating a dynamic backscatter-to-extinction ratio by constraining the LIDAR AOD with AERONET AOD. This is the reason that Model 2 (Fig. 4.5b) has performed far better than Model 1, showing a direct linear relationship between estimated and ground visibility. Most of the time estimated visibility from Models 2,

3, 5 and 6 (Fig. 4.5 b, c, f and g) falls within the expected error range of the proposed model (Blue Dashed lines) as well as the upper and lower limit of ± 20 % of the ground visibility at HKIA (Green Dotted lines). VR estimates using Models 5 and 6 are concentrated closest to the 1:1 line. Hence, if we rank the models based on R^2, R, RMSE and MAD, Model 5 performs best followed by Models 6 and 3.

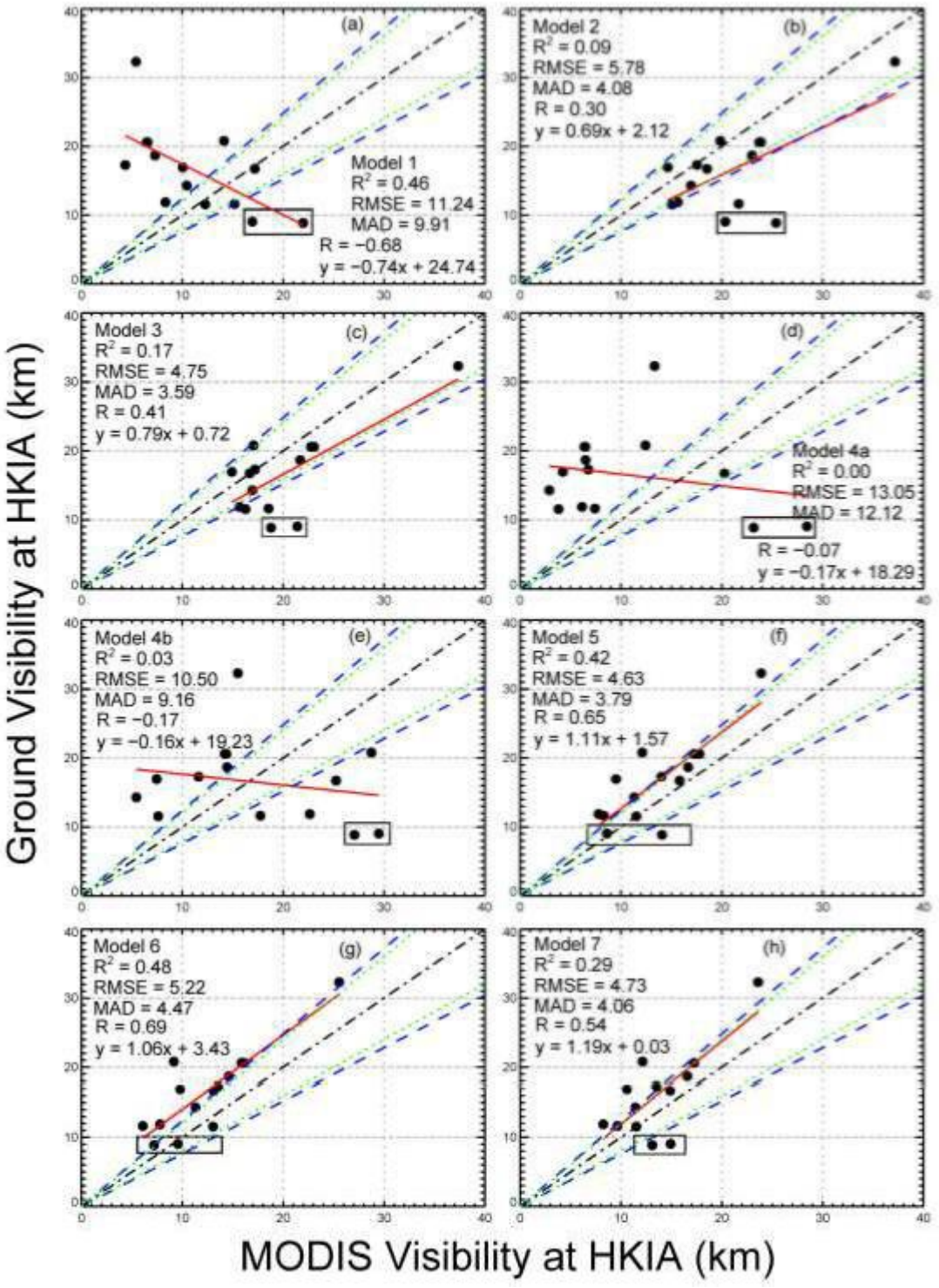

Figure 4.5. Scatter plot of V_{HKIA} and MODIS derived visibility at HKIA for each proposed model (Table 1). Black Dash-Dot line displays the 1:1 line, Blue Dashed lines show the upper and lower

limit of estimated error in the model, Green Dotted lines show the upper and lower limit of ± 20 % of the ground visibility at HKIA, Red solid line displays the fitted regression line and rectangles encompass data for 26 May 2011 and 31 May 2011. R^2, RMSE and MAD are described in Figure 4.3.

Performance of the proposed models greatly improves (Table 4.3) if we remove 26 May 2011 and 31 May 2011 from the validation, based on unusually low values of V_{HKIA} corresponding to low MODIS AOD for these anomalous days at HKIA. MODIS AOD for these two days was 0.18 (0.17) and 0.20 (0.35) respectively at HKIA (HKPU), whereas AERONET AOD was 0.33 and 0.32, respectively, at HKPU. Values of τ_{MA} and V_{HKIA} are low for these days relative to τ_{MU} and V_{HKPU}. This shows unusually low visibilities at HKIA when τ_{MA} was also low. Comparing values of R^2, R, RMSE and MAD, Model 3 replaces Model 5 as the strongest performer. Again, the only difference between Models 3 and 5 (Table 4.1) is the use of surface extinction from the ALS in Model 3. This once again shows that LIDAR data processed without using static Extinction-to-Backscattering ratio may result in better estimates of surface VR.

Table 4.3. Comparison of model performance before and after removal of data for 26 May 2011 and 31 May 2011. Note that an underlined value represents that of the best model.

	Before removal				After removal			
	R^2	RMSE	R	MAD	R^2	RMSE	R	MAD
Model 1	0.46	11.24	-0.68	8.91	0.28	11.45	-0.53	8.80
Model 2	0.09	5.78	0.30	4.08	0.49	3.35	0.70	2.65
Model 3	0.17	4.75	0.41	3.59	*0.44*	*2.96*	*0.66*	*2.48*
Model 4a	0.00	13.05	-0.07	12.12	0.22	13.29	0.46	12.25
Model 4b	0.03	10.50	-0.17	9.16	0.05	9.85	0.22	8.40
Model 5	*0.42*	*4.63*	*0.65*	*3.79*	0.59	4.77	0.77	3.95
Model 6	0.48	5.22	0.69	4.47	0.49	5.61	0.63	5.03
Model 7	0.29	4.73	0.54	4.06	0.59	4.67	0.77	3.89

From Table 4.1, Models 4a and 4b depend on concurrent values of ML heights and MODIS AOD, whereas Model 5 and 6 depend on concurrent values of V_{HKPU}, AERONET AOD and MODIS AOD. Therefore, being independent of τ_{LU} and σ_{LU}, a larger validation dataset for Models 4-6 can be arranged separately because Models 4 – 6 are independent of τ_{LU} and σ_{LU}. Hence, Models 4-6 were further analysed using respective extended validation datasets with corresponding numbers of data points (N) of 16, 16, 28 and 29 respectively (Fig 4.6). Model 5 still shows the best result,

followed by Model 6. This demonstrates the robustness of the respective models. For a region where the vertical spatial distribution of aerosol physical properties can be considered constant, Models 3 and 5 are more applicable. Therefore passive satellite remote sensing has the potential to estimate the surface VR to within an uncertainty of 20%, or that prescribed for a relatively simple visibility meter.

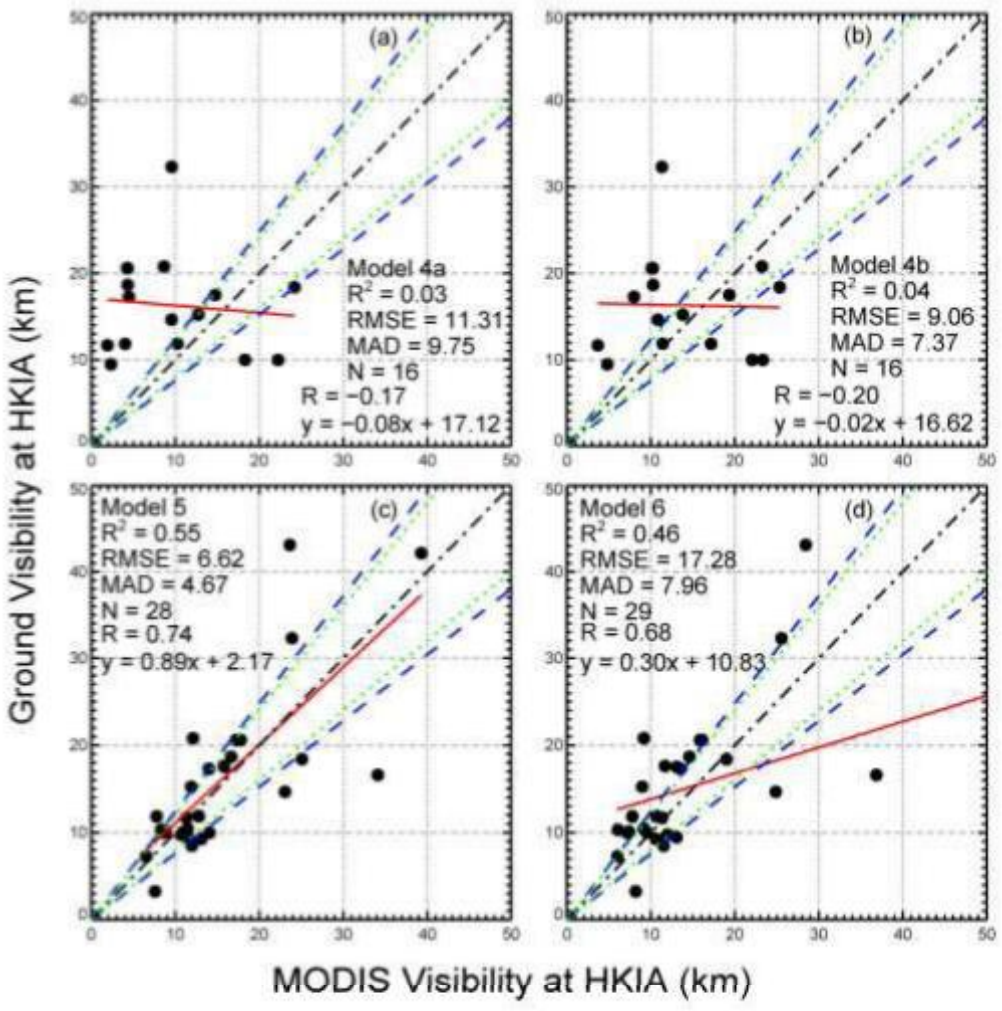

Figure 4.6. Scatter plot of V_{HKIA} and MODIS derived visibility at HKIA for Models 4-6 with extended validation data sets. Lines are described in Fig. 4.5. R^2, RMSE and MAD are described in Figure 4 and N is the available number of data points for validation.

Although HKIA and HKPU are 35 km apart, there is a significant difference in the visibilities at these locations (Fig. 4.1e, 4.1f and 4.5h). This suggests that a very dense ground based visibility-monitoring network is necessary in order to monitor the visibility of the entire Hong Kong domain. This is the reason that the reference model (Model 7) was unable to represent VR at HKIA (Fig. 4.5). Models 2, 3, 5 and 6 using MODIS data performed better than the reference model, which indicates that

inclusion of MODIS data is necessary for estimating VR at regional level. It also shows the merits of the proposed methods for estimating VR. Hence, passive satellite remote sensing techniques can be applied to optimize the use of a ground-based network and to fill gaps where no instruments are deployed. This will potentially help in reducing cost in monitoring regional air quality since VR estimates can be used as a surrogate for mass concentration of fine particulates ($PM_{2.5}$) (Chow et al., 2002; Vajanapoom et al., 2001).

4.5.3 Model Selection

The predictive power of a model is indicated by the uncertainties in its inputs as well as the deviation of its output from actual values. It is good to note that the outputs of the proposed models are within ± 20 % of the ground values. However, uncertainties in the input parameters applied have reduced the performance of some models. Among the input parameters the LIDAR data represents the greatest uncertainties due to the use of a static extinction-to-backscatter ratio. The extinction-to-backscatter ratio is necessary for retrieving the LIDAR extinction coefficient and LIDAR AOD as well as for scaling of LIDAR signal to the surface due to optical overlap of the instrument. In contrast, AOD from AERONET is considered to have the least uncertainty, though again we stress that the potential impact of optically thin cloud contamination of these data, and MODIS was ignored, due to the limited profiling range (175 m) during the daytime of the ALS. VR measurements from the visibility meter are also prone to uncertainty since they do not consider light absorption factors. However, the primary source of uncertainty involved in the estimation of VR in our models is the error term corresponding to the nonlinear regression step, since it is found to explain only 50% of the variations in σ_s and V_{HKPU}. A larger data set of σ_s and V_{HKPU} is needed to further improve the regression fitting.

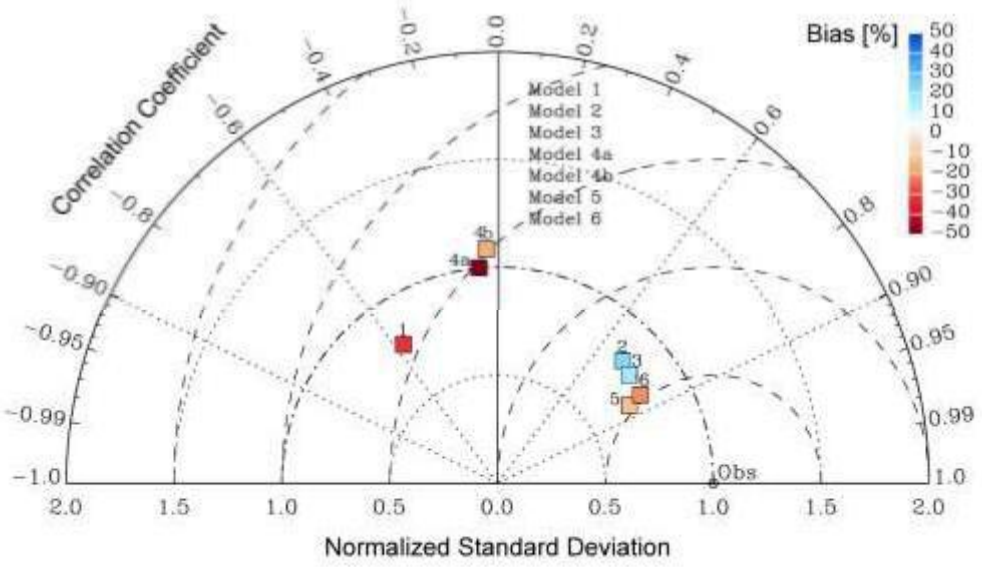

Figure 4.7. Pattern statistics (Taylor diagram; Taylor, 2001) describing the visibilities from the six models compared to observed visibilities at HKIA. The radial distance from the origin at '*0.0*' represents the normalized standard deviation. '*Obs*' represents the statistics of observed visibilities at HKIA. RMS difference for the modelled visibilities is proportional to the radial distances from origin at '*Obs*' (units same as normalized standard deviation). Normalized Pearson's correlation between observed and modelled visibilities is represented along the azimuthal position along the outer hemisphere. Color bar scales the normalized bias (%) in each model.

For better understanding of the performance of the proposed models a Taylor's diagram (Taylor, 2001) was built (Fig. 4.7). Taylor diagrams depict a statistical summary of how well patterns of estimated and observed values match based on their correlation, standard deviation and root mean square error. The radial distance from the origin at '*0.0*' represents the normalized standard deviation. '*Obs*' represents the statistics of observed visibilities at HKIA. RMS differences for the modelled visibilities are proportional to the radial distances from the origin at '*Obs*' (units same as normalized standard deviation). Normalized Pearson's correlations between observed and modelled visibilities are represented along the azimuthal position along the outer hemisphere. The color bar scales the bias (%) in each model.

Pattern statistics describing the six modelled visibilities compared to observed visibilities at HKIA show that Models 2, 3, 5 and 6 outperform models 1, 4a and 4b. The correlations for Models 5 and 6 are higher than for Models 2 and 3, whereas normalized standard deviations for Models 2, 3 and 6 are similar and higher for Model 5. Models 2 and 3 can be improved by using ALS data of better quality. However, the percentage biases for Models 5 and 3 are less than for Models 2 and 6. Overall Model 5 appears to be the best model for the estimation of VR using MODIS

AOD at HKPU and HKIA along with VR from HKPU (Fig. 4.7). Performance of these models is expected to further improve by retrieving AOD from MODIS at a high spatial resolution such as 3 by 3 km^2, which is planned for MODIS Collection 6 products (Levy, et al., 2013).

4.6 CONCLUSIONS

This study was designed to model and estimate VR using column-integrated aerosol physical properties from MODIS, ground-based LIDAR and AERONET sun photometer measurements of aerosol optical depth. Six models were developed under the assumption that the vertical distribution of aerosol physical properties for the study domain is constant regionally on any particular day, but that the aerosol amount may vary spatiotemporally and the shape of aerosol vertical profile may vary temporally. Results suggest that models utilizing satellite observations together with the near surface extinction coefficient from a visibility meter and ALS deployed at HKPU are reliable for estimation of VR 35 km away at HKIA. VR estimates from the proposed models were found to be within ± 20 % of ground values. The models did not overestimate or underestimate VR for clean and/or polluted days, as exhibited by previous studies of visibility modelling.

Chapter 5: Overall Conclusion and Recommendations

This study was designed to develop a remote sensing based methodology for measuring at-or-near ground level atmospheric visibility (Visual Range – VR). The relationship between the surface extinction coefficient (B_{ext}) and columnar Aerosol Optical Depth (AOD) from four spaceborne sensors (MODIS, MISR, CALIPSO and OMI) was examined. The potential of MODIS, MISR, OMI and CALIPSO AOD products for monitoring visibility in Hong Kong was evaluated at two visibility recording stations; the Hong Kong Observatory (HKO) and the Hong Kong International Airport (HKIA). The highest correlation at HKIA is for MISR AOD for kernel window of 1 by 1 (R = 0.60) followed by MISR AOD for kernel windows of 3 by 3 (R = 0.51) and Calipso for kernel window of 3 by 3 (R = 0.39) and the highest correlation at HKO is for MISR AOD for kernel window of 3 by 3 (R = 0.63) followed by MODIS AOD with kernel windows of 5 by 5 (R = 0.53) and 3 by 3 (R = 0.51) respectively. Although the correlation, RMSE and MAD for MISR AOD and B_{ext} is the highest at HKO and HKIA, the higher spatial and temporal resolution of MODIS AOD along with comparable RMSE and MAD made it a better candidate for use in regression modelling to simulate B_{ext} and VR. Selected MODIS AOD product was then subjected to regression analyses. A simple linear regression model M1was able to explain 58.1 % of variance in B_{ext} whereas a multiple linear regression model (M2) with climatic data (VT, RH and Q) explained 84.0 % of the variance in VR with a high accuracy depicted by a low RMSE of 0.27 km. The results of this study suggest that Q alone can explain the combined effect of P, T and RH on VR whereas VT alone is sufficient to explain the effects of WS and WD on dispersion of aerosols and hence VR.

This study also proposed another methodology to model and estimate VR using column-integrated aerosol physical properties from MODIS, ground-based LIDAR and AERONET sun photometer measurements of AOD. Six models were developed under the assumption that the vertical distribution of aerosol physical properties for the study domain is constant regionally on any particular day, but that the aerosol

amount may vary spatiotemporally and the shape of aerosol vertical profile may vary temporally. Using a 355 nm extinction coefficient profile solved from the LIDAR, MODIS AOD was scaled down to the surface to generate regional composite depictions of surface visibility. Results suggest that models utilizing satellite observations together with the near surface extinction coefficient from a visibility meter and LIDAR deployed at the Hong Kong Polytechnic University (HKPU) were reliable to estimate the VR 35 km away at HKIA. VR estimates from the proposed models were found to be within 20 % of ground values which is consistent with requirements of the International Civil Aviation Organization (ICAO). The models did not overestimate or underestimate VR for clean and/or polluted days, as exhibited by previous studies of visibility modelling. Results of the study demonstrate the potential for applying passive satellite depictions of broad-scale aerosol optical properties, and suggest that passive remote sensing exhibits the potential for enhancing the performance of pre-existing ground level visibility networks.

Results of this study can help devise methodologies for governments to more efficiently estimate VR at regional level. In addition to improvement in estimation of VR, this work can also lead to better understanding of environmental and health effects of ambient air quality in terms of atmospheric visibility for areas with no existing air pollution monitoring stations. The integration of the remotely estimated VR into a real time database network, such as Infusing Satellite Data into Environmental Applications (IDEA) by National Oceanic and Atmospheric Administration (NOAA) and Environment/Environmental Central Facility (ENVF) Environmental and Atmospheric Database in Hong Kong, can help civil authorities both in improving policy regulation and for control of transportation and navigation. With that in mind, our continuing goal is to facilitate the implementation and further testing of such infrastructure in order to meet the growing air quality-related issues faced by one of the world's largest metropolitan cities

Bibliography

Ackerman, S. A., Strabala, K. I., Menzel, W. P., Frey, R. A., Moeller, C. C., & Gumley, L. E. (Ackerman, S. A., Strabala, K. I., Menzel, W. P., Frey, R. A., Moeller, C. C., & Gumley, L. E. (1998). Discriminating clear sky from clouds with MODIS *Journal of Geophysical Research, 103*(D24), 32141-32157. doi:10.1029/1998JD200032

Aesthetics. (2011). Merriam-Webster dictionary, available at http://www.merriam-webster. com /dictionary/aesthetic.

Anderson, T. L., Masonis, S., Covert, D., Ahlquist, N., Howell, S., Clarke, A., & McNaughton, C. (2003). Variability of aerosol optical properties derived from in situ aircraft measurements during ACE-asia *Journal of Geophysical Research, 108*(D23ACE), 15-19. doi:10.1029/2002JD003247

Anderson, T. (1998). Determining aerosol radiative properties using the TSI 3563 integrating nephelometer *Aerosol Science and Technology, 29*(1), 13; 57-69.

Babari, R., Hautière, N., Dumont, É., Brémond, R., & Paparoditis, N. (2011). A model-driven approach to estimate atmospheric visibility with ordinary cameras. *Atmospheric Environment, 45*(30), 5316-5324. doi:10.1016/j.atmosenv.2011.06.053

Bäumer, D., Versick, S., & Vogel, B. (2008). Determination of the visibility using a digital panorama camera. *Atmospheric Environment, 42*(11), 2593-2602.

Bendix, J. (1995). Determination of fog horizontal visibility by means of NOAA-AVHRR, Paper presented at the *International geoscience and remote sensing symposium*, IGARSS '95*, 3* 1847-1849. doi:10.1109/IGARSS.1995.524045

Bhartia, P.K. & Wellemeyer, C.W. (2002). OMI TOMS-V8 Total O3 Algorithm, Algorithm Theoretical Baseline Document: *OMI Ozone Products*, P.K. Bhartia (ed.), Vol. II, ATBD-OMI-02, Version 2.0., Available online at: http://eospso.gsfc.nasa.gov/eos_homepage/for_scientists/atbd/docs/OMI/ATBD-OMI-02.pdf

Bian, Q. (2011). *Study of visibility degradation over the pearl river delta region: Source apportionment and impact of chemical characteristics* (PhD, The Hong Kong University of Science and Technology).

Bohren, C. F., & Huffman, D. R. (2004). *Absorption and scattering of light by small particles* . Weinheim: Wiley-VCH.

Bovensmann, H. (1999). SCIAMACHY: Mission objectives and measurement modes *Journal of the Atmospheric Sciences, 56*(2), 24; 127-150.

Brimblecombe, P. (1981). Long term trends in London fog. *Science of the Total Environment, 22*(1), 19-29. doi:http://dx.doi.org/10.1016/0048-9697(81)90078-4

Brimblecombe P., (1987). The Big Smoke. Routledge, London.

Burrows, J. (1995). SCIAMACHY: scanning imaging absorption spectrometer for atmospheric chartography, *Acta Astronautica, 35*(7), 445 - 451. doi:10.1016/0094-5765(94)00278-T

Burrows, J. P., Hölzle, E., Goede, A. P. H., Visser H., & Fricke, W. (1995). SCIAMACHY: Scanning imaging absorption spectrometer for atmospheric cartography, *Acta Astronautica,* **35(7)**, pp. 445-451.

Campbell, J. R., Reid, J. S., Westphal, D. L., Zhang, J., Tackett, J. L., Chew, B. N., . . . Winker, D. M. (2013). Characterizing the vertical profile of aerosol particle extinction and linear depolarization over southeast asia and the maritime continent: The 2007–2009 view from CALIOP. *Atmospheric Research, 122*(0), 520-543. doi:http://dx.doi.org/10.1016/j.atmosres.2012.05.007

Campbell, J. (2008). Elevated cloud and aerosol layer retrievals from micropulse lidar signal profiles. *Journal of Atmospheric and Oceanic Technology, 25*(5), 685-700. doi:10.1175/2007JTECHA1034.1

Caro, S., Cavallo, V., Marendaz, C., Boer, E. R., & Vienne, F. (2009). Can headway reduction in fog be explained by impaired perception of relative motion? *Human Factors, 51*(3), 378-392.

Chan, C. K., & Yao, X. (2008). Air pollution in mega cities in China. *Atmospheric Environment, 42*(1), 1-42. doi:10.1016/j.atmosenv.2007.09.003

Chan, M. N., Kreidenweis, S. M., & Chan, C. K. (2008). Measurements of the hygroscopic and deliquescence properties of organic compounds of different solubilities in water and their relationship with cloud condensation nuclei activities *Environmental Science & Technology, 42*(10), 3602-3608. doi:10.1021/es7023252

Chang, D., Song, Y., & Liu, B. (2009). Visibility trends in six megacities in China mainland 1973–2007 *Atmospheric Research, 94*(2), 161-167. doi:10.1016/j.atmosres.2009.05.006

Chang, W. L., & Koo, E. H. (1986). A study of visibility trends in Hong Kong (1968–1982). *Atmospheric Environment (1967), 20*(10), 1847-1858. doi:10.1016/0004-6981(86)90325-2

Charlson, R. J., Schwartz, S. E., Hales, J. M., Cess, R. D., Coakley, J. A.,Jr, Hansen, J. E., & Hofmann, D. J. (1992). Climate forcing by anthropogenic aerosols *Science (New York, N.Y.), 255*(5043), 423-430. doi:10.1126/science.255.5043.423

Cheng, A. Y. S., Chan, M. H., & Yang, X. (2006). Study of aerosol optical thickness in Hong Kong, validation, results, and dependence on meteorological parameters. *Atmospheric Environment, 40*(24), 4469-4477. doi:10.1016/j.atmosenv.2006.04.022

Cheung, H., Wang, T., Baumann, K., & Guo, H. (2005). Influence of regional pollution outflow on the concentrations of fine particulate matter and visibility in the coastal area of southern China. *Atmospheric Environment, 39*(34), 6463-6474. doi:10.1016/j.atmosenv.2005.07.033

Chew, B. N., Campbell, J. R., Reid, J. S., Giles, D. M., Welton, E. J., Salinas, S. V., & Liew, S. C. (2011). Tropical cirrus cloud contamination in sun photometer data *Atmospheric Environment, 45*(37), 6724 - 6731. doi:10.1016/j.atmosenv.2011.08.017

Chin, H. C. P. (1997). Visibility impairment in Hong Kong. Environmental Protection Department of Hong Kong. doi:EPD Technical Report: EPD/TP 1/97.

Chin, M., Diehl, T., Ginoux, P., & Malm, W. (2007). Intercontinental transport of pollution and dust aerosols: Implications for regional air quality *Atmospheric Chemistry and Physics, 7*(21), 5501-5517. doi:10.5194/acp-7-5501-2007

Chow, J. C., Watson, J. G., Lowenthal, D. H., & Richards, L. W. (2002). Comparability between PM2.5 and particle light scattering measurements. *Environmental Monitoring and Assessment, 79*(1), 29-45.

Chow, J. C., Watson, J. G., Shah, J. J., Kiang, C. S., Loh, C., Lev-On, M., . . . Molina, L. T. (2004). Megacities and atmospheric pollution *Journal of the Air & Waste Management Association (1995), 54*(10), 1226-1235.

Clean air act. (1993). Clean air act. UK, Available at http://www.legislation.gov.uk/ukpga/1993/11/pdfs/ukpga_19930011_en.pdf

Curier, R. L., Veefkind, J. P., Braak, R., Veihelmann, B., Torres, O., & de Leeuw, G. (2008). Retrieval of aerosol optical properties from OMI radiances using a multiwavelength algorithm: Application to western Europe *Journal of Geophysical Research, 113*(D17) doi:10.1029/2007JD008738

Delucchi, M. A., Murphy, J. J., & McCubbin, D. R. (2002). The health and visibility cost of air pollution: A comparison of estimation methods. *Journal of Environmental Management, 64*(2), 139-152. doi:10.1006/jema.2001.0515

Diner, D. J., Beckert, J. C., Reilly, T. H., Bruegge, C. J., Conel, J. E., Kahn, R. A., . . . Verstraete, M. M. (1998). Multi-angle imaging SpectroRadiometer (MISR) instrument description and experiment overview *IEEE Transactions on Geoscience and Remote Sensing, 36*(4), 1072-1087. doi:10.1109/36.700992

Diner, D. (1985). Influence of aerosol scattering on atmospheric blurring of surface features *IEEE Transactions on Geoscience and Remote Sensing, GE-23*(5), 618-624.

Dockery, D. W., Pope, C. A.,3rd, Xu, X., Spengler, J. D., Ware, J. H., Fay, M. E., . . . Speizer, F. E. (1993). An association between air pollution and mortality in six U.S. cities *The New England Journal of Medicine, 329*(24), 1753-1759. doi:10.1056/NEJM199312093292401

CRS. (2005). Clean Air Act: A Summary of the Act and Its Major Requirements. Available at http://fpc.state.gov/documents/organization/47810.pdf

Du, K., Mu, C., Deng, J., & Yuan, F. (2013). Study on atmospheric visibility variations and the impacts of meteorological parameters using high temporal resolution data: An application of environmental internet of things in China mainland *International Journal of Sustainable Development & World Ecology, 20*(3), 238-247. doi:10.1080/13504509.2013.783886

Dubovik, O., & King, M. D. (2000). A flexible inversion algorithm for retrieval of aerosol optical properties from sun and sky radiance measurements *Journal of Geophysical Research, 105*(D16), 20673. doi:10.1029/2000JD900282

Duda, R. O., & Hart, P. E. (1972). Use of the HT to detect lines and curves in pictures. *Comm.ACM, 15*(15), 11-15.

EPA, Environmental Protection Agency USA. (2011). *The benefits and costs of the clean air act from 1990 to 2020.*

Fernald, F. (1984). Analysis of atmospheric lidar observations: Some comments. *Applied Optics, 23*(5), 652. doi:10.1364/AO.23.000652

Finlayson-Pitts, B. J., & Pitts, J. N. (2000). *Chemistry of the upper and lower atmosphere* Academic Press.

Hadjimitsis, D. G., Clayton, C., & Toulios, L. (2010). Retrieving visibility values using satellite remote sensing data *Physics and Chemistry of the Earth, Parts A/B/C, 35*(1-2), 121-124. doi:10.1016/j.pce.2010.03.002

Han, Y., Lu, D., Rao, R. Z., & Wang, Y. J. (2009). Determination of the complex refractive indices of aerosol from aerodynamic particle size spectrometer and integrating nephelometer measurements. *Applied Optics, 48*(21), 4108-4117. doi:10.1364/AO.48.004108

Hansen, J. E., & Travis, L. D. (1974). Light scattering in planetary atmospheres *Space Science Reviews, 16*(4), 527-610. doi:10.1007/BF00168069

Haung, F., Hong, W., Junping, Q., & Guofu, W. (2006). Retrieval of atmospheric horizontal visibility by statistical regression from NOAA/AVHRR satellite data *Journal of Ocean University of China, 5*(3), 207-212. doi:10.1007/s11802-006-0003-4

He, Q. S. (2006). A study on aerosol extinction-to-backscatter ratio with combination of micro-pulse lidar and MODIS over Hong Kong. *Atmospheric Chemistry and Physics Discussion, 6*(2), 3099-3133. doi:10.5194/acpd-6-3099-2006

He, Q., Li, C., Mao, J., Lau, A. K., & Chu, D. A. (2008). Analysis of aerosol vertical distribution and variability in Hong Kong *Journal of Geophysical Research, 113*(D14) doi:10.1029/2008JD009778

Heath, D.F. & Park, H. (1978). The Solar Backscatter Ultraviolet (SBUV) and Total Ozone Mapping Spectrometer (TOMS) Experiment in The Nimbus–7, Users' Guide, edited by C. R. Madrid, NASA Goddard Space Flight Centre, Greenbelt, U.S., pp. 175.

Henry, R. C., Mahadev, S., Urquijo, S., & Chitwood, D. (2000). Color perception through atmospheric haze. *Journal of the Optical Society of America, Optics and Image Science, 17*(5), 831-835. doi:10.1364/JOSAA.17.000831

Henry, R. C. (2006). A field study of visual perception of complex natural targets through atmospheric haze by naïve observers. *Atmospheric Environment, 40*(27), 5251-5261.

HKEPD. (2007). Hong Kong Air Quality Objectives. Available at http://www.epd.gov.hk/epd/english/environmentinhk/air/air_quality_objectives/review_aqo.html

HKO. (2012). Hong Kong Observatory, Number of hours of Reduced Visibility observed at HKO, Hong Kong, Available at http://www.weather.gov.hk/cis/statistic/hko_redvis_statistic_e.htm

HKTB. (2003). Hong Kong Tourism Board, Annual report, Available at; http://www.discoverhongkong.com/eng/about-hktb/images/ 2003-2004-05.pdf

Ho, K. F., Lee, S. C., Cao, J. J., Chow, J. C., Watson, J. G., & Chan, C. K. (2006). Seasonal variations and mass closure analysis of particulate matter in Hong Kong. *Science of the Total Environment, 355*(1-3), 276-287.

Hoff, R. M., & Christopher. (2009). Remote sensing of particulate pollution from space: Have we reached the promised land?, (2009 critical review report). *Journal of the Air Waste Management Association, 59*(6), 645.

Hogg, C., 2004, Hong Kong chokes under thick smog, available at http://news.bbc.co.uk/go/pr/fr /- /2 /hi /asia-pacific/3579144.stm, accessed on 16/01/2012.

Holben, B. N., Eck, T. F., Slutsker, I., Tanré, D., Buis, J. P., Setzer, A., . . . Smirnov, A. (1998). AERONET—A federated instrument network and data archive for aerosol characterization *Remote Sensing of Environment, 66*(1), 1-16. doi:10.1016/S0034-4257(98)00031-5

Horvath, H., & Kaller, W. (1994). Calibration of integrating Nephelometers in the post-halocarbon era. *Atmospheric Environment, 28*(6), 1219-1223. doi:10.1016/1352-2310(94)90299-2

Horvath, H. (1971). On the applicability of the Koschmieder visibility formula. *Atmospheric Environment (1967), 5*(3), 177-184.

Horvath, H. (1981). The university of Vienna telephotometer. *Atmospheric Environment, 15*(12), 2537-2546.

Howes, E. P. (1913). Aesthetics. *Psychological Bulletin, 10*(5), 196-201. doi:10.1037/h0071344

Huang, D., Xu, J., & Zhang, S. (2012). Valuing the health risks of particulate air pollution in the Pearl River delta, China. *Environmental Science & Policy, 15*(1), 38-47. doi:10.1016/j.envsci.2011.09.007

Huang, W., Tan, J., Kan, H., Zhao, N., Song, W., Song, G., . . . Chen, B. (2009). Visibility, air quality and daily mortality in Shanghai, China. *Science of the Total Environment, 407*(10), 3295-3300. doi:10.1016/j.scitotenv.2009.02.019

Hudak, Andrew T., Evans, Jeffrey S., Falkowski, Michael J., Crookston, Nicholas L., Gessler, Paul E., Morgan, Penelope, Smith, Alistair M. S. (2005). Predicting plot basal area and tree density in mixed-conifer forest from lidar and Advanced Land Imager (ALI) data. In: Proceedings of the 26th Canadian Symposium on Remote Sensing; Wolfville, Nova Scotia, June 14-16, 2005. CD-ROM. 8 p.

Hyslop, N. P. (2009). Impaired visibility: The air pollution people see. *Atmospheric Environment, 43*(1), 182-195. doi:10.1016/j.atmosenv.2008.09.067

Ichoku, C., Chu, D.A., Mattoo, S., Kaufman, Y.J., Remer, L.A., Tanré, D., Slusker, I., & Holben, B.N. (2002). A spatio-temporal approach for global validation and analysis of MODIS aerosol products *Geophysical Research Letters, 29*(12) doi:10.1029/2001GL013206

Jacobson, M. Z. (2002). *Atmospheric pollution: History, science, and regulation*

Jiang, X., Liu, Y., Yu, B., & Jiang, M. (2007). Comparison of MISR aerosol optical thickness with AERONET measurements in Beijing metropolitan area *Remote Sensing of Environment, 107*(1-2), 45-53. doi:10.1016/j.rse.2006.06.022

Jung, J., Lee, H., Kim, Y. J., Liu, X., Zhang, Y., Gu, J., & Fan, S. (2009). Aerosol chemistry and the effect of aerosol water content on visibility impairment and radiative forcing in Guangzhou during the 2006 pearl river delta campaign *Journal of Environmental Management, 90*(11), 3231-3244. doi:10.1016/j.jenvman.2009.04.021

Kacenelenbogen, M., M. A. Vaughan, J. Redemann, R. M. Hoff, R. R. Rogers, R. A. Ferrare, . . . B. N. Holben. (2011). An accuracy assessment of the CALIOP/CALIPSO version 2/version 3 daytime aerosol extinction product based on a detailed multi-sensor, multi-platform case study. *Atmospheric Chemistry and Physics, 11*(8), 3981.

Kahn, R., Banerjee, P., & McDonald, D. (2001). Sensitivity of Multiangle imaging to natural mixtures of aerosols over ocean *Journal of Geophysical Research, 106*(D16), 18219-18238. doi:10.1029/2000JD900497

Kang, J. J., Ni, R., & Andersen, G. J. (2008). *Effects of reduced visibility from fog on car-following performance.* Available at http://www.academia.edu/182805/The_Effects_of_Reduced_Visibility_from_Fog_on_Car_Following_Performance

Kaufman, Y. J., & Fraser, R. S. (1982). Different atmospheric effects in remote sensing of uniform and nonuniform surfaces *Advances in Space Research, 2*(5), 147-155. doi:10.1016/0273-1177(82)90342-8

Kaufman, Y.J. & Tanré, D. (1998). Algorithm for remote sensing of tropospheric aerosols from MODIS, MODIS Algorithm Theoretical Basis Document, Product ID: MOD04, Revised 26 October, 1998. Available at http://modis.gsfc.nasa.gov/data/atbd/atbd_mod02.pdf

Kaufman, Y. J., Tanré, D., Gordon, H. R., Nakajima, T., Lenoble, J., Frouin, R., . . . Teillet, P. M. (1997). Passive remote sensing of tropospheric aerosol and atmospheric correction for the aerosol effect *Journal of Geophysical Research, 102*(D14), 16815-16830. doi:10.1029/97JD01496

Ke, D,. Chao, M,. Junjun, D., & Fang, Y., (2013), Study on atmospheric visibility variations and the impacts of meteorological parameters using high temporal resolution data: an application of Environmental Internet of Things in China, *International Journal of Sustainable Development & World Ecology,* Vol. 20, Iss. 3, 2013

Keckhut, P., Hauchecorne, A., & Chanin, M. L. (1993). a critical-review of the database acquired for the long-term surveillance of the middle atmosphere by the french rayleigh lidars. *Journal of Atmospheric and Oceanic Technology, 10*(6), 850-867. doi:10.1175/1520-0426(1993)010<0850:ACROTD>2.0.CO 2

King, M. D., Platnick, S., Yang, P., Arnold, G. T., Gray, M. A., Riedi, J., . . . Liou, K. (2004). Remote sensing of liquid water and ice cloud optical thickness and effective radius in the arctic: Application of airborne multispectral MAS data. *Journal of Atmospheric & Oceanic Technology, 21*(6), 857-875. Retrieved from http://search.ebscohost.com/login.aspx?direct=true&db=aph&AN=13424083&site=ehost-live

Klett, J. D. (1985). Lidar inversion with variable backscatter/extinction ratios. *Applied Optics, 24*(11), 1638. doi:10.1364/AO.24.001638

Koschmieder, H. (1924). *Theorie der horizontalen sichtweite* Beitr. Phys. Frei. Atmos.

Kovalev, V. A., & Eichinger, W. E. (2004). *Elastic lidar: Theory, practice, and analysis methods* . Hoboken, N.J.: John Wiley.

Kulesa, G. (2002). Weather and aviation: how does weather affect the safety and operations of airports and aviation, and how does FAA work to manage weather-related effects? The Potential Impacts of Climate Change on Transportation Workshop, USDOT Center for Climate Change and Environmental Forecasting, Washington DC. Available at http://climate.dot.gov/documents/workshop1002/kulesa.pdf.

Lai, L. Y., & Sequeira, R. (2001). Visibility degradation across Hong Kong: Its components and their relative contributions. *Atmospheric Environment, 35*(34), 5861-5872. doi:10.1016/S1352-2310(01)00395-8

Lee, F. Y. P., & Gervat, G. P. (1995). *Visibility degradation and its relationship to air quality.*. Hong Kong: Environmental Protection Department of Hong Kong. doi:EPD Technical Report: EPD TP/ 1/95.

Lee, Y. C., & Hills, P. R. (2003). Cool season pollution episodes in Hong Kong, 1996-2002. *Atmospheric Environment, 37*(21), 2927-2939.

Lee, Y. C., & Savtchenko, A. (2006). Relationship between air pollution in Hong Kong and in the pearl river delta region of south China mainland in 2003 and 2004: An analysis *Journal of Applied Meteorology and Climatology, 45*(2), 269-282. doi:10.1175/JAM2332.1

Lee, Y. L., & Sequeira, R. (2002). Water-soluble aerosol and visibility degradation in Hong Kong during autumn and early winter, 1998. *Environmental Pollution, 116*(2), 225-233.

Leung , Y. K., & Lam, C. Y. (2008). Visibility Impairment in Hong Kong – A Wind Attribution Analysis, Bulletin of Hong Kong Meteorological Society, Volume 18, report 838, p.33-48, Available at http://www.weather.gov.hk/publica/reprint/r838.pdf.

Leung, Y., Wu, M., & Yeung, K., (2009), A Study on the Relationship Among Visibility, Atmospheric Suspended Particulate Concentration, and Meteorological Conditions in Hong Kong, *Acta Meteor. Sinica*, 23(2):250-260

Levelt, P. F., van den Oord, G. H. J., Dobber, M. R., Malkki, A., Huib Visser, Johan de Vries, . . . Saari, H. (2006). The ozone monitoring instrument *IEEE Transactions on Geoscience and Remote Sensing, 44*(5), 1093-1101. doi:10.1109/TGRS.2006.872333

Levy, R. C., Mattoo, S., Munchak, L. A., Remer, L. A., Sayer, A. M., & Hsu, N. C. (2013). The collection 6 MODIS aerosol products over land and ocean *Atmospheric Measurement Techniques Discussions, 6*(1), 159-259. doi:10.5194/amtd-6-159-2013

Levy, R. C., Remer, L. A., Martins, J. V., Kaufman, Y. J., Plana-Fattori, A., Redemann, J., & Wenny, B. (2005). Evaluation of the MODIS aerosol retrievals over ocean and land during CLAMS *Journal of the Atmospheric Sciences, 62*(4), 974-992. doi:10.1175/JAS3391.1

Lin, T., Christina Hsu, N., Tsay, S., & Huang, S. (2011). Asian dust weather categorization with satellite and surface observations *International Journal of Remote Sensing, 32*(1), 153-170. doi:10.1080/01431160903439932

Lind, J. A., & Kok, G. L. (1999). Emission strengths for primary pollutants as estimated from an aircraft study of Hong Kong air quality. *Atmospheric Environment, 33*(5), 825-831.

Liu, P., Zhao, C., Zhang, Q., Deng, Z., Huang, M., Ma, X., & Tie, X. (2009). Aircraft study of aerosol vertical distributions over Beijing and their optical properties *Tellus B, 61*(5), 756-767. doi:10.1111/j.1600-0889.2009.00440.x

Liu, P., Zhao, C., Zhang, Q., Deng, Z., Huang, M., Ma, X., & Tie, X. (2009). Aircraft study of aerosol vertical distributions over Beijing and their optical properties. *Tellus B, 61*(5), 756-767. doi:10.1111/j.1600-0889.2009.00440.x

Livingston, J. M., Redemann, J., Russell, P. B., Torres, O., Veihelmann, B., Veefkind, P., . . . Zhang, Q. (2009). Comparison of aerosol optical depths from the ozone monitoring instrument (OMI) on aura with results from airborne sunphotometry, other space and ground measurements during MILAGRO/INTEX-B *Atmospheric Chemistry and Physics, 9*(18), 6743 -6765. doi:10.5194/acp-9-6743-2009

Loehman, E. T., Park, S., & Boldt, D. (1994). Willingness-to-pay for gain and losses in visibility and health. *Land Economics, 70*, 478-498.

Lolli, S., Sauvage, L., Loaec, S., & Lardier, M. (2011). EZ Lidar: A new 780 compact autonomous eye-safe scanning aerosol Lidar for extinction measurements and PBL height detection. Validation of the performances against other instruments and intercomparison campaigns. Opt. Pura Appl. 44:33–41.

Louie, P. K., Chow, J. C., Chen, L. W., Watson, J. G., Leung, G., & Sin, D. W. (2005). PM2.5 chemical composition in Hong Kong: Urban and regional variations *The Science of the Total Environment, 338*(3), 267-281. doi:10.1016/j.scitotenv.2004.07.021

Lowenthal, D. H., Rogers, C. F., Saxena, P., Watson, J. G., & Chow, J. C. (1995). Sensitivity of estimated light extinction coefficients to model assumptions and measurement errors. *Atmospheric Environment, 29*(7), 751-766. doi:10.1016/1352-2310(94)00340-Q

Lu, W. Z., & Wang, X. K. (2004). Interaction patterns of major air pollutants in Hong Kong territory. *Science of the Total Environment, 324*(1-3), 247-259.

Mahadev, S. (1999). Application of a color-appearance model to vision through atmospheric haze *Color Research and Application, 24*(2), 9; 112-120.

Mallows, C. L. (1973). Some comments on CP. *Technometrics, 15*(4), 661-675. Retrieved from http://www.jstor.org/stable/1267380

Malm, W. C., Day, D. E., Kreidenweis, S. M., Collett, J. L., & Lee, T. (2003). Humidity-dependent optical properties of fine particles during the big bend regional aerosol and visibility observational study. *Journal of Geophysical Research: Biogeosciences, 108*(D9) doi:10.1029/2002JD002998

Malm, W. C., Gebhart, K. A., Molenar, J., Cahill, T., Eldred, R., & Huffman, D. (1994). Examining the relationship between atmospheric aerosols and light extinction at mount rainier and north cascades national parks. *Atmospheric Environment, 28*(2), 347-360. doi:10.1016/1352-2310(94)90110-4

Malm, W., Molenar, J., & Chan, L. L. (1982). Photographic simulation techniques for visualizing the effect of uniform haze on a scenic resource. *Journal of the Air Pollution Control Association, 33:2*, 126-129.

Malm, W., & Malm. (1981). Human perception of visual air quality (uniform haze). *Atmospheric Environment, 15*(10-11), 1875-1890. doi:10.1016/0004-6981(81)90223-7

Mang, L,. Jun T., Chuen-Yu, C., Jun-Ji, C., Zhi-Sheng, Z., Li-Hua, Z., & Ren-Jian, Z.,Characterization of Regression Relationship between Recent Air Quality and Visibility Changes in Megacities at Four Haze Regions of China, *Aerosol and Air Quality Research*, x: 1–13, xxxx, ISSN: 1680-8584 print / 2071-1409 online doi: 10.4209/aaqr.2011.11.0220

Martonchik, J. V., Diner, D. J., Kahn, R. A., Ackerman, T. P., Verstraete, M. M., Pinty, B., & Gordon, H. R. (1998). Techniques for the retrieval of aerosol properties over land and ocean using multiangle imaging *IEEE Transactions on Geoscience and Remote Sensing, 36*(4), 1212-1227. doi:10.1109/36.701027

Martonchik, J. V. (1997). Determination of aerosol optical depth and land surface directional reflectances using multiangle imagery *Journal of Geophysical Research, 102*(D14), 17015. doi:10.1029/96JD02444

Martonchik, J. (1998). Techniques for the retrieval of aerosol properties over land and ocean using multiangle imaging *IEEE Transactions on Geoscience and Remote Sensing, 36*(4), 16; 1212-1227.

Middleton, W. E. K. (1952). Vision through the atmosphere. University of Toronto press, 1952. pp. xiv, 250; 120 figs., 26 tables. 2nd edition. 68s. *Quarterly*

Journal of the Royal Meteorological Society, 81(347), 128-131. doi:10.1002/qj.49708134734

Mishchenko, M. I., Geogdzhayev, I. V., Liu, L., Ogren, J. A., Lacis, A. A., Rossow, W. B., . . . Muñoz, O. (2003). Aerosol retrievals from AVHRR radiances: Effects of particle nonsphericity and absorption and an updated long-term global climatology of aerosol properties. *Journal of Quantitative Spectroscopy and Radiative Transfer, 79–80*(0), 953-972. doi:10.1016/S0022-4073(02)00331-X

More, S., Kumar, P., P., Gupta, P., Devara, P., C., S., & Aher, G., R., (2013), Comparison of Aerosol Products Retrieved from AERONET, MICROTOPS and MODIS over a Tropical Urban City, Pune, India, *Aerosol and Air Quality Research*, 13: 107–121, ISSN: 1680-8584 print / 2071-1409 online, doi: 10.4209/aaqr.2012.04.0102

Morel, G., & Chauvin, C. (2006). A socio-technical approach of risk management applied to collisions involving fishing vessels. *Safety Science, 44*(7), 599-619. doi:10.1016/j.ssci.2006.01.002

Mui, K. W., Wong, L. T., & Chung, L.Y. (2009). Mathematical models for accurate prediction of atmospheric visibility with particular reference to the seasonal and environmental patterns in Hong Kong, *Environ Monit Assess,* 158(1-4):333-41. doi: 10.1007/s10661-008-0587-9. Epub 2008 Oct 26.

Mui, K. W., Wong, L. T., & Hui, P. S. (2009). Screening strategies of an indoor air quality express assessment protocol (EAP) for air-conditioned offices *Indoor and Built Environment, 18*(1), 77-82. doi:10.1177/1420326X08101529

NCEP, National Centers for Environmental Prediction/National Weather Service/NOAA/U.S. Department of Commerce (2000), NCEP FNL Operational Model Global Tropospheric Analyses, continuing from July 1999, http://rda.ucar.edu/datasets/ds083.2, Research Data Archive at the National Center for Atmospheric Research, Computational and Information Systems Laboratory, Boulder, Colo.Nichol, J. E., Wong, M. S., & Wang, J. (2010). A 3D aerosol and visibility information system for urban areas using remote sensing and GIS. *Atmospheric Environment, 44*(21–22), 2501-2506. doi:10.1016/j.atmosenv.2010.04.036

Otterman, J. (1985). Satellite measurements of surface albedo and temperatures in semi-desert. *Journal of Climate and Applied Meteorology, 24*(3), 228-235. doi:10.1175/1520-0450(1985)0242.0.CO 2

Pejovic, T., Williams, V. A., Noland, R. B., & Toumi, R. (2009). *Factors affecting the frequency and severity of airport weather delays and the implications of climate change for future delays*

Peters, J., Hedley, A. J., Wong, C. M., Lam, T. H., Ong, S. G., Liu, J., & Spiegelhalter, D. J. (1996). Effects of an ambient air pollution intervention and environmental tobacco smoke on children's respiratory health in Hong Kong. *International Journal of Epidemiology, 25*(4), 821-828.

Pope, C. A.,3rd, Thun, M. J., Namboodiri, M. M., Dockery, D. W., Evans, J. S., Speizer, F. E., & Heath, C. W.,Jr. (1995). Particulate air pollution as a predictor

of mortality in a prospective study of U.S. adults *American Journal of Respiratory and Critical Care Medicine, 151*(3 Pt 1), 669-674.

PRB. (2012). World population data sheet - 2012-population-data-sheet_eng.pdf Retrieved 7/17/2013, 2013, from http://www.prb.org/pdf12/2012-population-data-sheet_eng.pdf

Qun, L. S., Mang, L., Ming, W. J., Yu, C. C., & Fang, S. X. (2009). Characterization and relationship of long-term visibility and air pollutant changes in the Hong Kong region. *China Environmental Science, 29*(4), 351-356.

Rainwater, M., & Gregory. L. (2005). Cimel Sun Photometer (CSPHOT) Handbook. ARM TR-056, U.S. Department of Energy, Office of Science, Office of Biological and Environmental Research, Available at http://www.arm.gov/publications/tech_reports/handbooks/csphot_handbook.pdf?id=38

Riffler, M., Schneider, C., Popp, C., & Wunderle, S. (2009). Deriving atmospheric visibility from satellite retrieved aerosol optical depth Paper presented at the *EGU General Assembly 2009, Held 19-24 April, 2009 in Vienna, Austria Http://meetings.Copernicus.org/egu2009,* http://adsabs.harvard.edu//abs/2009EGUGA..1110928R. 10928.

Road traffic accidents statistics, Transport Department, Hong Kong. (2010). Available at; http://www.td.gov.hk/en/road_safety/road_traffic_accident_statistics/2010/index.html, accessed on 16/01/2012.

Ross, D. M., Malm, W. C., & Iyer, H. K. (1997). Human visual sensitivity to plumes with a gaussian luminance distribution: Experiments to develop an empirical probability of detection model. *Journal of the Air Waste Management Association, 47*(3), 370-82.

Seinfeld, J. H., & Pandis, S. N. (2006). *Atmospheric chemistry and physics: From air pollution to climate change* . Hoboken, N.J.: J. Wiley.

Sequeira, R., & Lai, K. (1998). The effect of meteorological parameters and aerosol constituents on visibility in urban Hong Kong *Atmospheric Environment, 32*(16), 2865-2871. doi:10.1016/S1352-2310(97)00494-9

Taylor, K. E. (2001). Summarizing multiple aspects of model performance in a single diagram. *Journal of Geophysical Research: Atmospheres, 106*(D7), 7183-7192. doi:10.1029/2000JD900719

Thach, T. Q., Wong, C. M., Chan, K. P., Chau, Y. K., Chung, Y. N., Ou, C. Q., . . . Hedley, A. J. (2010). Daily visibility and mortality: Assessment of health benefits from improved visibility in Hong Kong *Environmental Research, 110*(6), 617-623. doi:10.1016/j.envres.2010.05.005

Tiao, G. C., Box, G. E. P., & Hamming, W. J. (1975). Analysis of Los Angeles photochemical smog data: A statistical overview *Journal of the Air Pollution Control Association, 25*(3), 260-268. doi:10.1080/00022470.1975.10470082

Torres, O. (2005). Total ozone mapping spectrometer measurements of aerosol absorption from space: Comparison to SAFARI 2000 ground-based observations *Journal of Geophysical Research, 110*(D10) doi:10.1029/2004JD004611

Tsai, Y. I. (2005). Atmospheric visibility trends in an urban area in Taiwan 1961–2003 *Atmospheric Environment, 39*(30), 5555-5567. doi:10.1016/j.atmosenv.2005.06.012

Vajanapoom, N., Shy, C. M., Neas, L. M., & Loomis, D. (2001). Estimation of particulate matter from visibility in Bangkok, Thailand *Journal of Exposure Analysis and Environmental Epidemiology, 11*(2), 97-102. doi:10.1038/sj.jea.7500148

Van De Hulst, H. C. (1957). Light scattering by small particles *Physics Today, 10*(12), 28.

Vincent, D. A., (2003), Visibility over land from contrast analysis of multi-spectral satellite observations, M.Sc. Theses, Nnaval postgraduate school, USA

Wan, J., Lin, M., Chan, C., Zhang, Z., Engling, G., Wang, X., . . . Li, S. (2011). Change of air quality and its impact on atmospheric visibility in central-western Pearl River delta. *Environmental Monitoring and Assessment, 172*(1), 339-351.

Wang, J., Christopher, S. A., Reid, J. S., Maring, H., Savoie, D., Holben, B. N., . . . Yang, S. (2003). GOES 8 retrieval of dust aerosol optical thickness over the Atlantic Ocean during PRIDE. *J.Geophys.Res., 108*, 8595. doi:10.1029/2002JD002494

Wang, J., & Martin, S. T. (2007). Satellite characterization of urban aerosols: Importance of including hygroscopicity and mixing state in the retrieval algorithms. *J.Geophys.Res., 112*, D17203. doi:10.1029/2006JD008078

Wang, K., Dickinson, R. E., & Liang, S. (2009). Clear sky visibility has decreased over land globally from 1973 to 2007 *Science (New York, N.Y.), 323*(5920), 1468-1470. doi:10.1126/science.1167549

Watson, J. G. (2002). Visibility: Science and regulation. *Journal of the Air Waste Management Association, 52*(6), 628; 628-713; 713.

White, W. H. (1990). The components of atmospheric light extinction: A survey of ground-level budgets. *Atmospheric Environment - Part A General Topics, 24 A*(10), 2673-2679.

Williams, D. H., & Cogan, J. L. (1991). Estimation of visibility from satellite imagery *Applied Optics, 30*(400), 414. doi:10.1364/AO.30.000414

Winker, D. M. (2003). The CALIPSO mission: Spaceborne lidar for observation of aerosols and clouds Paper presented at the Proceedings of SPIE*, 4893* 1-11. doi:10.1117/12.466539

Winker, D. M., Hunt, W. H., & McGill, M. J. (2007). Initial performance assessment of CALIOP *Geophysical Research Letters, 34*(19) doi:10.1029/2007GL030135

Winker, D., Pelon, J., Coakley, J., Ackerman, S., Charlson, R., Colarco, P., . . . Wielicki, B. (2010). The CALIPSO mission: A global 3D view of aerosols and clouds *Bulletin of the American Meteorological Society, 91*(9), 1211-1229. doi:10.1175/2010BAMS3009.1

Wong, m. s., Lee, k., Nichol, J. E., & Li, z. (2010). Retrieval of aerosol optical thickness using MODIS 500 x 500 m^2, a study in Hong Kong and the pearl river delta region. *IEEE Transactions on Geoscience and Remote Sensing, 48*(8), 3318-3327. doi:10.1109/TGRS.2010.2045124

Wong, C., Atkinson, R. W., Ross Anderson, H., Hedley, A. J., Stefan, M., Chau, P. Y., & Lam, T. -. (2002). A tale of two cities: Effects of air pollution on hospital admissions in Hong Kong and London compared. *Environmental Health Perspectives, 110*(1), 67-77.

Wong, C. M., Lam, T. H., Peters, J., Hedley, A. J., Ong, S. G., Tam, A. Y. C., . . . Spiegelhalter, D. J. (1998). Comparison between two districts of the effects of an air pollution intervention on bronchial responsiveness in primary school children in Hong Kong. *Journal of Epidemiology and Community Health, 52*(9), 571-578.

Wong, C., Ma, S., Hedley, A. J., & Lam, T. -. (2001). Effect of air pollution on daily mortality in Hong Kong. *Environmental Health Perspectives, 109*(4), 335-340.

Wong, C., Vichit-Vadakan, N., Kan, H., Qian, Z., Vajanapoom, N., Ostro, B. . . . Liu, W. (2008). Public health and air pollution in asia (PAPA): A multicity study of short-term effects of air pollution on mortality. *Environmental Health Perspectives, 116*(9), 1195-1202.

Wong, T. W., Wun, Y. T., Yu, T. S., Tam, W., Wong, C. M., & Wong, A. H. S. (2002). Air pollution and general practice consultations for respiratory illnesses. *Journal of Epidemiology and Community Health, 56*(12), 949-950.

Wu, D., Tie, X., Li, C., Ying, Z., Lau, A. K., Huang, J., . . . Bi, X. (2005). An extremely low visibility event over the Guangzhou region: A case study. *Atmospheric Environment, 39*(35), 6568-6577.

Xiao, F., Brajer, V., & Mead, R. W. (2006). Blowing in the wind: The impact of china's Pearl River delta on Hong Kong's air quality. *Science of the Total Environment, 367*(1), 96-111. doi:10.1016/j.scitotenv.2006.01.010

Xue, M., Kong, F., Thomas, K. W., Wang, Y., Brewster, K. , Gao, J., Wang, X., Weiss, S. J., Clark, A. J., Kain, J. S., Coniglio, M. C., Du, J., Jensen, T. L., & Kuo, Y. H. (2010). CAPS Realtime Storm Scale Ensemble and High Resolution Forecasts for the NOAA Hazardous Weather Testbed 2010 Spring Experiment. *25th Conf. Severe Local Storms*, Denver, CO, Amer. Meteor. Soc., Paper 7B.3.

Yang, D., Li, C., Lau, A. K., & Li, Y. (2013). Long-term measurement of daytime atmospheric mixing layer height over Hong Kong. *Journal of Geophysical Research: Atmospheres, 118*(5), 2422-2433. doi:10.1002/jgrd.50251

Yang, X., Gu, X., Chen, L., (2008), Estimation Of Atmospheric Horizontal Visibility From Satellite Remote Sensing Data, *IEEE International Geoscience & Remote Sensing Symposium*, July 6-11, Boston, Massachusetts, U.S.A.

Yu, H. B., Dickinson, R. E., Chin, M., Kaufman, Y. J., Holben, B. N., Geogdzhayev, I. V., & Mishchenko, M. I. (2003). Annual cycle of global distributions of aerosol optical depth from integration of MODIS retrievals and GOCART model simulations. *Journal of Geophysical Research, 108*(D3) doi:10.1029/2002JD002717

Yuan, C., Lee, C., Liu, S., Yuan, C., Yang, H., & Chen, C. A. (2002). Developing strategies for improving urban visual air quality. *Aerosol and Air Quality Research, 2*(1), 9-22.

Zajonc, A. (1993). Catching the light: The entwined history of light and mind *Physics Today, 46*(9), 64.

Zhang, Q. H., Zhang, J. P., & Xue, H. W. (2010). The challenge of improving visibility in Beijing *Atmospheric Chemistry and Physics, 10*(16), 7821-7827. doi:10.5194/acp-10-7821-2010

Zhang, Q., Ma, X., Tie, X., Huang, M., & Zhao, C. (2009). Vertical distributions of aerosols under different weather conditions: Analysis of in-situ aircraft measurements in Beijing, China mainland *Atmospheric Environment, 43*(34), 5526-5535. doi:10.1016/j.atmosenv.2009.05.037

Zhou, J. C., Swietlicki, E., Berg, O. H., Aalto, P. P., Hameri, K., Nilsson, E. D., & Leck, C. (2001). Hygroscopic properties of aerosol particles over the central arctic ocean during summer. *Journal of Geophysical Research: Biogeosciences, 106*(D23), 32111-32123. doi:10.1029/2000JD900426

Zhuang, H., Chan, C. K., Fang, M., & Wexler, A. S. (1999). Size distributions of particulate sulfate, nitrate, and ammonium at a coastal site in Hong Kong. *Atmospheric Environment, 33*(6), 843-853. doi:10.1016/S1352-2310(98)00305-7

Zieger, P., Weingartner, E., Henzing, J., Moerman, M., de Leeuw, G., Mikkilä, J. . . . Baltensperger, U. (2011). Comparison of ambient aerosol extinction coefficients obtained from in-situ, MAX-DOAS and LIDAR measurements at Cabauw *Atmospheric Chemistry and Physics, 11*(6), 2603-2624. doi:10.5194/acp-11-2603-2011